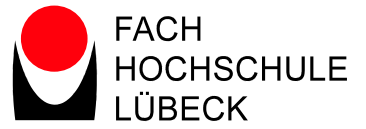




UNIVERSITÄT ZU LÜBECK



University of Applied Sciences

## **Master's Program: Biomedical Engineering**

### **Master's Thesis**

# *IMPROVEMENT, COMPLETION AND VERIFICATION OF AN ARTIFICIAL MUSCLE BIOMECHANICAL RACK (AMBR)*

**For receiving the Degree of Master of Science in  
Biomedical Engineering.**

**University of Lübeck  
Lübeck University of Applied Sciences**



**Deutsches Zentrum  
DLR für Luft- und Raumfahrt**

**Author: Manuela Paulina Trejo Ramírez**

**University's Supervisor: Dr. rer, nat, Floris Ernst**

**External Supervisor: Dipl. Ing. Andreas Kriechbaumer**

**Date: July 3rd, 2014**



## DECLARATION FOR THE MASTER'S THESIS

I warrant, that the thesis is my original work and that I have not received outside assistance. Only the sources cited have been used in this draft. Parts that are direct quotes or paraphrases are identified as such.

Lübeck, (date) \_\_\_\_\_

\_\_\_\_\_  
(Signature)

I hereby grant the Luebeck University of Applied Sciences the right to publish; reproduce and distribute my work, especially when it is to be presented to a third party for inspection.

Lübeck, (date) \_\_\_\_\_

\_\_\_\_\_  
(Signature)



A mis padres, por su amor y apoyo incondicional



## SUMMARY

During spaceflight astronauts undergo different physiological adaptations. One of them is bone tissue density decay in the lower region of the leg. Engineering tools are needed to understand the mechanisms of bone (re-)modelling and to design proper countermeasures. A computer model involving the Finite Element Method (FEM) is being developed; it calculates muscle forces from a known bone deformation. For this purpose a biomechanical rig will be useful for verifying the results obtained from the computer model as well as to better understand the influence of muscle forces on the tibia bone.

This Master's thesis describes the improvement, reconstruction and verification of an Artificial Muscle Biomechanical Rig (AMBR) which is capable of simulating specific lower leg muscle forces obtained from the FEM approach. Once these forces are applied the deformation on the chosen specimen is recorded to compare it with the initial deformation fed to the computer model.

The rack implements different mechatronic technologies in order to replicate muscle contraction and force application into a tibia-like specimen, as well as additional systems to record output data from the biomechanical tests.

The control system applies the desired muscle forces using pneumatic actuators. The process is managed through a valve system and force sensors. The operator, by using a custom-designed computer interface is able to define the force application parameters as well as to monitor the state of the biomechanical tests.

For recording reaction forces and moments a force plate was installed. To gather information on the specimen deformation when controlled forces are applied an innovative method developed at the German Aerospace Center, Deutsches Zentrum für Luft- und Raumfahrt (DLR), based on Motion Capturing was used.

Different tests focused on the functionality of the technologies used were made in order to know their accuracy and repeatability. Once their efficacy was proven, the necessary elements were integrated into a single-structure arrangement. Final tests showed that during operation all mechanisms were well integrated and didn't hinder the function of the others. The final results show that the information obtained is appropriate and the data from future tests will help to validate the computer model.





# CONTENTS

<b>SUMMARY .....</b>	<b>V</b>
<b>LIST OF ABBREVIATIONS .....</b>	<b>IX</b>
<b>1. INTRODUCTION .....</b>	<b>1</b>
<b>2. BACKGROUND AND FUNDAMENTALS .....</b>	<b>3</b>
2.1. PRELIMINARY WORK AT THE DLR.....	3
2.2. INVERSE FE MODEL .....	4
2.3. PREVIOUS MECHANICAL TEST RACK FRAME .....	5
2.4. GENERAL REQUIREMENTS OF THE PROJECT .....	6
2.5. EXAMPLES OF BIOMECHANICAL TEST RIGS .....	7
2.5.1. <i>Oxford rig</i> .....	7
2.5.2. <i>The Tübingen knee simulator</i> .....	8
2.5.3. <i>Lower Extremity Loading Device LELD</i> .....	9
2.6. MUSCLE BEHAVIOUR.....	10
2.7. TECHNOLOGIES NECESSARY FOR TEST RACK DEVELOPMENT .....	12
2.7.1. <i>Actuators</i> .....	12
2.7.2. <i>Control system</i> .....	14
2.7.3. <i>Reaction forces sensor</i> .....	17
2.7.4. <i>Motion capturing system</i> .....	18
<b>3. REALIZATION .....</b>	<b>21</b>
3.1. IMPROVEMENT OF RIG STRUCTURE AND INTERFACES .....	21
3.2. CONTROL SYSTEM .....	26
3.2.1. <i>Main concept</i> .....	27
3.2.2. <i>Pneumatic Hardware</i> .....	27
3.2.3. <i>Software</i> .....	30
3.3. CONTROL BIOMIMETICS OF MUSCLE BEHAVIOUR.....	35
3.4. MOTION CAPTURING SYSTEM .....	37
3.5. REACTION FORCES SENSOR PREPARATION .....	38
<b>4. EVALUATION AND DISCUSSION.....</b>	<b>41</b>
4.1. CONTROL SYSTEM .....	41
4.2. MOTION CAPTURING SYSTEM .....	44
4.3. REACTION FORCES SENSOR.....	47

4.4. LOAD CELLS.....50

4.5. REDIRECTION EFFECT ..... 53

4.6. FINAL SETUP TEST ..... 54

**5. CONCLUSIONS .....63**

**6. REFERENCES.....65**

**7. ACKNOWLEDGEMENTS.....69**

**LIST OF TABLES.....71**

**LIST OF FIGURES.....73**

**APPENDICES.....77**

## LIST OF ABBREVIATIONS

AMBR. Artificial Muscle Biomechanical Rack  
DLR. Deutsches Zentrum für Luft- und Raumfahrt  
FEM. Finite Element Method  
LELD. Lower Extremity Loading Device  
MoCap. Motion Capture  
MUST. Muscle induced Strains in the Tibia  
OST. Optical Segment Tracking  
PID. Proportional-Integrative-Derivative  
PWM. Pulse-Width Modulation  
VI. Virtual instrument



# 1. INTRODUCTION

During sojourns under microgravity, astronauts experience muscle and bone atrophy. To develop proper countermeasures one first needs to understand the basic mechanisms of bone (re-)modelling. Results obtained from different studies and surveys do not offer a complete view of the entire mechanisms responsible for bone tissue remodelling. For example, the magnitude of the forces applied by muscles to a bone is not well known.

Until now muscle contributions are not well understood and might be underestimated. Muscular forces play an even bigger role than expected, and some movement patterns are more influential than others. The aim for this project is to gather information on which muscle activation patterns have a greater impact on bone remodelling.

Therefore a computer model is being developed involving FEM (Finite Element Method), where the deformation of the bone will be reversely attributed to muscle forces. When the computer model is finally validated, it will help to correlate the deformations that bone experiences during locomotion. Future advances and therapies might be developed in order to counteract bone atrophy in astronauts and understand and prevent the mechanisms causing bone diseases on earth such as osteoporosis in patients.

To validate the computer model the construction of a biomechanical test rig is proposed. The rig should be capable of simulating specific lower leg muscles and apply their corresponding forces into a tibia specimen of known mechanical properties and obtain its deformation information.

This Master's thesis describes the improvement, reconstruction and verification of the Artificial Muscle Biomechanical Rack (AMBR) developed at the Space Physiology Department of the Institute of Aerospace Medicine at the German Aerospace Center in Cologne, Germany.

During previous studies at the Space Physiology Department tibial deformation within specific points was recorded in subjects while performing different positions of human locomotion [1]. The deformation information is entered into the computer model and the outcome is the magnitude of muscle forces that contribute to that specific tibial bending. The forces will be replicated by artificial muscles in a specimen and the outcome will be the deformation that should resemble the one measured during the locomotion studies.

For this purpose a mechatronic system is designed, implemented and tested. The main purpose of the system is to generate, transmit and control specific muscle forces during the simulation of different leg movements. The system is based on an artificial muscle mechanism using pneumatic cylinders to contract and simulate muscle forces activated via pneumatic valves. The control portion is carried out by a custom-made software interface developed in LabVIEW 2012 SP1 to allow the operator to select actuating muscles and define the force application parameters during regular biomechanical testing. The software communicates with a special hardware interface that gathers digital and analogue data from sensors and activates control outputs according to testing needs. The output data from the test is collected using different systems such as a force plate for obtaining ground reaction forces and moments, and a motion capturing system using high resolution cameras and retro-reflective markers for recording specimen deformation.

In order to verify the functionality of the different control, actuation and data recording systems, several tests are performed and their corresponding statistical analysis is made. The results indicate the suitability for their application in the rack as well as their limitations. Finally system integration tests were made to corroborate the complete setup functionality and its capacity to carry out biomechanical test procedures that involve simulating different muscle forces during specific positions of human locomotion. Measures for improvement are suggested for future testing and redesign of the setup.

## 2. BACKGROUND AND FUNDAMENTALS

For this thesis the foundation is composed of previous work performed by researchers at the Space Physiology department of the German Aerospace Center, the Deutsches Zentrum für Luft- und Raumfahrt (DLR) as well as other similar studies performed by other entities. The general goals of this project are summarized in order to find the appropriate technologies suitable for it. A background on studies and outcomes from the DLR will be explained, and then research on other test rack functionalities and characteristics will be presented. Finally the theory behind diverse technologies necessary for the AMBR is explained.

### 2.1. Preliminary work at the DLR

In order to understand the remodelling mechanisms on bones due to the application of muscle forces, a series of studies were performed at the Space Physiology department. Bearing in mind that bone remodelling is induced by mechanical stress due to load application either by muscular forces or bodyweight, the transformation it undergoes is a function of the force magnitude, and the way those loadings affect the bone, for example during dynamic conditions like walking and running. These mechanisms are exemplified in the Mechanostat model. The model describes bone density growth and loss due to different stress conditions. When bone is in a long unloaded state, bone tissue density decreases, for example in patients with limited mobility or astronauts. When stress is present during normal periods, bone is said to be in an adapted state. If the bone is stimulated through certain exercises or therapies, a density gain is present. This model was the first attempt to find an adequate function for describing bone tissue adaptation [2].

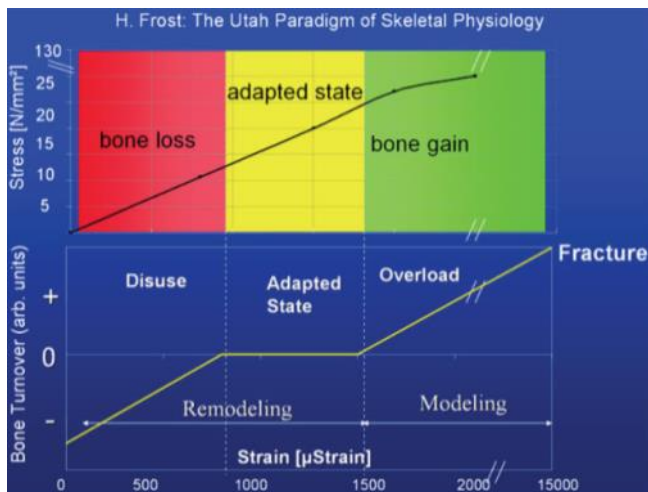


**Figure 2.1: Mechanostat model [2]**

With the development of *in vivo* bone deformation measurements researchers have been able to record data and correlate, to a certain extent, using methods like strain gauges, how activities such as standing, walking and running, load and bend bones [3]. As this technique is highly invasive and has many drawbacks, a new method was developed at the Space Physiology Department by substituting strain gauges by retro-reflective marker clusters from commercial Motion Capturing (MoCap) systems like Vicon [4]. This approach was investigated in the MUST study (**M**uscle **ind**Uced **S**trains in the **T**ibia).



**Figure 2.2 MUST study. A MoCap system recorded tibial deformation during human locomotion [1]**

## 2.2. Inverse FE model

At the Space Physiology Department a novel approach for calculating lower leg muscle forces from known tibial deformations is being developed by Dipl. Ing. A. Kriechbaumer. The computer model developed starts from the assumption that the bone adaptation triggered by mechanical loading is largely due to the application of muscle forces during normal activities, and their contribution to the loading is even higher than the load induced by bodyweight.

As muscles play a significant role in bone remodelling, an approach to determine specific muscle forces during certain activities from bone deformation needs to be developed. Because measuring muscle forces *in-vivo* is complicated, a computer model might enable the determination of to what extent the muscles acting on a bone contribute to its loading and therefore adaptation.



The algorithm works by using tibial deformation data as an input. This information was obtained by the MUST study explained previously. The data is processed using mechanical principles like Hooke's law (a displacement is directly proportional to the force) and the superposition principle (a net result of different stimuli is equal to the sum of their result) to calculate the magnitude of the forces.

$$F = -kx \quad (\text{Eq.1})$$

In Equation 1 the Hooke's law is shown.  $F$  is the amount of force applied in N,  $x$  is the displacement in the spring in meters and  $k$  is the spring constant or force constant

The program optimizes the magnitude of the force for each muscle by minimizing the error between the measured displacement and the calculated one.

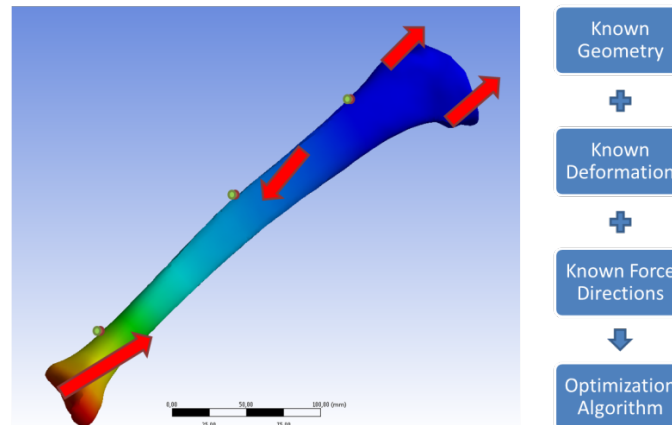


**Figure 2.3 Basic principle of the computer model**

For the validation of this approach, a mechanical test rig will be implemented. The objectives of the AMBR are to simulate the forces calculated from the model and retrieve bone deformation information. The recorded deformation should match, as closely as possible, the input from the MUST study.

## 2.3. Previous mechanical test rack frame

A former student working at the Space Physiology Department focused on the design, construction and testing of a mechanical frame for the AMBR [5]. First the general requirements of functionality of the AMBR rack were defined because these will have a direct/indirect impact on the design of the mechanical frame. The main requirements were:

- Apply a set number of forces, in a uniform way for its closeness to the computer model;
- Resolution of  $\leq 1\%$ ;
- Maximum total forces to be applied on the specimen should not exceed 15kN;
- Suitable specimen attachment and loading device;
- A system for recording deformation data and ground reaction forces and moments
- Define a suitable specimen for testing.

After considering these aspects the outcome generated was a 2-bar vertical frame which allowed the deformation capturing system to record tibial bending with enough space for its installation and an unobstructed field of view. The muscle-like actuators are mounted in a custom made plate on their respective alignment angles. The ropes coming from the actuators are redirected through hooks to the attachment point screws on the specimen. The specimen is mounted on top of a force plate, upon which is a fixation plate for applying a simulated bodyweight and inertial forces.

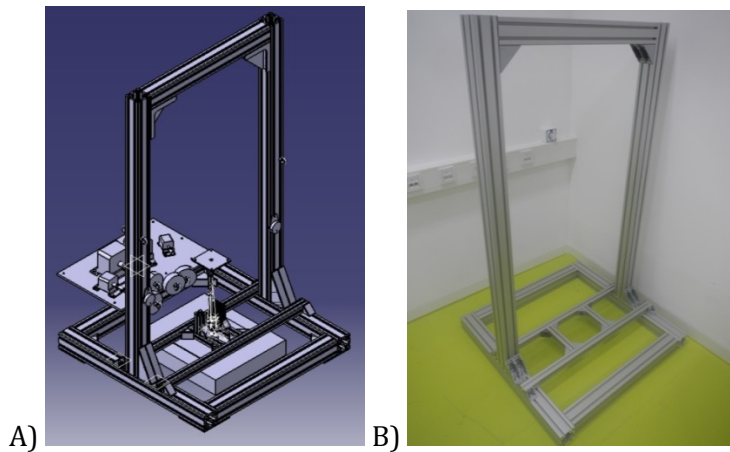


**Figure 2.4 First mechanical frame for AMBR rack. A) Computer design, B) Physical configuration [5]**

Some issues were observed with this first setup when tested for its verification. First the force plate was moving towards the rack during testing making it difficult to align, so was advised for future studies to fix it to the main structure. A considerable amount of movement and vibration in the rack was observed. For this, a base structure that holds the whole mechanical frame could avoid these movements that might cause force direction misalignments as well as deformation recording errors. The actuator plate was mounted in a cantilever position so whenever a force was applied there was a significant bending of the base plate; also the plate thickness (5mm) was too small. During testing the specimen was fixed at the bottom by a screw and this method was proven to be invalid because of the deformation misbehaviour as well as the stress induced crack at the bottom of the specimen. Finally, the force sensor readings were inaccurate due to the need of a better mechanical mounting.

## 2.4. General requirements of the project

Bearing in mind the previous work done in the project, it is important to clarify the specific requirements of the test rig for it to be completed and verified. This will set the goals that each of the different components and systems of the rack should meet in order to allow a smooth operation as well as the flexibility for testing and record data appropriately.

The main requirements for the AMBR are:

- Redesign and reconstruct the current mechanical frame to provide it with greater stability, it needs to be able to prevent unwanted vibrations and mechanical disturbances that alter other systems and components. The frame should be capable of combining all systems into one setup. A force plate should be positioned underneath the specimen to gather reaction forces and moments. The motion capturing system needs to have a suitable view of the specimen sensors for deformation recording.
- Implement a lower leg artificial muscle system capable of contracting and applying forces of the same magnitude and in a similar way as the ones observed in humans. The actuators will recreate static and semi-static conditions only. For this only lower leg muscles pulling downwards are needed. Implementing actuators capable of a high speed operation for future dynamic tests is a plus.
- Design a computer interface that allows the operator to perform biomechanical tests and permits the modification of contraction application parameters like filling, force and other specific control settings. The front panel should display information regarding the current state of the system for monitoring purposes, and important graphs and values to facilitate test and evaluation procedures.

- Arrange the control hardware to keep good component integration. Components that represent a risk to the user should be kept close to the rack and away from the operator.
- Install a force plate capable to recording reaction forces and moments in three coordinate axes.
- Implement a system based in MoCap able to record small specimen deformations during testing and return information of the changes in position of markers collocated in defined regions of the anatomy of the specimen.
- All the aforementioned systems should be integrated in one fixed setup. Their individual operation should be optimal and not hinder the function of the other systems while functioning.

These requirements provide enough information for investigating technologies suitable for those tasks as well as to guide the redesign, reconstruction and validation of the AMBR.

## 2.5. Examples of biomechanical test rigs

In general, several approaches to obtain biomechanical information like bending of lower leg bones and movement have been developed. Experimental studies use human joint and lower leg specimens for experiments that will be difficult to be carried out *in vivo*. These mechanical setups employ different mechanisms of force application as well as a variety of sensors for motion/deformation recording. These setups frequently use cadaveric legs and reuse tendons to apply a known muscular force in a particular point. Considering the fact that solutions employed by this racks might be of great interest for the AMBR project, an investigation on the different rigs built previously was made, and the most significant ones will be discussed. Even though the main purpose of the construction of those rigs is different, it is important to acknowledge how complications were addressed and specific elements built in order to apply a similar solution in the AMBR.

### 2.5.1. Oxford rig

The Oxford Rig was designed for biomechanical tests applied to cadaveric human knee joints. The different positions tested were focused on simulating a certain level of knee flexion during activities like bike riding, standing from a chair or climbing stairs. Its main intention is to allow the knee to have full spatial freedom by adding hip and knee joints. These joints were constructed in a specific setup with fixed degrees of freedom to allow flexion/extension, abduction/adduction and internal/external tibial rotation, allowed by the kinematical chain of hip-knee-ankle joints.

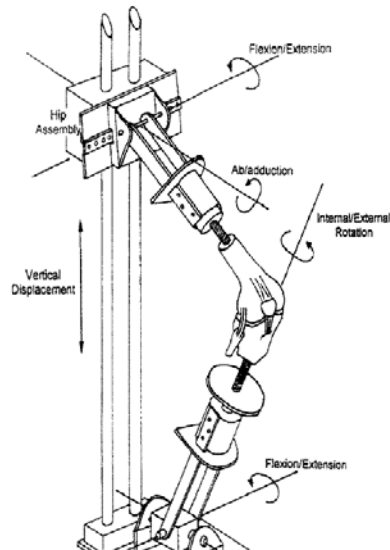


**Figure 2.5 The Oxford Knee-Testing Rig [6]**

The Oxford Rig focuses in the kinematic study of knee movement during specific activities; from this it can be learned that the hip and ankle joints allow the simulation of these activities. For the purpose of the AMBR, it could be considered for the future to design and build custom-made joints to allow movement of the specimen in different directions. As mentioned before, the AMBR will be intended for static biomechanical conditions tests, but it should be flexible enough for future dynamic applications and modifications. From this rig the main structure idea is important to design a proper mechanical frame.

### 2.5.2. The Tübingen knee simulator

The Tübingen knee simulator also performs in-vitro studies of knee kinematics. It was constructed following the kinematic chain of the Oxford Rig. Its purpose is to simulate knee movement under physiological muscle loading in order to improve surgical procedures and rehabilitation therapies. The simulator can apply five knee muscles to assess a fixed amount of body weight using the force read at the ankle joint as the target force of the control system.

The muscle force application was in charge of electrical servo motors attached to tendons via muscle clamps. It is important to note that the forces generated by such actuators were small, with a maximum achieved muscle force of 250N.

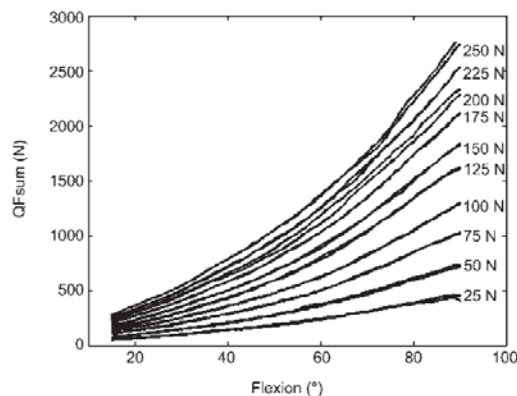


**Figure 2.6 Total forces in three simulated quadriceps muscles. Forces applied during various knee loading conditions for one specimen [7]**

The mechanical design includes a vertical frame as well as hip and ankle joint assemblies with fixed degrees of motion to allow unconstrained knee joint movement in six degrees of freedom. The muscles simulated included three knee extensors and two flexors using electrical servomotors attached via steel cables. Uniaxial force sensors were collocated between the tendon clamps and the steel cables to monitor the applied forces. The movement of bone segments was recorded using an ultrasonic MoCap system.



**Figure 2.7 The Tübingen knee simulator [7]**

The simulator has two control schemes: position-control and force-control. The position-control scheme is aimed to match the needed knee flexion and the force-control scheme uses a proportional control to produce a desired ankle bearing reaction force. Custom-made control software developed in LabVIEW was used to control the system via serial communication. It has to be noted that applying a Proportional-Integrative-Derivative (PID) control required a delay in the control loop so the speed of knee angle movement was reduced to 1 deg/s with a proportional control only [7].

### 2.5.3. Lower Extremity Loading Device LELD

Before the development of the MUST study at the DLR, a validation study was carried out to verify if an Optical Segment Tracking (OST) approach could be valid for recording bone deformation during in-vivo studies. For this purpose the Lower Extremity loading Device (LELD) rig was constructed at the German Sports University in Cologne. It is capable of simulating physiological muscle contractions in human cadaveric lower extremities for the MUST study [8].

The deformation of tibial segments was recorded by the relative movement between two marker clusters with three non-collinear retro-reflective markers fixed on the distal and proximal regions of the tibia. The aim was to record a more detailed picture of the deformation. The muscle forces simulated were applied in low magnitudes up to a maximum of 505N. The OST was capable of tracking the tibia bending angles during muscular loading. The actuators chosen for this task were pneumatic cylinders. These were activated in different cycles depending of the position to be simulated. Several lower leg muscles which have an impact on tibial loading were simulated.

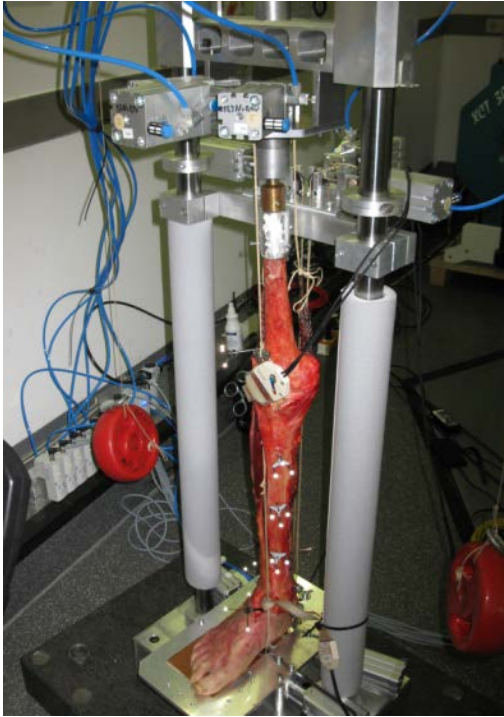


**Figure 2.8 The LELD rig**

It can be said that this specific rig is the direct predecessor of the AMBR and its design will serve as a basis for the development of the AMBR.

## 2.6. Muscle behaviour

It is important to know the natural mechanisms that dictate biological muscle behavior for its correct application into any biomimetic setup. Skeletal muscle is the main contributor to human locomotion and directly impacts joint movement, bone loading and support. Muscles are able to use chemical energy and transform it into force and movement.



**Figure 2.9 The muscles responsible for human locomotion have a direct impact on bone remodelling during specific activation patterns [9]**

The skeletal muscle structure is based on cells called muscle fibers having diameters between 10 and 100 $\mu$ m and lengths of up to 20cm [10]. When a group of fibers are bound together by connective tissue, it creates what is called muscle. Usually muscles are connected to bones by bundles of collagen fibers called tendons [10]. It is well known that there are different ways in which muscle fibers are arranged within

muscles and this is the reason why certain muscle contractions are different from others e.g. joint angle generation.

Striated skeletal muscle has the ability to contract, it does not necessarily mean it will shorten, but it makes reference to the capacity of generating force within muscle fibers. One important part of the biomechanical behaviour of muscles is the excitation-contraction coupling. This refers to the sequence of events driven by the application of an action potential in a muscle fiber leading to the biochemical process that in turn leads to muscle fiber contraction. If a single action potential is applied, the mechanisms of contraction are expected to last around 100ms or more, following a well-known behaviour.

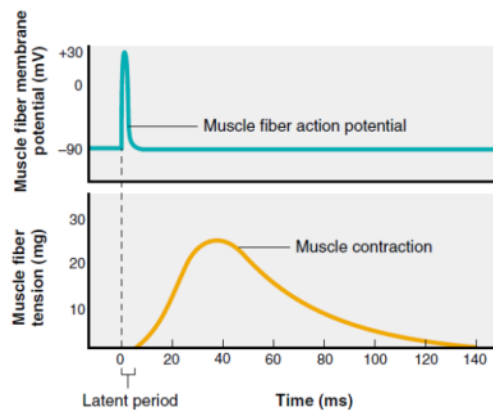


**Figure 2.10 Time relations between a skeletal muscle fiber action potential. Resulting contraction and relaxation of the muscle fiber [10]**

By definition, a force exerted on an object by a contracting muscle is called muscle tension and the force exerted by the object to the muscle is a load. When the muscle generates tension but does not contract it is called isometric (constant length) contraction.

The most important series of events to be replicated is the tension generation mechanism in muscles. As the purpose of the AMBR rack is to apply isometric contractions, the following model will be used as a reference:

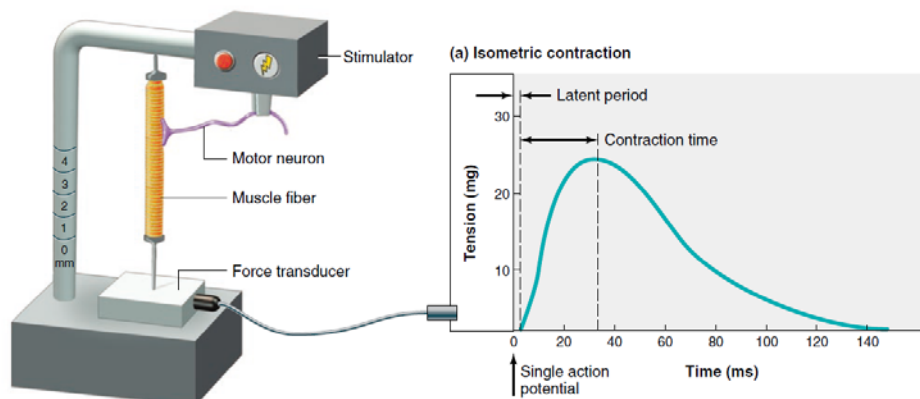


**Figure 2.11 Measurement of tension during a single isometric twitch of a skeletal muscle fiber [10]**

As it can be depicted in Figure 2.11, when a stimulus is applied to a muscle fiber, after a latent period, a tension curve is generated with respect of time. Depending on the muscle fiber or the whole muscle in question, the contraction time varies. However in general the contraction is generated in a matter of milliseconds.



The chain activation-contraction-force generation within time is what defines the biomechanical behaviour to be achieved within the AMBR. As a first stage the test rig will focus on static positions; the contraction time e.g. speed of contraction will not be fully taken into account when choosing for an appropriate actuator, this is however important as in the future, time will be a vital parameter. So it is advised that from the beginning an actuator type capable of achieving a contraction speed close to the normal range of biological muscle should be chosen.

Another important parameter for searching and choosing actuators is the amount of force these should be capable of exerting. As known from physiological studies and human locomotion simulations, forces of the lower leg muscles are very high. On the following chart, extracted from a paper which studied vertical jump, it is evident that the magnitude of the forces required by such muscles ranges in hundreds and even thousands of newtons, implying that the type of actuators needed for the rig should be able to generate such high forces.

TABLE III Values of the maximum isometric strength of each muscle ( $F_o^m$ ), optimal muscle-fiber length ( $l_o^m$ ), muscle pennation angle ( $\alpha$ ), and tendon slack length ( $l_s^T$ ) assumed in the model. Actuators on the left and right sides of the body are assumed to have the same parameter values

	Actuator	$F_o^m$ [N]	$l_o^m$ [m]	$l_s^T$ [m]	$\alpha$ [deg]
FDH	flexor digitorum longus/brevis flexor hallucis longus/brevis	1184	0.0400	0.3900	8
EDH	extensor digitorum longus/brevis extensor hallucis longus/brevis	760	0.1100	0.3200	7
DFIN	tibiablis anterior extensor hallucis longus	1003	0.1050	0.2600	5
DPEV	peroneus tertius extensor digitorum	609	0.1000	0.3000	9
PFIN	tibialis posterior flexor digitorum longus flexor hallucis longus	2149	0.0400	0.3700	10
PPEV	peroneus brevis peroneus longus	1556	0.0500	0.3000	7
SOL	soleus	3016	0.0500	0.2540	25

Figure 2.12 Sample of values of the maximum isometric strength of each muscle [11]

## 2.7. Technologies necessary for test rack development

### 2.7.1. Actuators

An important component of the AMBR rack is to have a device or set of devices capable of simulating muscle contraction mechanisms as well as applying a specific force appropriate to the singular muscle to be simulated. For this, an investigation on different actuator options was made, then those options were compared, and finally a decision was made for their implementation in the rack

- Muscle wires

Muscle wire is a generic term that includes muscle-like actuators capable of contracting when stimulated by an electrical current. Flexinol is an actuator wire made of a NiTi alloy which behaves similar to memory alloys. Flexinol can be found in the form of a wire or coil shape that when an electrical current is applied (heat) it contracts, generating tension on the object it is connected to. When cooled it returns to its initial length. There is another type of this alloy in the shape of ribbons capable of exerting higher forces than those of wires. For example, a ribbon with a width of 0.805mm and a thickness of 0.040 mm can generate a pull force of 0.572 kg with a current of 1.75 Amperes [12].



The advantage is that the contraction mechanism of this actuator resembles quite closely that of biological muscle. Its main disadvantage is the high amount of energy consumption it requires when compared to the very small amount of force it can generate.

- Electric actuators

Electric motors were another option considered for this project. There is a wide range of manufacturers that offer linear electrical actuators with high ranges of forces. Within the different options common setups were found; either a normal rotating electric motor on which a gear reduction was installed to transform rotation into linear translation of the end shaft, for example Maxxon motors [13]. This requires purchasing extra accessories when acquiring these motors, as well as an increment in the cost. Other options of actuators with high force capacities demand high electrical energy consumption as well as special electrical characteristics like three-phase configuration like those used in Exlar motors [14]. This actuator might not be a suitable option due to the complexity of implementation and high complementary costs.

- Pneumatic actuators

Other existing commercial actuators that behave like biological muscle are the pneumatic muscles. These actuators are relatively small compared to the high magnitude of forces they are able to exert. Their costs are lower compared to other actuators of similar power and have contraction behaviour very close to the real biological model. Due to their size and low weight these are a practical option for muscles pulling upwards on the lower leg for future applications. The actuation concept and direct contraction draw the attention of considering the possibility of implementing pneumatic actuators in the test rack.

Keeping in mind the magnitude of forces to be applied, an investigation through the catalogues of pneumatic actuator manufacturers was done. In the end the manufacturer chosen was Festo AG. & Co. due to their large range of actuators as well as their resources for design and construction of pneumatic systems. Another advantage is the lower cost compared to other actuation types and its high availability.

For a quick assessment on how actuators could be chosen Festo provides an online tool that helps consumers select a pneumatic cylinder that suits their needs as well as suggest appropriate accessories depending on the actuator specifications such as pressure, force, etc. While researching different models available, the compact cylinders of the AEVUZ series were found [15]. These are compact cylinders that with a small size can achieve relatively high forces. Since for the AMBR setup only muscles of the lower leg pulling downwards will be simulated, the weight of the cylinders is not an issue, as long as they can achieve the range of forces desired.



**Figure 2.13 AEVUZ pneumatic cylinder [16]**

An important advantage of the AEVUZ cylinders and of pneumatic actuators in general is that these are made for pulling applications, discarding the need of mechanical

adaptations in order to obtain such linear movement. Also, this movement allows it to generate tensional force at a very high speed. For example, in Figure 2.14 is an image result from Festo's online engineering tool finder and shows the AEVUZ pneumatic cylinder with a capacity of 4,222N at 6bar, while pulling a load of 400kg [16]. The position/speed/time diagram shows the high speed capacity of this actuator. Again it should be kept in mind that speed is not a current parameter for operation but in the future this characteristic will be of vital importance.



**Figure 2.14 Position/speed/time diagram. Obtained from Festo online engineering tool [15]**

### 2.7.2. Control system

An automatic control system is defined as an interconnection of elements that form a configuration denominated system, which make it capable of regulating itself. [17] This applies to design systems with a desired behaviour, and to an external stimulus able to modify its response in order to keep a specific variable within desired levels.

Depending on the desired control system, its components might range from electronics, e.g. sensors, mechanics like actuation elements, to computer processing units. A control system has a specific configuration that makes it able to react to external signals. In an open-loop control system we have an input to a system or process, and then an output according to the input obtained.

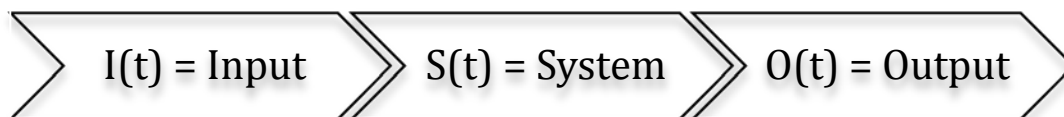


**Figure 2.15 Open-loop control system**

For these kinds of systems it could be inferred that the control action, up to a certain extent, is independent of the output. Similar to a washing machine, these systems generally employ a timer in order to self-regulate.

On the other hand there are systems whose control action depends on the output; such systems employ sensors that detect the real response and compare it to a set reference input. The feedback in this is used to compare the real output against the desired behaviour, so the system will know what kind of corrective action to apply.

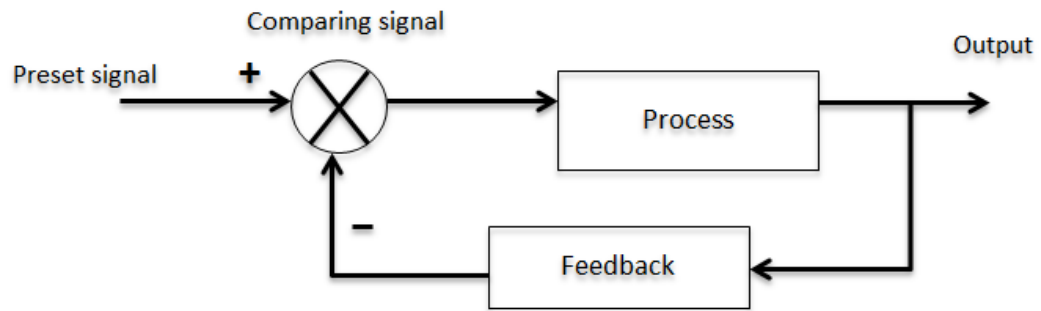


**Figure 2.16 Closed-loop control system**

For any kind of mechatronic application, it is important to have a clear idea of the process to be regulated, how it will be monitored and the magnitude of the desired levels for performing a specific task. For the AMBR, the application of muscle-like forces has to be set in order to accomplish a user-defined force magnitude, and an appropriate sensor to monitor the force level should be in place.

The closed-loop control to be implemented will be defined according to the control needs as well as the hardware available to perform such a task.

According to the actuator investigation done in the intership of the author of this thesis, pneumatic actuators have clear advantages compared to other actuators. Lower cost, high force with lower power consumption and direct linear movement are their advantages. The disadvantages include the noise present during operation as well as vibrations due to fast activation movement. [18]

As the most suitable choice of actuation for the AMBR are pneumatic actuators, either artificial muscles or cylinders, such actuators have special configuration needs for their regulated operation. There are many different configurations that can be used each with advantages and disadvantages. For this project the best alternative or combination of different alternatives might be used. As there is no unique solution, different applications will be explored and the optimal one will be implemented.

- Proportional pressure regulators

One of the most evident choices is to implement an commercial off-the-shelf proportional pressure regulator. These are electropneumatic devices that contain all of the needed components for regulation in a single device. Generally they have high speed valves, one to fill the actuator with compressed air and one for release. Because this configuration might be limiting, an extra controller is included, for example a microcontroller for regulating pressure or flow rate via Pulse-Width Modulation (PWM). The advantages are that it doesn't require any extra hardware and is easy to connect to other interfaces; the disadvantages are the high cost of this elements and the innacurate positioning of the actuator.

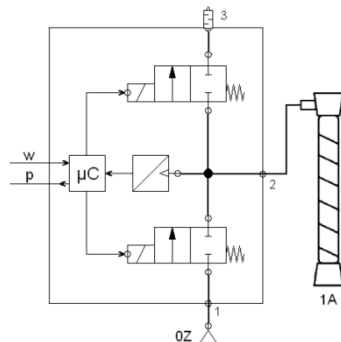


**Figure 2.17 Inner connection of proportional pressure regulator [19]**

In Figure 2.17 the inner connection shows an arrangement of two 2/2 way valves, one connected to the main supply and the other to a silencer for compressed air release. Their activation is controlled by a microcontroller that regulates the pressure of the actuator regarding the desired one.



**Figure 2.18 Proportional Pressure regulator form Festo [20]**

- Cascade of throttle valves

While some hardware control options imply a hard control system with a complex setup, other options use a cascade of throttle valves. The basic operation principle is the same, using high speed valves for pressurizing/depressurizing an actuator. The difference is that the number of valves increases and they are connected in parallel. Each valve has a different flow rate or pressure level. When these are combined in different arrangements, different unique pressure levels or flow rates can be achieved. The number of levels is equal to  $2^n$ , where  $n$  is the number of valves in the assembly.

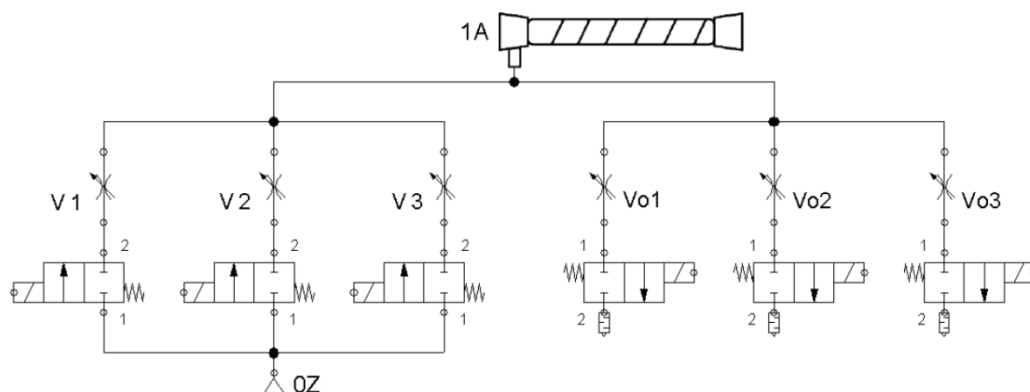


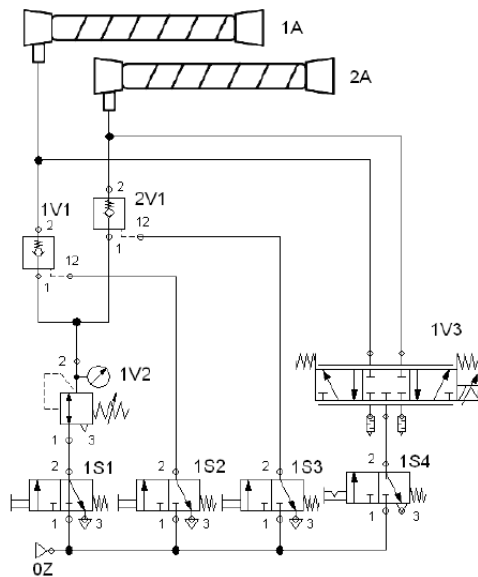
**Figure 2.19 Diagram of cascade throttle valves assembly [19]**

In Figure 2.19, a cascade of 2/2 way valves in parallel is shown. Each valve is coupled with a flow control valve. This setup allows having a combination of flow rates depending on the valve couple selected.

The advantages are the smoother movement of the actuators and its flexibility to be implemented with another control systems; the disadvantages are the requirement of a higher number of pneumatic components and of a special driver to control all the valves.

- Proportional directional control valves

Another option for controlling pneumatic actuators are proportional directional control valves. Usually this scheme is used for position control of double-acting cylinders. In this case the valves can be used to control an antagonistic setup of muscles.



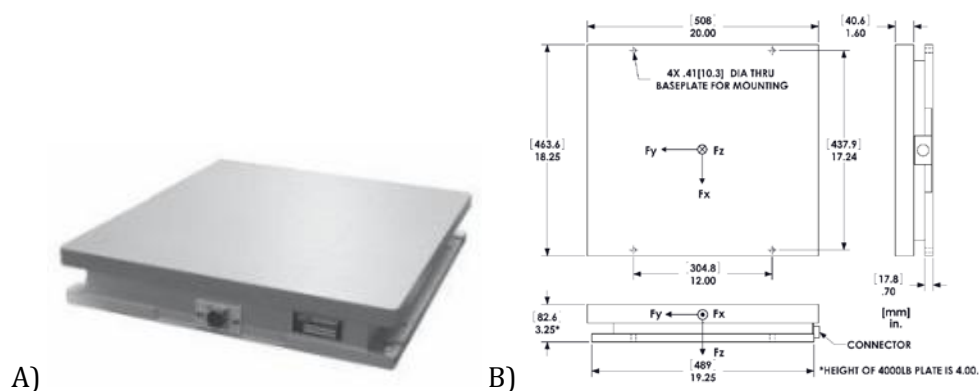
**Figure 2.20 Circuit of a control system using a proportional valve [19]**

Figure 2.20 shows how a proportional directional valve is implemented to control an antagonistic setup of muscles. The design requires the installation of additional check and position valves.

These valves are unlike other common directional valves. Proportional directional valves not only manage direction of flow but also the flow rate of the inlet and outlet of an actuator. This application can achieve precise position and flow control. The disadvantages are the high cost of the valves, the requirement of special additional hardware components and the complex control implementation.

### 2.7.3. Reaction forces sensor

A system for recording ground reaction forces is already available at the DLR. The sensor is a force plate from AMTI force and motion model OR6-6-2000. This force plate is specially designed for gait studies and it has a high sensitivity, excellent repeatability and a long-term stability. This sensor is also highly recommended for research and clinical studies.



**Figure 2.21 A) AMTI Force plate B) Dimensions and orientation of the force plate [21]**

The plate uses a six-component transducer that measures three force components ( $F_x$ ,  $F_y$ ,  $F_z$ ) and three moment components ( $M_x$ ,  $M_y$ ,  $M_z$ ) which act on the dynamometer. For its operation, an input voltage is applied on each channel and for each of the six

components there is a corresponding output voltage. The ratio of output to input for each channel is called sensitivity.

The forces and moments are measured to a defined coordinate system. The shear center of the unit is defined from the manufacturer and is the point where the application of force in either coordinate axis will theoretically produce a zero moment output.

The general force plate specifications are shown on Table 2.1.

<b>Dimensions (WxLxH)</b>	18.25 x 20 x 3.25 in	<b>Mounting hardware</b>	Recommended
<b>Weight</b>	40 lb.	<b>Sensing elements</b>	Strain gage bridge
<b>Channels</b>	Fx, Fy, Fz, Mx, My, Mz	<b>Amplifier</b>	Required
<b>Top plate material</b>	Composite	<b>Analog outputs</b>	6 Channels
<b>Temperature range</b>	0 to 125°F	<b>Digital outputs</b>	None
<b>Excitation</b>	10V maximum	<b>Crosstalk</b>	< 2% on all channels
<b>Fx, Fy, Fz hysteresis</b>	± 0.2% full scale output	<b>Fx, Fy, Fz non-linearity</b>	± 0.2% full scale output

Channel	Fx	Fy	Fz	Units	Mx	My	Mz	Units
Capacity	500	500	1000	lb	10000	10000	5000	in-lb
Sensitivity	3	3	0.75	µv/v-lb	0.18	0.18	0.38	µv/v-in-lb
Natural frequency	400	400	1000	Hz	-	-	-	Hz

**Table 2.1 AMTI Force plate OR6-6-2000**

#### 2.7.4. Motion capturing system

Considering the drawbacks present in previous bone deformation recording systems, (e.g. strain gauges); a viable option for recording real time bone deformation is by using motion capturing systems. MoCap is a way to digitally record desired human movements which can then be mapped to a digital model in 3D space. Therefore information on position, speed, velocity, etc. can be processed and interpreted. The most publicly known application of MoCap is in the animation of digital characters for the entertainment industry.

One of the main applications of MoCap is in life sciences research. Needs for varying clinical studies are resolved through MoCap; for example by assessing clinical patients and designing appropriate rehabilitation therapies by analyzing gait patterns. Subject's joints and extremity positions can be recorded to diagnose motion problems and assess them based on quantitative data.

The MoCap system available at the DLR is from Vicon and uses Bonita B3 cameras. This camera system has a resolution of 0.3 Megapixels at a maximum frame rate of 240, at full frame resolution, allowing for the capture of fast moving objects. The cameras are compact and easy to mount in nearly any type of configuration. The cameras are easy to set up and capable of performing tests on gait analysis, sports biomechanics, animal studies and rehabilitation [4]. The B3 model is suitable for recording lower limb gait and records in small volume virtual environments, making it adequate for its implementation in the AMBR.



**Figure 2.22 Vicon Bonita B3 camera [4]**

The technical data of this system is show in Table 2.2.

Resolution (Megapixels)	Maximum frame rate at full frame resolution	Sensor	On-Board Marker processing	On-Board Data selection	Power
0,3	240	CMOSIS	Yes	No	POE/Giganet
Lens options	Field of view (H° x V^°)	Strobe options	Shutter type	Connection type	Updateable firmware
4-12mm zoom	82 x 66, 32 x 24	NIR	Electronic freeze frame shutter	RJ45-RJ45, RJ45-Lemo	Yes

**Table 2.2 Vicon Bonita B3 specifications [4]**





## 3. REALIZATION

In this section the different technologies implemented in the AMBR will be explained. The designed and constructed systems range from the mechanical frame to the different control mechanisms, like actuators and sensors. Data recording systems are also in place to gather output data from the biomechanical tests to be performed. The main task of this work is to set the aforementioned systems in place as well as to focus on the control design and implementation. It is important to clarify that the reconstruction tasks shown on 3.1 were not made by the author, although all the modifications of the AMBR that have an impact on the operation of the system are described.

### 3.1. Improvement of rig structure and interfaces

As mentioned at the beginning of this thesis, a former student at the Space Physiology Department designed and constructed the mechanical frame for the AMBR. The task was to design a frame capable of handling the different testing elements like actuators, specimen and data capturing systems in one main structure. This should be strong enough to resist forces present during the tests of muscle contraction, specimen deformation as well as force redirection.

During the preliminary tests some issues regarding construction and components in general were observed. For the second iteration of the rig the mechanical frame was redesigned and reconstructed in order to eliminate disturbances that might hinder proper testing procedures and data recording.

- Force plate

The force plate for capturing reaction forces and moments was positioned under the bottom plate under the specimen using high friction Gecko tape. A wooden base common to all structures was mounted underneath, so the force plate as well as the rack frame can be mounted using screws and no deviations will be present. This will also ensure that no changes on the coordinate systems are present while performing different tests due to the change in position. Previously, it was observed that during tests the rig and force plate move closer to each other due to the high forces applied.

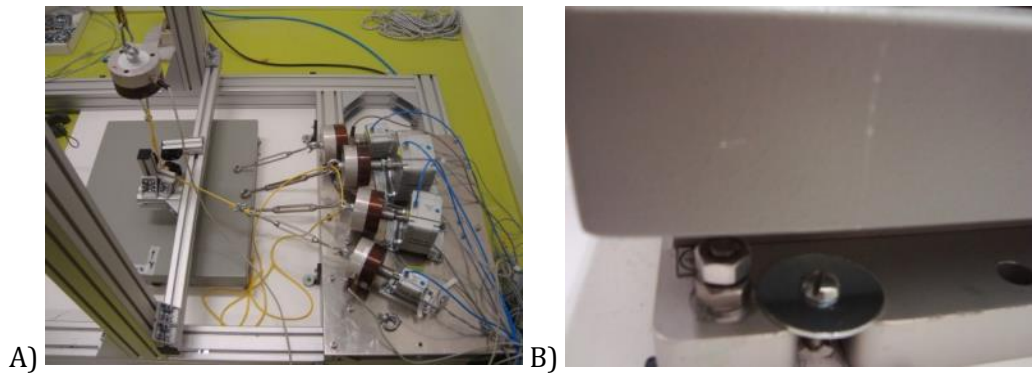


**Figure 3.1 Force plate. A) Alignment of force plate B) Fixation of the plate to the wooden base using screws**

- Actuator platform

The actuator's base plate was replaced with a thicker (10 mm) high resistance plate; and mounted on two beams; one at the front and one at the back, therefore no bending will be present when actuators generate high forces.

- Specimen preparation

The specimen used was an artificial bone manufactured especially for biomechanical tests from the manufacturer SAWBONES. The model is a size large left tibia (405mm in length).

## AVERAGE MATERIAL PROPERTIES

### **SIMULATED CORTICAL BONE (SHORT FIBER FILLED EPOXY)**

Density	Longitudinal Tensile		Compressive	
	Strength	Modulus	Strength	Modulus
(g/cc)	(MPa)	(GPa)	(MPa)	(GPa)
1.64	106	16.0	157	16.7
Density	Transverse Tensile		Note: Material property data based on ASTM D-638 and D-695	
	Strength	Modulus		
(g/cc)	(MPa)	(GPa)		
1.64	93	10.0		

### **SIMULATED CANCELLOUS BONE (RIGID POLYURETHANE FOAM)**

	Compressive		
	Density	Strength	Modulus
	(g/cc)	(MPa)	(MPa)
<b>Solid</b>	0.27	6.0	155
<b>Cellular</b>	0.32	5.4	137

**Note:** Material property data based on ASTM D-1621.

A)

B)



**Figure 3.2 Artificial tibia model. A) Material properties, B) Model [22]**

The actuators were connected to the bone using M6 screws drilled into the bone. The marker clusters were those used in the MUST study and positioned in specific anatomical locations on the tibia that were applicable to this study.

To fix the specimen during tests, the tibia was mounted to a metal plate disc using a M12 screw. Due to the placement of this screw, when forces were applied the specimen started cracking along the screw hole generating an undesirable mechanical behaviour and increasing the risk of total mechanical failure. A custom made bottom mold in aluminium was manufactured, and the specimen was fixed to it using epoxy resin.

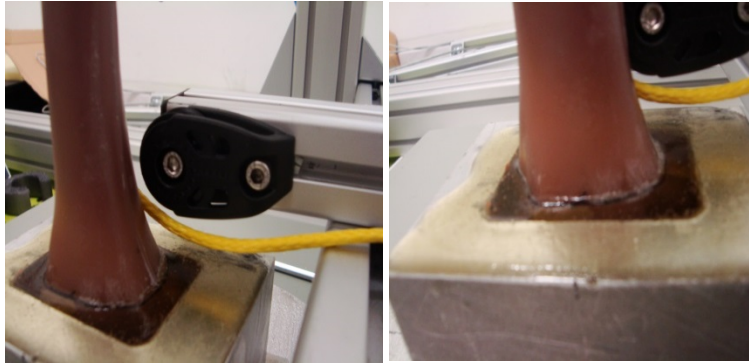


**Figure 3.3 Bottom fixation. Bottom mold attachment of the specimen**

At the top of the tibia four screws were attached through a small metal plate, this was used to mount the plate that holds the machine weights for the bodyweight force application. Because the small metal plate was flat and the tibial plateaus are irregularly shaped, the weight wasn't uniformly distributed therefore not according to the biological model. For this the metal plate was shaped using a CNC drilling machine to match the specimen geometry and ensure regular force application and was then fixed using screws.



**Figure 3.4 New specimen top attachment. The plate was drilled in order to match the geometry of the tibia specimen**

- Force redirection system

Considering that it is not feasible to mount actuators in a way that the desired force is applied with respect to the normal angle as muscles have during contraction, a redirection system was constructed to guide ropes from the specimen attachments to the actuators in the correct directions.

The first system used metal beams and hooks to redirect the ropes to the actuators. This system was proven incorrect due to the high forces applied through the hooks, deforming them along the screw attachments of the hook to the metal beam

Other redirection alternatives were tested but the conclusion reached was that using pulleys is the best option for redirection of the ropes. Pulleys are specially manufactured to reduce the force-loss effect due to friction, although it still might be present, it should be kept to a minimum in order to improve force control performance. The ropes chosen for this task are high-load sailing ropes; their material is special for handling high forces with a low elongation.

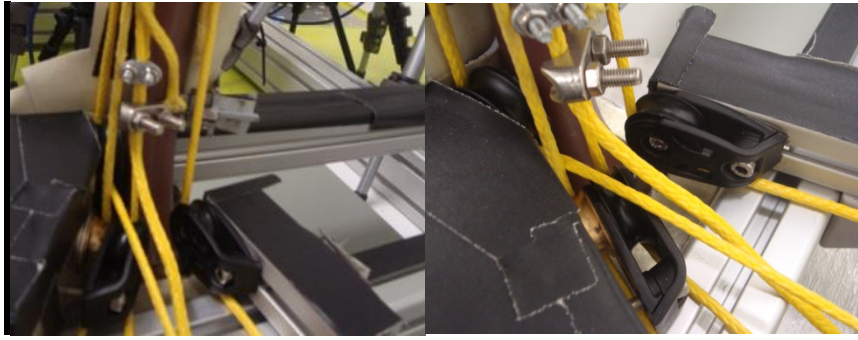


**Figure 3.5 New redirection system. Pulley wheels and special high-load pulleys were employed to construct the force redirection mechanism**

It was observed that still by employing high load pulleys a force loss due to redirection was present. For this a test to understand and address this loss was made. The results will be explained in the following chapter.

- Load cells mounting

The force sensors are load cells with internal strain gages whose deformation gives information regarding the amount of tension/compression applied. A quick setup was made at the beginning in order to mount the load cell and let the actuator pull from one sensor end and attach the redirection rope to the main sensor structure.

In order to have a stable mechanical arrangement, special flanges provided by the manufacturer were adapted to the sensors to allow compression/tension readings in one end only. The screws for attaching the base to the sensors were fixed with a moment of 6 N-m applied by a special torque wrench. As the flange was heavy, if left hanging it could introduce force reading variations. The base was attached to the piston rod by custom-made adapters. Because the force readings changed when the sensor was fixed to its flange, the force deviation was investigated as will be shown in the following chapter.

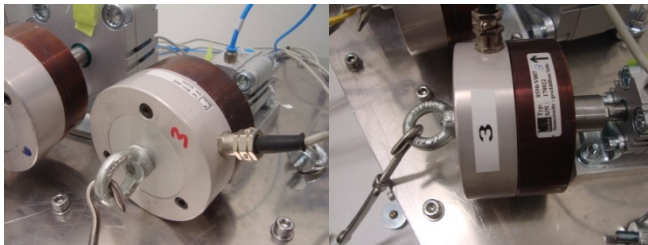


**Figure 3.6 New load cell mountings. Metal flanges mounted on the force sensors**

- Pressure control system

As stated at the beginning of the chapter, the latter reconstruction tasks were performed by the other people involved in the project. The work of the author regarding the AMBR started with the rearrangement of the pneumatic control system. The pneumatic setup controlling the air pressure fed to the actuators was mounted on an aluminium plate on the table where the user monitors the test. This is a risky setup due to the closeness of opening/closing valves and compressed air released near the user. To avoid disturbances to the operator the components were mounted on two different plates. One containing all control and configuration valves collocated next to the rig, and the other on the control table for user operation, i.e. setting up the main pressure system and the emergency stop valve.

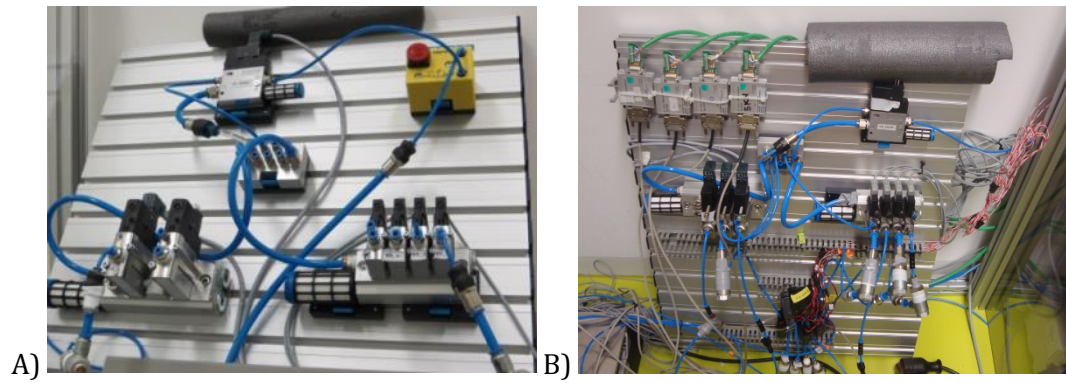


**Figure 3.7 Pneumatic configuration. A) Previous arrangement of pneumatic components. All the control valves were next to the user causing disturbances and exposure to potential risk. B) New arrangement of components. Only the main valve and emergency stop are next to the user**

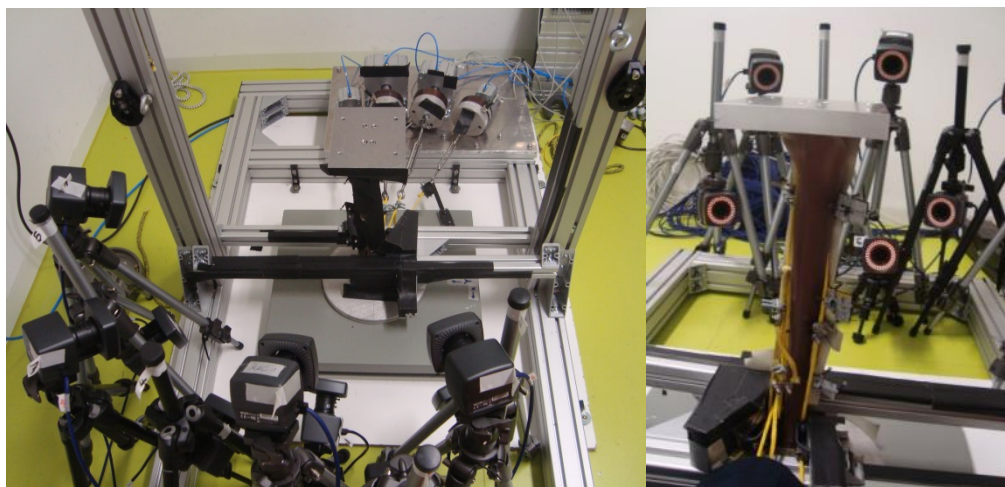


**Figure 3.8 AMBR final setup after redesign and reconstruction**



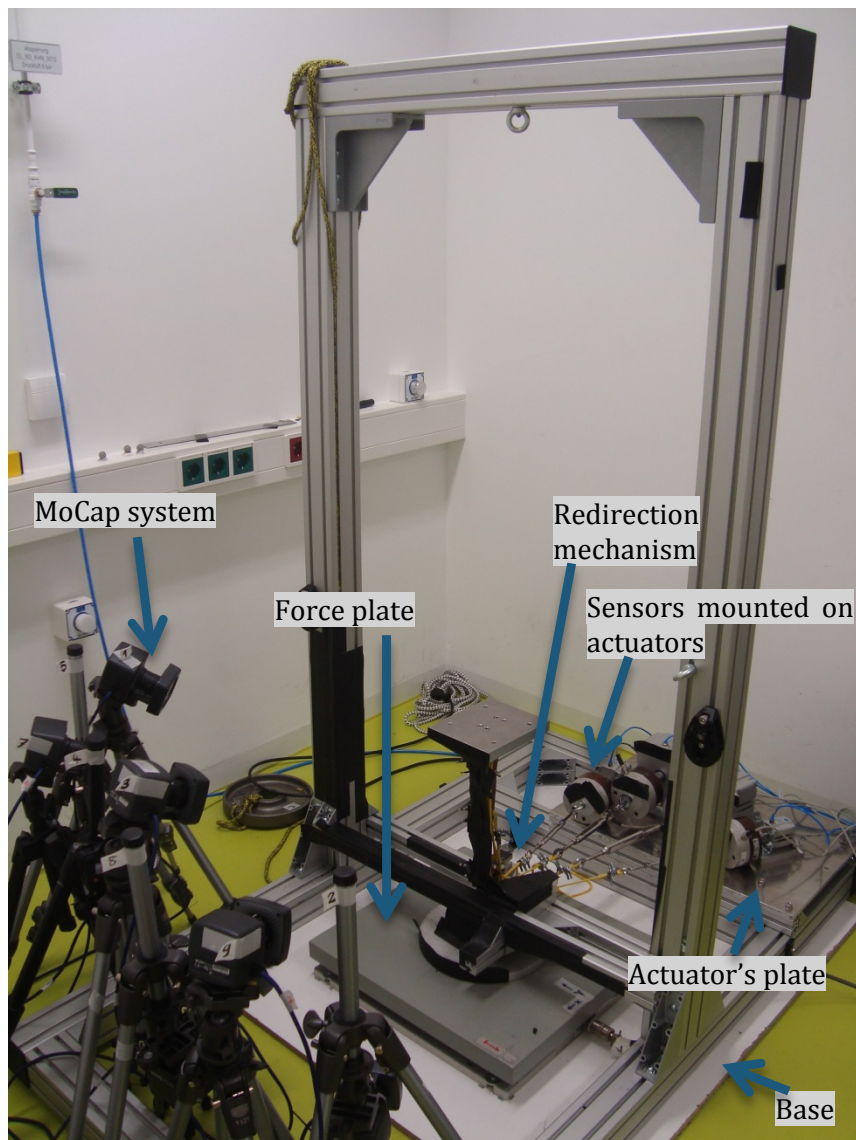


**Figure 3.9 Final AMBR configuration of main elements**

## 3.2. Control system

As an important part for operating the test rack, a control system was designed, built and tested. The main objective of this system is to enable the operator to manage the general operation of the rack, the forces applied within certain muscles as well as to obtain status information regarding the current operation during the test procedures.

The general requisites for the control system were the following:

- Activate/ deactivate the muscle actuators, either simultaneously by user selection or one at a time.
- Define the force application parameters: magnitude, control window, initial load cell error.
- Obtain and process analogue data from the load cells and present it as the real force applied by the actuator.
- Manage the air release from the actuators.
- Implement an emergency button to deactivate all outputs when hazardous conditions appear.

- Show information about the status of the actuators as well as the real force applied.

For a better understanding on how this systems works and the steps involved in translating user parameters into specific actions of the test rack, the hardware and software design required for this task will be explained.

### 3.2.1. Main concept

To explain the main idea behind the control system we might recall the function on a simple temperature control system like a thermostat. When the temperature sensor detects a difference between the real and desired temperature the heater turns on and off accordingly.

The idea behind the implemented control system works in a very similar way. The control was designed for the installation of a pair of valves regulating air pressure (force). By determining a set point such as desired force and a regulation window, the control activates and deactivates a couple of valves when the pressure magnitude is outside the boundaries of the regulation window.

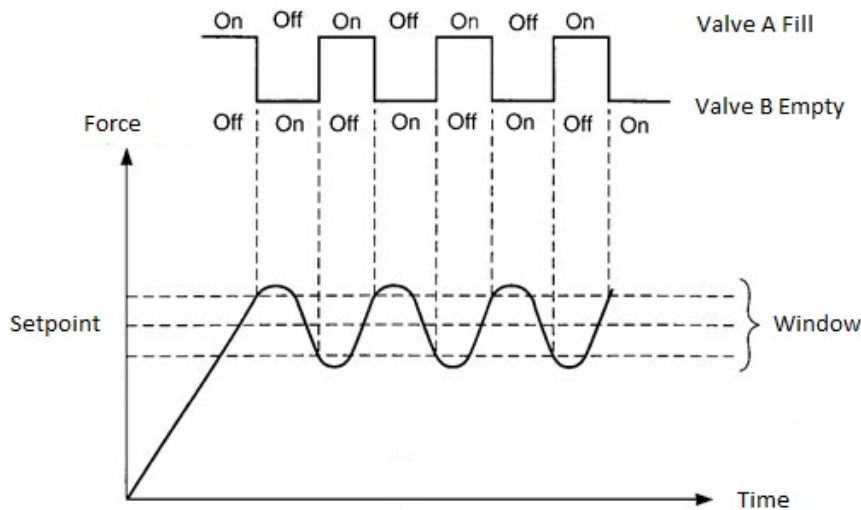


**Figure 3.10 ON/OFF control system for managing force (pressure) in pneumatic actuators**

One valve fills the actuator with compressed air and the other empties it, maintaining the force applied within the user specified window. Keeping this ON/OFF control in mind, the hardware and software will be implemented accordingly.

As it will be explained in detail in the following section, a prefilling phase was implemented in order to improve force application, regarding the speed of the muscles; currently the main objective is to simulate static loadings whereas the filling phase is merely for testing different options that in the future might be applied to simulate dynamic conditions in the lower leg.

### 3.2.2. Pneumatic Hardware

Recalling the advantages of implementing pneumatic actuators, Festo cylinders were chosen according to the force requirements for the muscles implemented on the rack. The product code of the model works by enumerating its characteristics such as: model - piston diameter in mm – stroke in mm – male thread piston rod (A-P-A)/ female thread (P-A).

The following table shows the muscles, force magnitudes and cylinders chosen for their application.

Muscle	Approximate maximum force	Actuator chosen and force capacity at 6 bar	Label
Soleus	2.8~3.1 KN	AEVUZ-100-10-A-P-A, 4222N	Actuator A
Tibialis posterior	1270~1600 N	AEVUZ-80-10-A-P-A, 2733N	Actuator B
Tibialis anterior	600~900 N	AEVUZ-50-10-A-P-A, 999N	Actuator C
Flexor digitorum longus	~310 N	AEVUZ-32-10-A-P-A, 382N	Actuator D

**Table 3.1 Actuators employed to simulate lower leg muscles**

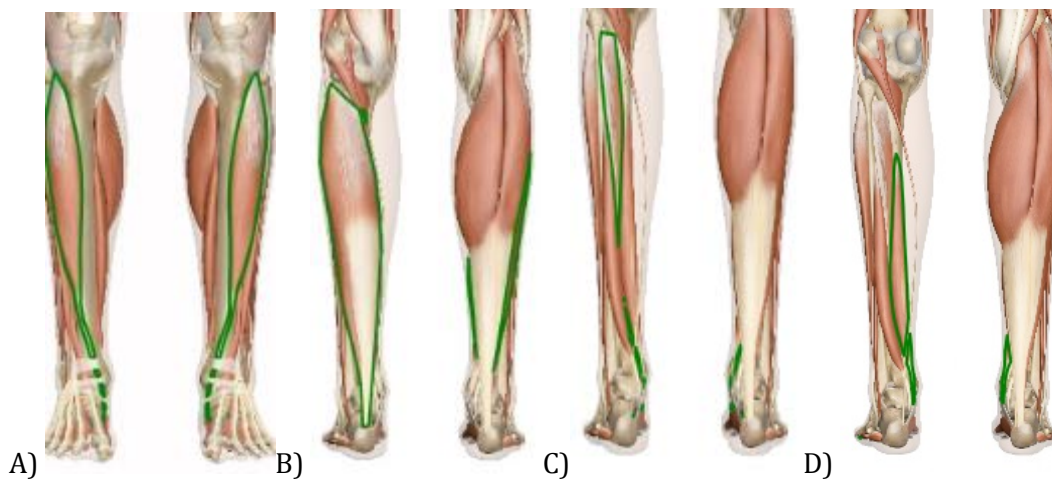


**Figure 3.11 Muscles simulated by actuators. A) Tibialis anterior, B) Soleus, C) Tibialis posterior, D) Flexor digitorum longus [23]**

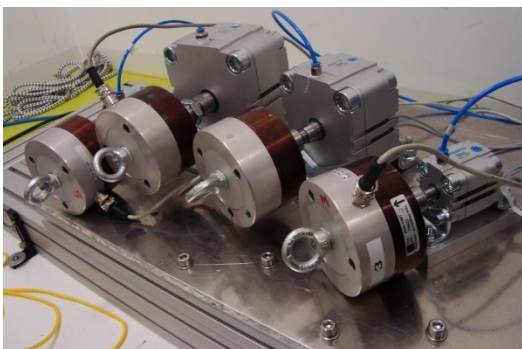


**Figure 3.12 Actuators mounted on the metal plate. The actuators are already aligned in the correct angles for force application**

By selecting pneumatic cylinders, the hardware to control them has to be chosen accordingly. Using the Festo actuator engineering online application the manufacturer suggests valves to activate/deactivate the input of compressed air. Another reason for valves is to manage flow speed on the actuator either for enhancing control actions and potentially in the future to experiment with the actuator contraction speed.

The basic configuration for controlling the actuator force application is the following:



**Figure 3.13 Actuator control configuration**



The following circuit shows the physical configuration for managing the actuators:

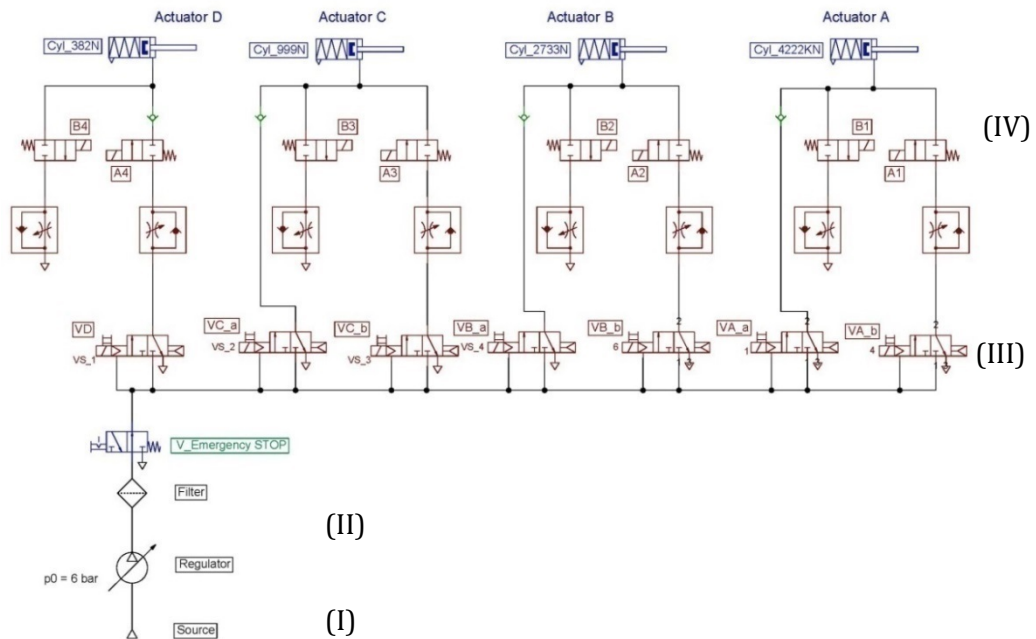


**Figure 3.14 General circuit for actuation control**

I. First we have the main source of compressed air, working at a maximum of 6 bars

II. Then a filter regulator was set to remove dust, moisture and other impurities present on the air as well as to set the pressure level fed to the circuit.

III: The first point of control is the main valves controlling each phase of the actuators filling process. For actuators A, B and C we have 2 valves, one for a prefilling phase ( $V_{x,a}$ ) and the other for the control phase ( $V_{x,b}$ ), for actuator D only the latter is implemented due to its small force capacity. For example, for actuator A the prefilling valve is  $VA_a$  and the control phase valve is  $VA_b$ .

The overall circuit for each actuator is set as follows:

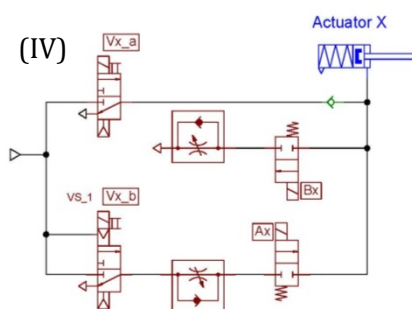


**Figure 3.15 Detailed circuit for individual actuator activation**

IV. The next control phase is the ON/OFF mechanism. For each actuator a valve A is set to fill and valve B to release the compressed air. Each window ON/OFF valve is coupled with a flow control valve that regulates the flow of compressed air supplied to and released from the actuator. This enhances the control regulation itself. Because of the speed of the valves a slower flow allows the system to manage the pressure to remain within the window with no major overshoots that might lead to an unstable oscillatory behaviour. It is important to note that depending on the force applied, the opening level of this flow control valves changes and has to be tuned manually each

time a new force is applied. The labels of the control valves (A1, B1...A4, B4), correspond to the actuators A to D.

When the user decides that the force achieved is satisfactory, one requirement for maintaining the force is to deactivate the actuator valves. Due to the hardware configuration the air is not released, maintaining the pressure as well as the force exerted by the muscle on the specimen.

A non-return valve is implemented on each actuator so the compressed air won't be released unless the user activates the release air function in the control. Nevertheless force and pressure losses are present due to small leaks, and the behaviour of mechanical elements, such as rope slacking due to high tensional forces.

For sensing of applied forces by the actuators, load cells were attached to the actuators piston rods. For the four cylinders it required three load cells (8531, Burster). The measuring range is 0 - 2000N and for one 0 - 5000N. These are made of high-strength aluminium and consist of foil strain gauges. As the sensor has terminals on both sides for measuring compression/ tension a special flange was mounted so the actual tension applied can be read. Coupled with the sensor there is a factory calibrated amplifier of the model 9235. This amplifier is operated at voltages between 15V and 30V. The measurement signals of the sensor ranging between 0 - 10 mV for bridge-connected strain gauges, are amplified to analogue 0 - 10 V. Compression is expressed in positive volts and tension in negative volts.

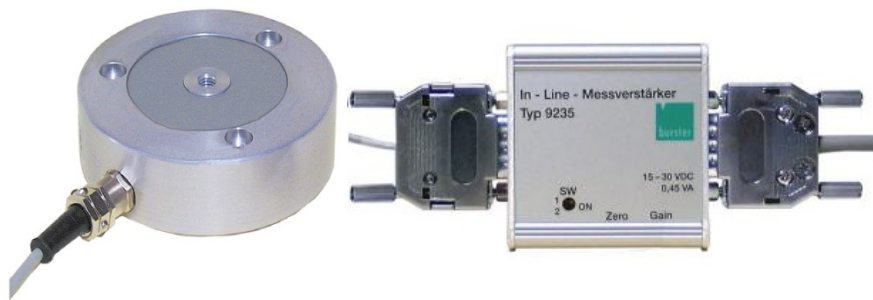


**Figure 3.16 Sensing element. Load cells model 8531 and In-Line amplifier model 9235**

The electronic circuits that show the control of the valve's solenoids will be explained on the next section of the control software.

### 3.2.3. Software

The design and implementation of the software is oriented to translate the user instructions into the operation of the artificial muscles. The computer interface for the user was developed in LabVIEW 2012 SP1, as it is an easy tool for mechatronic applications and there is already plenty of hardware available on the market for control applications either from National Instruments or other manufacturers.

Because a system capable of handling electric and pneumatic components is needed, it was decided to implement an EasyPort USB from Festo. The EasyPort is a process interface used for the bidirectional transmission of process signals between an actual control process and a PC [24]. The advantages of this interface are the low-voltage technology (24V DC) and the control program for the process in question can be written in a variety of languages. For our purpose it already included some examples implemented in LabVIEW. Finally being from the same manufacturer as the previous implemented hardware the wiring and general construction is easier and more intuitive.

The general characteristics of the EasyPort that are important for the design of the mechatronic system are the following:

EasyPort USB D16A process interface
Operating voltage: 24 V DC $\pm 10\%$
Power consumption: 3 VA
Number of outputs: 16 digital: 24 V DC, 2 analogue: 0...10 V DC or 10...+10 V DC, 12 bit resolution
Number of inputs 16 digital: 24 V DC, 4 analogue: 0...10 V DC or 10...+10 V DC, 12 bit resolution
Digital input switching threshold: 12 V DC
Digital input hysteresis: 3 V
Filter: 5 ms
Communication interfaces: RS 232, electrically isolated, USB 2.0, electrically isolated

**Table 3.2 EasyPort characteristics [24]**

The EasyPort hardware ports are labelled Port 1 and Port 2 each with 8 digital inputs/outputs and Port 3 has four analogue inputs.

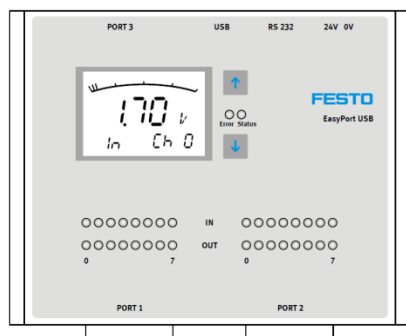


**Figure 3.17 Physical configuration of Festo EasyPort**

The control concept of the program written in LabVIEW will be explained in Figure 3.18. For the purposes of the application, the Control Design & Simulation package was used.

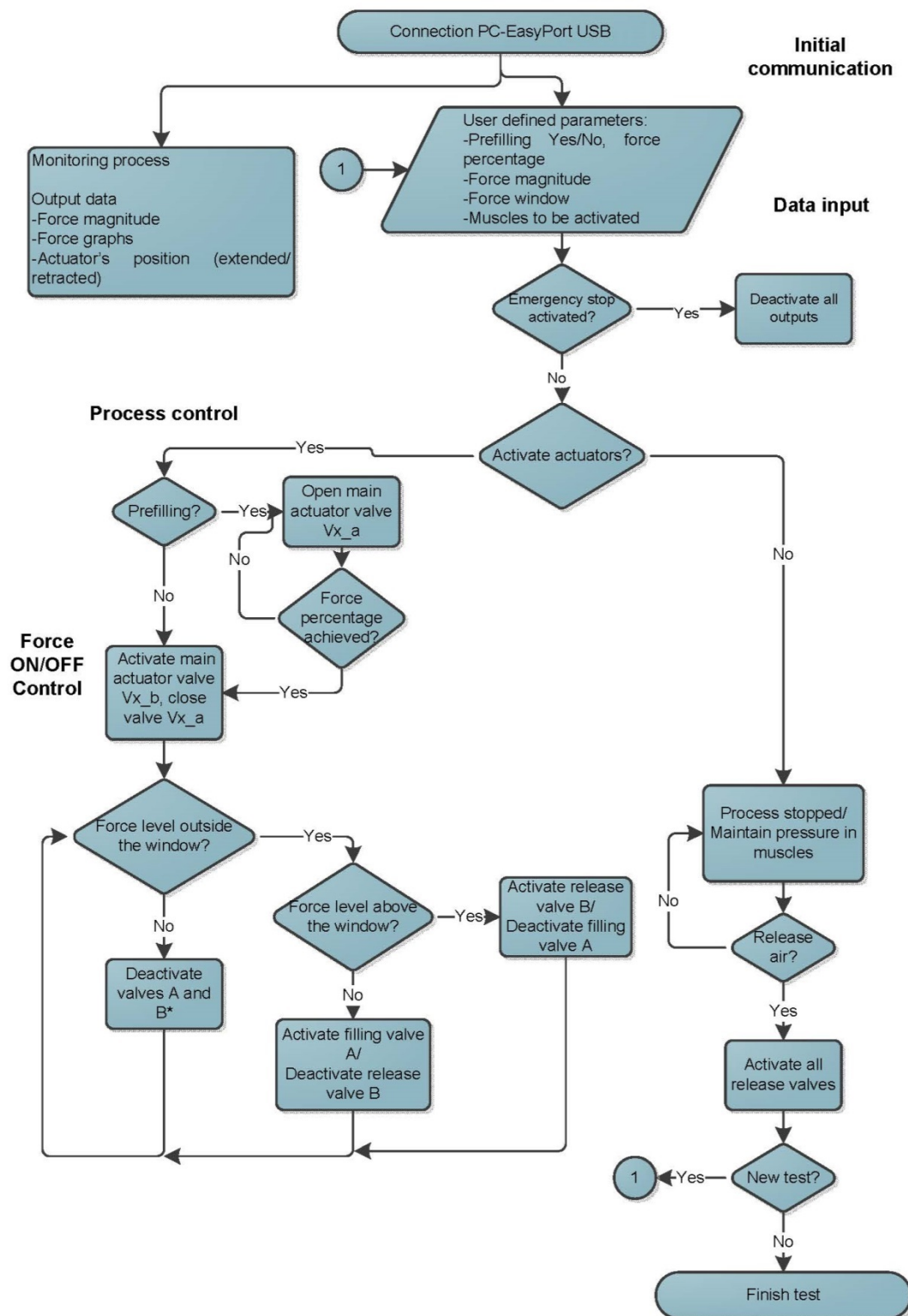


**Figure 3.18 Flow chart showing the main logic applied in the control software**

The flow chart shows the steps necessary to perform biomechanical tests in the rig. Three phases are necessary: Initial communication, data input and process control. The full control panel and program diagram can be found in the appendices.

The Initial communication phase starts when the program in LabVIEW is executed; the software checks the USB ports for an EasyPort module. Once the communication is established, the main program cycle starts running.

During the execution of the program, independently of the actuator activation and control process present at the moment, a monitoring process takes place at all times. The monitoring process is in charge of reading the system inputs and shows the user information that might be useful for decision making.

Digital inputs tell the state of the position sensors collocated on each cylinder that inform if it is extended or retracted. The analogue inputs are voltage levels coming from the force sensors. When the hardware receives the signal the software converts the voltage amplitude into Newtons using the custom made Analogue\_to\_newtons VI. Each analogue input has its own VI. During the conversion of Volts to Newtons, a multiplication factor of two was added to generate the real force value because it was observed that the value obtained was the half of the real reading.

As the signal for tensional force is in negative volts, it was converted into positive values for monitoring purposes as it will not be used to measure compressive forces. The force level for each sensor is show in graphs and in output text fields.

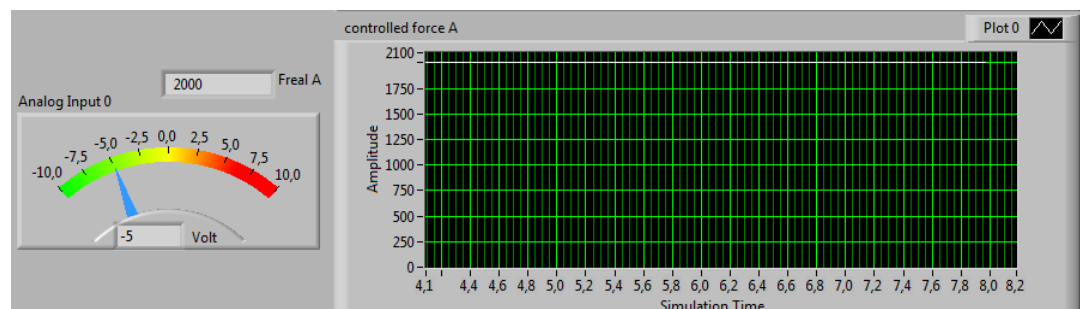


**Figure 3.19 Front panel displaying graphically force level as well as current voltage**

The next step is the data input. The user can define which muscles to activate and if they will be activated individually or simultaneously.

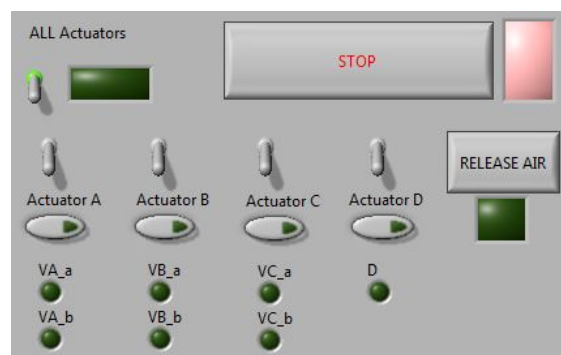


**Figure 3.20 Front panel for selecting and activating actuators**

The user can decide to apply a prefilling phase. This phase allows full pressure filling in an actuator, for example, for actuator A the main valve VA\_a is activated, pressurizing the cylinder with no flow and pressure restrictions, allowing a faster force raise. The prefilling can be applied until a percentage of the force defined by the user is achieved. If the user decides to not to implement prefilling the percentage input field can be set to zero.

The other parameters to be defined in the data input step is the desired force magnitude to be applied by the actuator and the force window around this force for control purposes. Depending on the actuator and flow rate, a broader or narrower window allows the system to be more precise and less oscillatory. Generally this parameter is set to a few Newtons. Another available input is the initial error; this is present when the readings of the load cells in unloaded state are not zero. This error

will be set as initial zero, so the force achieved by the control already takes into account this deviation.

Actuator	Fdesired	Window F	Init err
A	3200	10	0
B	2000	6	0
C	700	4	5
D	150	6	0

**Figure 3.21 Front panel for force settings**

Once the user inputs the data necessary to perform the test and activates the actuators, the process control step is performed. The first part checks for prefilling parameters, if a prefilling percentage was defined then the corresponding action is applied. Once the prefilling percentage is achieved or if it was left on zero, the Force ON/OFF control starts operating. To disable the prefilling valve VA\_a is deactivated and valve VA\_b is activated (in the case of actuator A, for example).

The valves implemented for switching between the prefilling and control phases were standard Festo solenoid valves using models CPE18 M1H-3GLS-1/4 for actuators A and B, CPE14 M1H-3GLS-1/8 for actuators C and D. The criteria for choosing those valves were based on the online engineering design tool from Festo.

This is the step in which the real control management is executed; once the condition is met the software calculates within the ON\_OFF controller VI if the force read is within the force window set by the user and turns the control valves ON or OFF. If the force is under the lower value of the window it turns on the filling valve A and deactivates release valve B, if the value is above the upper limit of the window then it turns on valve B and deactivates valve A. If the force is within the force window then both valves are deactivated. Because of the relatively slow response of the valves the condition of both valves being closed within the window was never met, but the influence of the width of the window could be seen in the oscillatory behaviour of the control process when the read force was close to the desired force. For the control valves it was used 2-way valves V1A02 from Isonic with a response time of ten milliseconds.

The control valves had a slow response time, and in order to maintain a certain force for a longer period, once the actuators activation button was pushed to “turn them off”, it closed all valves and maintained the pressure. The only way to exit the control loop is by deactivating the actuators.

When the test is over or the user desires to stop applying force, a release button on the front panel allows depressurizing all actuators and return to the initial position.

Another important point is the security employed in the software. At the front of the control panel an emergency stop button is located so the user can press it and immediately deactivate all outputs no matter what setting is currently running. This will be implemented whenever the user predicts an imminent risk during testing. Once the risk is assessed the user has the option of resuming the operation by pushing the button once again.



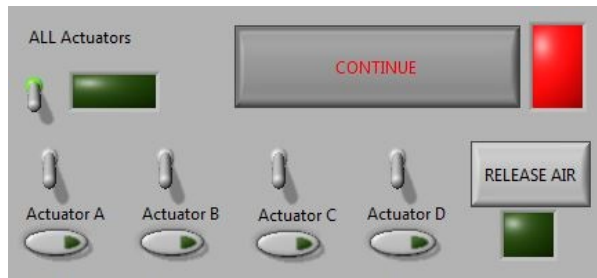


**Figure 3.22 Stop button activated. When the button is pushed it remains in that state and deactivates all outputs until user pushes the button again to continue with testing**

### 3.3. Control biomimetics of muscle behaviour

Reminding muscle behaviour explained at the beginning of this work, muscle contraction is applied in a very specific manner. For some investigational purposes this might be of interest, especially for dynamic biomechanical testing where the force application within time varies in a certain way, influencing the speed and position of a joint and how the bone deforms.

Recalling Figure 2.11, force application varies within a certain period of time and is inherent to muscle. For this purpose the focus is on the isometric contractions, and once the force is achieved it is maintained and then released. Also for now, the focus is on static conditions of mechanical loading of the tibia, therefore the goal is to provide a control tool for future applications based on a PID system. The hardware implementation in this case was the same as that used for the ON/OFF control except without the prefilling phase. This is due to the fact that the PID control used for this has to handle error differences and changes within time.

The PID control is useful in control applications where a specific output behavior over time is required. By modifying the gains of each part the curve behavior due to force and error changes over time, this can be managed and adjusted until a specific behaviour is achieved.

Recalling the LabVIEW flow chart of the ON/OFF control system in Figure 3.18, the program for the PID control implements the same elements with small differences. One is the elimination of the pre-filling phase and the other is the change in logic regarding how the control valves will be managed according to the output error.

In Figure 3.23, the PID logic can be seen. First, the desired force is converted into a voltage and compared to the voltage level read by the corresponding load cell analog input. If a difference (error) is obtained then the next phase in which Proportional, Integrative and Derivative actions are applied with the gains set by the user. The PID control panel and program diagram can be found in the appendices.

The manipulated signal obtained after this process has to be translated into ON/OFF commands for the control valves. One way to do this is to calculate the derivate of the signal and use the sign of the slope for the control. If the slope is positive it activated the filling valve A/ deactivated release valve B and if it is negative it activated release valve B/deactivated filling valve A. This is done in a very similar way as the ON/OFF control system but in this case the control logic is carried out by a PID system and of course a force window or deadband is not present.

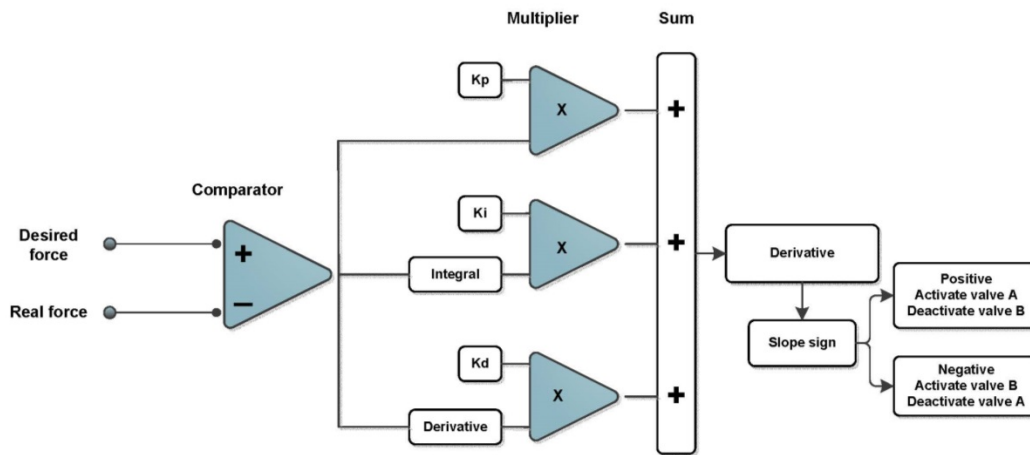


**Figure 3.23 PID control diagram**

To obtain the correct PID-gains for the setup, a test was carried out by using a specific PID tuning technique where a known algorithm for tuning can be followed in order to obtain a biomimetic muscle contraction behavior [25].

The purpose of this control is to mimic muscular contraction conditions. A test was performed with only one actuator for demonstration purposes. In this case actuator C with a set target force (600N). It has to be kept in mind that due to the slow operation of the control valves the curve obtained might resemble in shape the isometric contraction although it could be only achieved within a period of a few seconds instead of milliseconds.

The first step was to find an appropriate proportional gain. It is recommended by the tuning algorithm to set it to a low value like 1. As the response obtained was highly oscillatory, the Proportional gain was set to 0.1.

Then the Integrative gain was obtained. For this the gain was incremented geometrically and during the iterations the resultant curves were recorded.

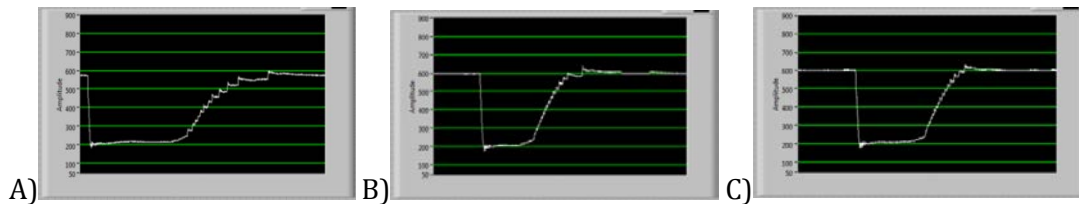


**Figure 3.24 Tuning of integral gains. Curves with different Integrative gains recorded. A) 2, B) 64, C) 128**

Considering various curves involving muscular contraction and relaxation for this case the I-gain chosen was 128 because of its stable and smooth behavior in achieving the desired 600N force.

Finally for this test the Derivative gain was implemented in the same way as the Integral gain.

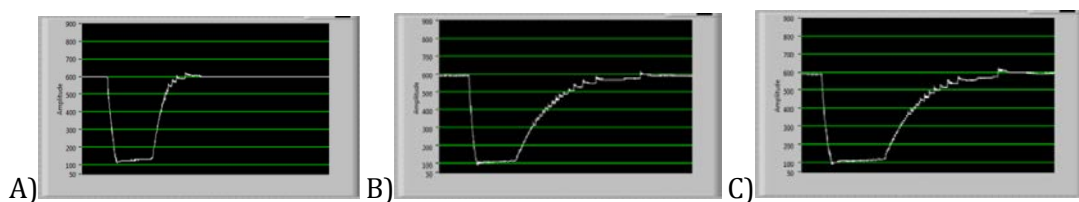


**Figure 3.25 Tuning of derivative gains. A) 2, B) 4, C) 16**



Looking at the curves obtained by incrementing geometrically the D-gain, a gain with a desired behaviour might be chosen. In this case a gain of 4 might be adequate for mimicking muscle behaviour contraction by applying a force of 600N, making the final PID configuration 0.1/128/4.

It should be remembered that for each actuator and for a specific force, the PID tuning must be performed in order to have clear biomimetic behaviour. As the practical implementation of this control system is not within the boundaries of this thesis, a test for the range of forces for all actuators wasn't performed.

### 3.4. Motion capturing system

A crucial part of the test rack is its ability to obtain information regarding the deformation during different force applications. The most important part of the test is to be able to record the specimen bending data and compare it with the computer model data for its verification.

For this purpose a motion capture system (Vicon Motion Systems [4]) similar to that used in the MUST study will be implemented. Motion capture can be defined as the recording of movement by a set of cameras, and subsequently reproduce the data digitally gathering information regarding position, speed, etc.

The system applied was a 9 camera array of the Bonita B3 model [4]. Recalling the preliminary study performed by [1], the cameras were set in a near umbrella configuration placing the specimen less than 90cm away. The reasons are that the range of motion of the specimen can be recorded, and the closer the cameras are to the subject in question the better the resolution.

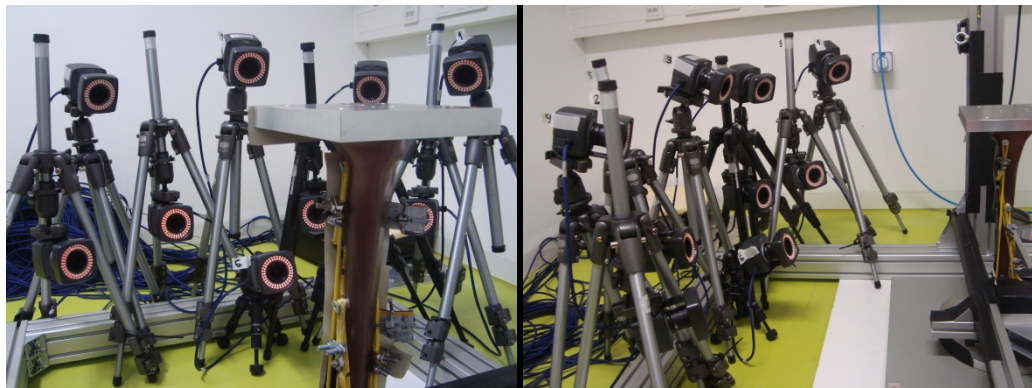


**Figure 3.26 Physical configuration of the MoCap system**

The software used was Vicon Nexus. This program is designed for capturing marker information during biomechanical tests in subjects, interpreting and translating data into physiological parameters..

A set of steps has to be followed before starting capturing motion data. First the camera views need to be fixed. The cameras should be able to see all of the retro-reflective markers and differentiate them from other markers and objects. This is achieved by adjusting strobe and threshold individually for each camera. Strobe intensity controls the brightness of the LED array around the camera lense. The threshold determines the pixels to be considered for centroid fittings of markers.

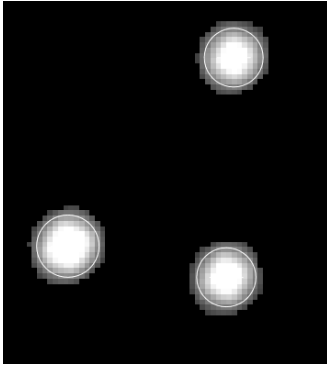


**Figure 3.27 Example of optimal strobe intensity and threshold view on the markers**

Once the cameras have an optimal view of the markers, sources of disturbances should be eliminated. The AMBR is built with metal beams which easily reflect the light in the room and generate unwanted bright shadows and so-called *phantom markers*. This problem was resolved by manually painting the reflective beams with a black marker or covering them with a non-reflective black material.

Once the cameras are calibrated these are arranged in the 3D virtual workspace with one of them defined as the coordinate origin. To define the origin of the coordinate system in a desired position the wand can be set in a certain spot of the rack (close to the specimen) and use the “Set volume origin” function of the Nexus software.

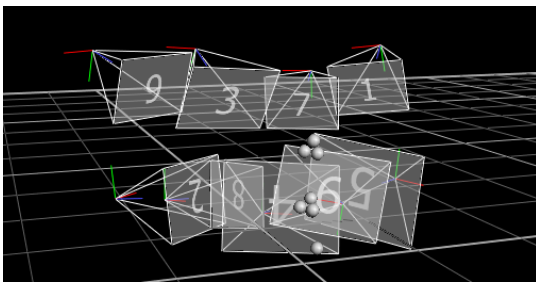


**Figure 3.28 Position of the cameras in the virtual workspace**

In figure 3.28 the markers mounted in the specimen can be seen. For this example two marker clusters and one single marker were attached to the specimen. The camera positions in the 3D space are shown so the user can understand the position of the cameras in the defined coordinate system.

When all previous steps are completed, the MoCap setup is fully operational and ready to record data of the marker clusters attached to the specimen.

### 3.5. Reaction forces sensor preparation

One important parameter to be known is the magnitude of the ground reaction forces. Other biomechanical studies in this field have gathered information on these reaction forces and moments during certain positions such as gait, running, jumping, etc. As the main purpose of the Biomechanical Test Rack is to simulate those positions and more, it is appropriate to setup a device capable of collecting that information.

The option chosen for this was to install a force plate at the base of the rack that will be under the specimen during testing. From the previous rack the mechanical design showed that installing the specimen above the force plate with Gecko tape was fixation enough for the testing purposes. Gecko tape employs a principle similar to that found

on gecko's feet. It has a high coefficient of kinetic friction, eliminating the need of any mechanical fixation like screws or welding.

The force plate used was an AMTI model OR6-6-2000 [21]. It is designed to be used in research and clinical studies looking at balance, gait and sports performance. The plate is used with a Gen5 signal conditioner that uses a six-channel strain gage amplifier.



**Figure 3.29 Physical configuration for force plate data capturing using the Gen 5 amplifier [21]**

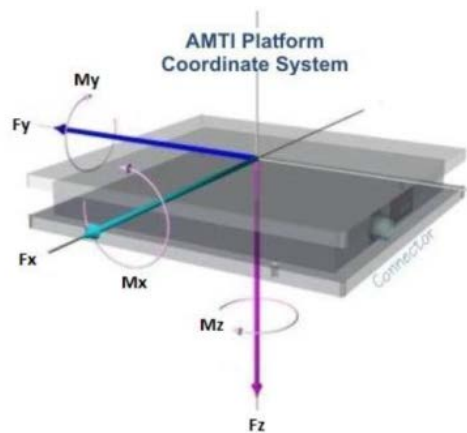


**Figure 3.30 Force plate coordinate system**

The coordinates of the origin for our specific force plate are  $X_o=0.8\text{mm}$ ,  $Y_o=-1.0\text{mm}$  and  $Z_o=-39.6\text{mm}$ . Using the configuration window the initial settings for the tests purposes are defined, such as Acquisition Rate and the units of the Digital Outputs. For the test purposes all forces ( $F_x$ ,  $F_y$ ,  $F_z$ ) and all moments ( $M_x$ ,  $M_y$ ,  $M_z$ ) will be recorded in Metric Units. The data rate will be defined during the test. The acquisition time also will be set depending on the test task in play.

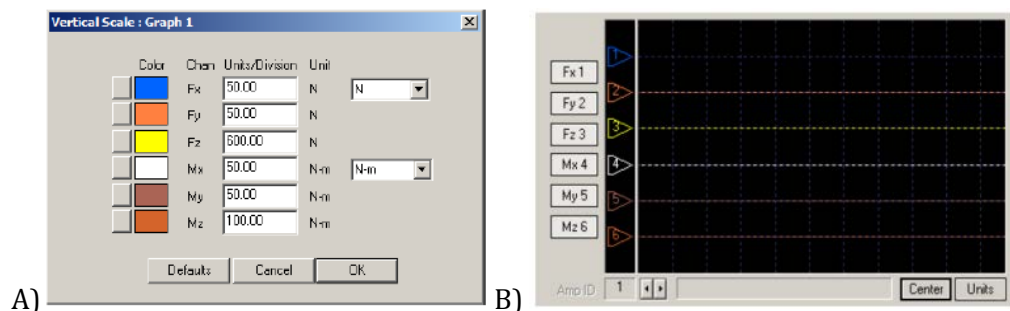


**Figure 3.31 Graph configuration. A) Force and moments units configuration. B) Graph showing the values of the three forces and three moments**

By implementing the aforementioned settings, the force plate is ready to operate and functional. In the following section a test for verifying accuracy and repeatability of the force plate is shown.



## 4. EVALUATION AND DISCUSSION

One of the main tasks of this work is to verify the functionality of the systems implemented in the rig. Special tests were performed for each main component of the rig functionality and the resulting data was recorded. Depending on the setup, analyses regarding accuracy, repeatability and reproducibility were made. Once the systems were validated individually, a final integration test was performed to verify the complete functionality of the rig during normal conditions of biomechanical testing. The efficacy of the systems and of the overall setup is discussed as well as their limitations.

### 4.1. Control system

In order to validate the performance of the control system a test was carried to obtain information regarding the accuracy and repeatability of the system. The physical configuration for testing was a series of hooks, fasteners and rope to connect the actuator with the mounted load cell to a hook mounted on a metal beam attached to the rack structure.

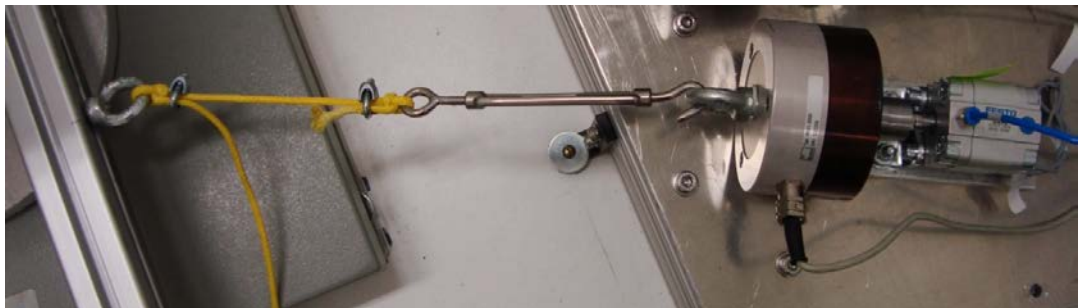


**Figure 4.1 Physical configuration for actuator control testing**

The test was made for each of the four actuators in the following way:

1. Different forces within the range of operation of the selected actuator were set on the control panel and maintained within a certain period of time at a frequency of 250Hz.
2. The load cell readings were exported and averaged over 250 data frames.
3. The different forces were applied and maintained five times.
4. The five different readings of each force were averaged and the standard deviation was calculated.

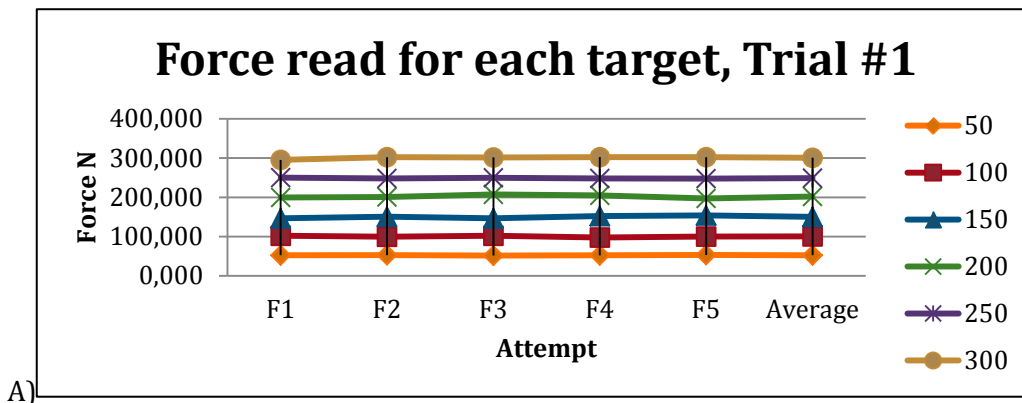
The first trial was made by incrementing the target forces in ascending order and in the second trial in a random order. For each desired force the opening level of the flow control valves had to be set in order to avoid high oscillations during the control action. The control window around the setpoint force was set depending on the actuator and desired force level. In general the windows were established in a range of 3 to 10 N.

In Table 4.1 an example of the force results for actuator D is shown. For each desired force the test was done five times. The average and standard deviation of the five repetitions were calculated. The last column shows the order in which the desired forces were implemented.

TRIAL #1									
Force desired	F1	F2	F3	F4	F5	Average	Standard Dev	Order	
50	52,599	52,895	51,848	52,451	53,284	52,615	0,534	1	
100	102,249	99,810	102,257	97,647	100,230	100,439	1,925	2	
150	146,788	150,823	146,764	152,402	154,211	150,198	3,346	3	
200	199,485	201,092	207,329	204,905	197,185	201,999	4,098	4	
250	250,419	248,104	249,956	248,291	247,715	248,897	1,207	5	
300	295,292	302,373	301,696	302,556	302,342	300,852	3,125	6	
TRIAL #2									
Force desired	F1	F2	F3	F4	F5	Average	Standard Dev	Order	
50	52,206	49,965	52,401	50,770	52,397	51,548	1,117	3	
100	99,892	99,588	99,966	100,837	99,394	99,935	0,555	2	
150	146,399	154,600	146,185	146,858	146,780	148,164	3,608	1	
200	198,827	196,703	198,469	195,427	201,278	198,141	2,228	4	
250	247,509	249,299	248,299	247,925	255,617	249,730	3,357	6	
300	300,895	298,953	302,338	299,658	303,093	300,987	1,744	5	

**Table 4.1 Forces applied and results on Actuator D. Cylinder of 32mm diameter. Maximum force of 382N at 6 bar. Mounted to load cell #3**

Graphs showing the average read forces in Trial #1 and #2 are displayed in Figure 4.2.



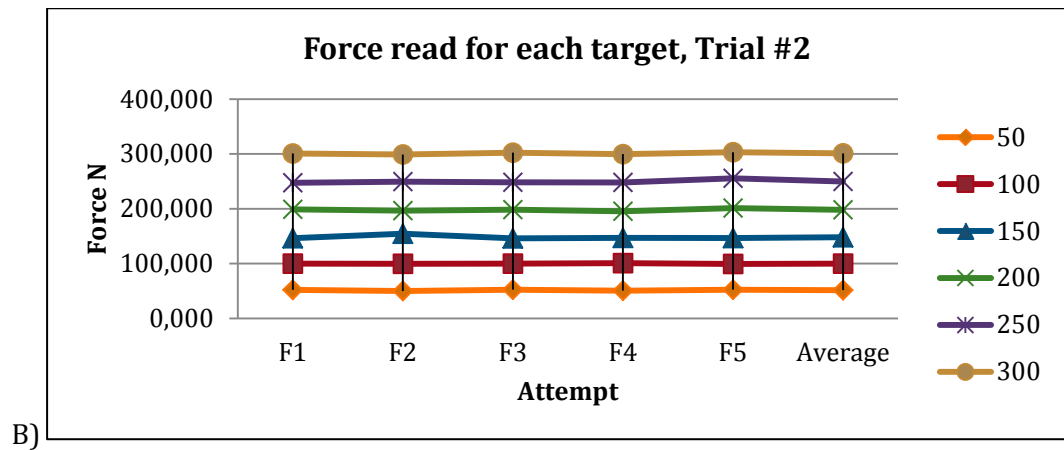


**Figure 4.2 Forces read on each trial for actuator D. A)Ascending order  
B) Random order**

The graphs and tables showing the force control results of all actuators can be consulted in the appendices.

#### • Discussion

To verify the capacity of the control system, a statistical analysis was performed. Using the Statgraphics Centurion XV statistical software; analyses on repeatability, reproducibility and accuracy were performed for the results on each actuator.

By using the SnapStat R&R of the calibrator, the five measurements on each trial were compared to each other for repeatability and the two trials were compared for reproducibility. The statistical method used was of Range and Average. The repeatability will tell if the force applied within each trial can be obtained again. The reproducibility will show if the system is capable of retrieving the same force even if the order of force application changes within trials.

Actuator	Repeatability within trials	Reproducibility between trials
A	0.354%	0.0%
B	1.07%	0.113%
C	1,028%	0.212%
D	2,444%	0.688%

**Table 4.2 Repeatability and reproducibility results for each actuator**

The repeatability and reproducibility percentage shows the estimation of the total error measurement, calculated by adding variances due to repeatability and reproducibility. The lower the error percentage the better the results are. Depending on the quality approach generally a percentage under 10% is usually acceptable. The percentages shown are lower than 3%, demonstrating the high capacity of the control system for repeatability and reproducibility. An interesting result showed that for actuator A a reproducibility error percentage of 0.0%, consequently for that specific actuator the influence in the change of force application between trials is null.

Subsequently an analysis of accuracy is performed. The different force measurements are compared to a reference number, in this case the desired force. The function employed in Statgraphics was Exactitude and linearity. This calculates the exactitude of a system over the average. The main calculation focuses on obtaining the bias of the system:

$$Bias = average - Real\ value \quad (Eq.2)$$



A process is said to be accurate if the bias is small. The resulting bias percentage is calculated by Equation 3.

$$\%Bias = |Bias|/(variation\ of\ the\ process) \text{ (Eq.3)}$$

Actuator	Bias percentage
A	1,165%
B	0.012%
C	0.013%
D	0.117%

**Table 4.3 Accuracy of the control system for each actuator. The analysis was done with a 95% confidence interval**

The bias percentage is low, being slightly higher for actuator A and up to certain extent for actuator D. It is possible that the bias percentage is higher for actuator D considering that the error difference with respect to the desired force (~5N) is high regarding the small range of force this actuator is capable of generating (382N). For actuator A the higher bias percentage might be a sign of the difficulty of applying high forces to a rigid object, introducing mechanical disturbances. In general this bias is acceptable for now, but further improvements should be made to refine the system and not to impede the deformation seen on the specimen due to inaccurate force application.

## 4.2. Motion capturing system

To validate the motion capturing system setup, a preliminary test was performed. The intention was to verify the accuracy and repeatability of the system. The method used employed a digital sliding calliper and two 5mm reflective markers attached to the top of the measuring tips.

The calliper was fixed using a vise mounted to an aluminium beam fixed to the main rig structure. Once the Vicon system was calibrated the calibration wand was positioned on the top of the vise to define the origin of the coordinate system. The calliper was aligned approximately parallel to the three coordinate axes. The opening of the measuring tips by 20, 30 and 40 mm was made in three different positions. The variations were intended to be along the three different coordinated axes but there was an unknown offset present.



**Figure 4.3 Configuration of motion capturing system test. A) Markers attached to the calliper measuring tips of the fixed jaw blades of the calliper at an initial span of 20mm B) Example showing the calliper mounted on the mechanical vise C) Example of coordinate system setup of the Vicon system using the calibration wand. The wand was positioned above the vise**





**Figure 4.4 Examples of the different offsets present on marker's mounting as well as marker imperfections**

One disadvantage of the test was that the position of the markers relative to the calliper is unknown. The reason is that the positioning of the markers on the calliper wasn't precise. There were many offsets present (deviation of the calliper position from the different axes, deviation of the position of the markers on the measuring tips such as tilting and varied heights). Therefore it wasn't possible to calculate the position variations by taking the position values directly. Nevertheless by using trigonometric and vector calculations the errors can be assessed in order to obtain corrected marker position data and calculate the accuracy and repeatability of the test.

The test was done by recording the different variations along the three different axes chosen. The calliper was opened to distances of 20, 30 and 40 mm approximately along the coordinated axes. For each opening distance the position data was recorded three times.

- Results

Keeping in mind the initial deviations of the setup from the established motion capturing coordinate system, the processing of the data obtained needs to be managed accordingly. For this a method for re-calculating data and compensate for the deviations present was devised. Consequently the general accuracy and repeatability of the Vicon system can be calculated.

As the distance between markers cannot be calculated simply because of the deviations present, a method was applied for verifying data within acceptable parameters. To do this, a two dimensional plane was chosen, for instance the XY plane, and the marker variations within that plane were seen by projecting a two dimensional vector component. By taking the two markers coordinates in three dimensions (XYZ) and calculate the vector from fixed marker A to moving marker B, the real distance between the markers in three dimensions can be seen. For assessing all variations within the same reference, and eliminating the Z variation on each variation step, a projected two-dimensional vector in XY was obtained from the original three-dimensional distance vector. When the distance variations were made approximately along the Z axis, the vector was projected in the XZ plane and the variation in the Y axis was eliminated.

The vectors and their respective distances were as follows: VD0 (20mm initial distance), VD1 (30mm), and VD2 (40mm). The angle between the three-dimensional vectors and the two-dimensional vectors was calculated as shown in Equation 4:

$$\alpha = \arccos \frac{VDx \text{ in } 2D}{VDx \text{ in } 3D} \quad (\text{Eq.4})$$

Then the corrected vector was calculated in order to minimize the error obtained from the vector projection on the two-dimensional plane.

$$VDx' = \frac{VDx}{\cos \alpha} \quad (\text{Eq. 5})$$

After calculating the corrected vectors, the differences between each marker in the calliper openings were calculated; VD0-VD1, VD1-VD2 and VD2-VD0 respectively.

The calculations were done three times with three pairs of vector readings, one for each distance (20, 30 and 40mm). The results show the average, standard deviation and variation coefficient  $Cv$  (standard deviation  $\sigma$  divided by average  $\mu$ )

$$Cv = \frac{\sigma}{\mu} \quad (\text{Eq. 6})$$

	Trial 1			Trial 2			Trial 3		
	VD1'-VD0'	VD2'-VD1'	VD2'-VD0'	VD1'-VD0'	VD2'-VD1'	VD2'-VD0'	VD1'-VD0'	VD2'-VD1'	VD2'-VD0'
Average	9,936	10,002	19,938	9,959	10,012	19,971	10,079	10,010	20,088
Standard deviation	0,062	0,018	0,059	0,065	0,021	0,066	1,614	0,024	1,616
Variation coefficient	0,006	0,002	0,003	0,007	0,002	0,003	0,160	0,002	0,080

**Table 4.4 Variations made approximately along X-axis in mm**

	Trial 1			Trial 2			Trial 3		
	VD1'-VD0'	VD2'-VD1'	VD2'-VD0'	VD1'-VD0'	VD2'-VD1'	VD2'-VD0'	VD1'-VD0'	VD2'-VD1'	VD2'-VD0'
Average	9,988	10,153	20,141	9,994	10,151	20,145	9,996	10,147	20,144
Standard deviation	0,016	0,025	0,019	0,016	0,021	0,019	0,016	0,022	0,018
Variation coefficient	0,002	0,002	0,001	0,002	0,002	0,001	0,002	0,002	0,001

**Table 4.5 Variations made approximately along Y-axis in mm**

	Trial 1			Trial 2			Trial 3		
	VD1'-VD0'	VD2'-VD1'	VD2'-VD0'	VD1'-VD0'	VD2'-VD1'	VD2'-VD0'	VD1'-VD0'	VD2'-VD1'	VD2'-VD0'
Average	10,024	9,981	20,005	10,028	9,979	20,007	10,029	9,981	20,010
Standard deviation	0,019	0,011	0,018	0,011	0,019	0,017	0,011	0,011	0,010
Variation coefficient	0,002	0,001	0,001	0,001	0,002	0,001	0,001	0,001	0,001

**Table 4.6 Variations made approximately along Z-axis in mm**

With one exception (trial 3, variation on X-axis), the variation coefficient percentage is low for each calculation of the vector difference, showing consistency in the data captured. Each average, standard deviation and variation coefficient calculation was done over time with 241 data frames (1 sec approximately), consistent with the 241.935Hz of the motion capturing system. It is important to mention that for each dataset, a Grubbs outlier test was performed for discarding data that was not useful [26]. The theory behind the presence of these outliers is in the quality of the reflective coating used on the markers was not ideal, generating data spikes during readings on each of the three position coordinates of the markers.

For testing the repeatability of the marker positions on each calliper spanse in every coordinate axis, a comparison calculation was made. For example, for the approximate variations made along the X-axis, three trials on the 20, 30, and 40mm openings were compared.

	Trial 1 vs Trial 2	Trial 2 vs Trial 3	Trial 1 vs Trial 3
VD1'-VD0'	-0,023	-0,119	0,142
VD2'-VD1'	-0,010	0,002	0,008
VD2'-VD0'	-0,033	-0,117	0,150

**Table 4.7 Comparison of variations made approximately along X-axis. Error difference in mm obtained by comparing both results**

	Trial 1 vs Trial 2	Trial 2 vs Trial 3	Trial 1 vs Trial 3
VD1'-VD0'	-0,005	-0,001	0,005
VD2'-VD1'	0,002	-0,002	0,000
VD2'-VD0'	-0,003	-0,002	0,005

**Table 4.8 Comparison of variations made approximately along Y-axis. Error difference obtained by comparing both results**

	Trial 1 vs Trial 2	Trial 2 vs Trial 3	Trial 1 vs Trial 3
VD1'-VD0'	-0,006	-0,002	0,008
VD2'-VD1'	0,003	0,003	-0,006
VD2'-VD0'	-0,003	0,001	0,002

**Table 4.9 Comparison of variations made approximately along Z-axis. Error difference obtained by comparing both results**

After calculating the differences between the measuring gauge, it is seen in the different axis variations that the repeatability of the system is adequate for the application. With the exception of the X-axis data, where the differences are 0.15mm or less, the differences for the other axes are 0.01mm or less. It is possible that the higher variations in the X-axis are present because the damaged areas of the markers were facing the cameras while performing the test in that particular orientation. Considering the standard deviations shown in Tables 4.4 to 4.6, the magnitudes are smaller than the differences calculated.

In order to obtain a specific repeatability percentage, a statistical analysis similar to the one performed on the control system was made. The test was designed to check the repeatability percentage within the three different variation measurements along the three coordinate axes. The results showed a Repeatability percentage of the system of 0.408627%, proving the high repeatability capacity of the MoCap system.

For accuracy of the entire MoCap system, a linearity and accuracy test was made and the result was a Bias percentage of 0.333%. This is a low value proving the high accuracy of the system for detecting small variations.

Considering the data shown from this preliminary test, the motion capturing system is suitable for detecting variations in markers in the three different coordinate axes with a high repeatability, verifying it to be appropriate for capturing specimen deformations on the rack mechanical setup.

### 4.3. Reaction forces sensor

A simple functionality test for the force plate was performed to verify how sensitive the system was in detecting weight and torque changes. If the plate sensors proved to be adequate, then it will be suitable for mounting to the AMBR. The test made was a simple comprobation of repeatability and accuracy, keeping in mind that the sensor is certified and calibrated by the manufacturer. The idea is to see if there are any unusual readings on the plate and ascertain if it is fit for testing.

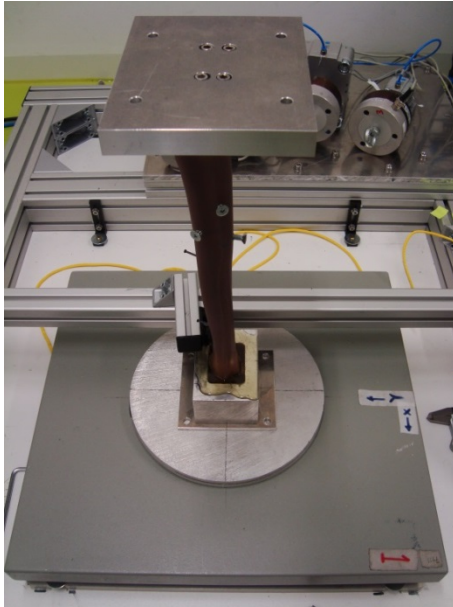


**Figure 4.5 Force plate loading with specimen. The specimen has attached top and bottom flanges**

After configuring the force plate and performing the zero-platform function, an initial test was done for further references. This was first done by mounting the tibia specimen with its base and custom made tope flange only in an arbitrary position on top of the force plate. The readings were captured in a period of 10 seconds with a 300 frames per second frequency. The average and standard deviation were calculated within those 300 frames. The initial readings obtained from the force plates were as follows.

Reaction	Fx N	Fy N	Fz N	Mx N-m	My N-m	Mz N-m
Average	1,44	-3,07	47,87	-0,15	0,27	0,03
Standard deviation	0,19	0,2	0,82	0,08	0,08	0,04

**Table 4.10 Specimen reaction forces and moments**

The main intention was to see if the force plate was capable of detecting slight variations in forces and moments applied to the specimen and gather the ground reaction forces. After reading the initial specimen configuration, the top plate was mounted on top of the specimen for accuracy purposes, the test was repeated three times and the average values are shown below.

Reaction	Fx N	Fy N	Fz N	Mx N-m	My N-m	Mz N-m
Average	0,22	-4,47	146,94	-0,31	0,38	-0,09
Standard deviation	0,57	0,37	1,05	0,1	0,13	0,05

**Table 4.11 Specimen reaction forces and moments due to top plate mounting**

A small force was applied to the top plate of the specimen and the whole setup began vibrating. This vibration was of a low intensity and was barely visible. To determine if the force plate could read such small variations, the data was captured.

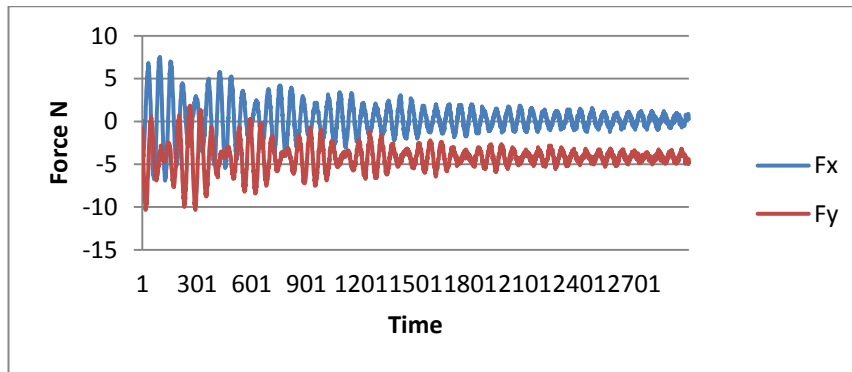


**Figure 4.6 Vibration on Fx and Fy due to vibrations**

In Figure 4.6 the force readings in Fx and Fy are shown, the effect of vibration on reading is highly visible, even in small force windows the vibration presence is clear.

To observe the force plate operation during a common setup for testing, three different 20kg weights were mounted on the top plate. The weights #12 (20,282 kg), #11 (20,118 kg) and #10 (20,677 kg) were stacked top of the other in that order.

Reaction	Fx N	Fy N	Fz N	Mx N-m	My N-m	Mz N-m
#12	1,27	-3,89	340,94	-2,52	1,46	0,1
SD	0,19	0,22	0,81	0,08	1,46	0,04
#12+#11	1,26	-4,29	538,56	-3,84	1,26	0,06
SD	0,2	0,21	0,8	0,08	1,26	0,04
#12+#11 +#10	1,19	-4,72	741,89	-5,47	1,3	0,02
SD	0,2	0,22	0,89	0,08	1,3	0,04

**Table 4.12 Average readings of reaction forces and moments due to weight stacking. Also the standard deviation of the measurements is shown**

A statistical analysis similar to those performed with the systems was also done for the force plate. To check for accuracy, the different Fz force readings were analysed against the real weight values while stacking weights and mounting the top plate. A bias percentage of 1.062% was obtained. This was a low bias value for the accuracy of the force plate.

To check if it is possible to apply precisely moments to the tibia head, moment measurements along the X and Y axes were made by shifting the weights a specific distance and recording the resulting moment three times. Approximate moments of -30 N-m were applied to the X axis and -10 N-m applied to the Y axis in separate setups.

Capturing 10 frames of moment readings during the three trials, the repeatability test was performed and the result obtained was a Repeatability percentage of 1.11%. This is also a low value that shows that it is possible to apply moments to the tibia head when simulating specific loading patterns.

The conclusion reached was that the system is capable of sensing small differences in forces and moments applied to the specimen and is reliable enough to capture ground reaction data during testing procedures.

## 4.4. Load cells

The load cells model, 8531 from Burster, came calibrated from the factory with a combined value consisting of non-linearity, hysteresis and no repeatability in constant installation position of  $\leq \pm 0.15\%$ . When the load cells were in an unloaded state it was observed in LabVIEW some readings that might suggest a deviation within the real force against the displayed force.

The load cells were labelled using numbers from #3 to #7. These labels were already set by the manufacturer and helped to not confuse the calibrated amplifiers. Load cell #7 is also referred as 5KN because is the only sensor with a range of -5000 to +5000N.

In order to observe and assess this deviation, a functionality test was completed to gather information about readings of the load cells while bearing a known weight. Each load cell was tested through different fixed setups, and the LabVIEW readings at a 0.1 second time step for 5 seconds duration. For the 50 values dataset obtained for each setup the average and standard deviation were calculated.

Some data points appeared to be out of the normal readings and for this case an outlier detection Grubbs' test was made with a P value of 0.05. Meaning that when no outliers are detected there is a 5% or less chance that an outlier far from the others might be encountered [26].

The outliers found were erased and a new average and standard deviation were calculated. The decision of deleting the outliers was made because the values obtained revealed nothing relevant about the weight tested. It was decided that the appearance of those rare readings might be due to small spikes in voltage that can be disregarded because the nature of the test was static and no physical disturbances were found.

Once the outliers were discarded and the new calculations were done, the following results were obtained:

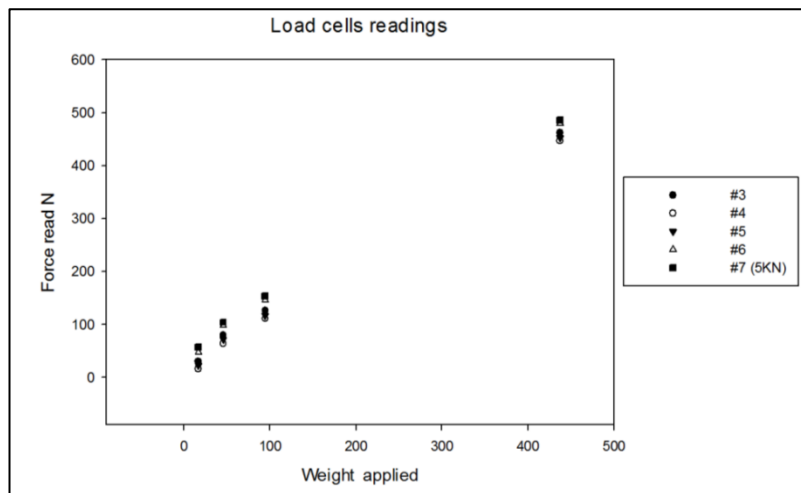
	#3		#4	
Weight	Average	Standard Dev	Average	Standard Dev
16,579	29,901	1,654	15,683	0,720
45,600	79,162	0,479	63,329	0,491
94,200	125,569	1,372	110,393	0,431
437,200	461,689	0,647	446,570	1,878

	#5		#6		#7 (5KN)	
Weight	Average	Standard Dev	Average	Standard Dev	Average	Standard Dev
16,589	21,772	1,550	46,837	2,165	56,283	2,093
45,600	70,525	1,323	97,141	2,213	103,389	6,354
94,200	115,889	0,647	145,760	0,741	152,793	3,069
437,200	453,158	0,706	478,510	2,483	486,079	1,974

**Table 4.13 Average force readings on load cells due to the application of a known weight**

It was observed that in every load cell a force offset was present on the weight readings and this can lead to irregularities when processing data from the computer model. The following figure shows the initial average results for the weight readings of each load cell. The deviations are even evident between sensors. Considering that the load cells and amplifiers were configured on a linear manner, a linear regression will be applied in order to fit a linear function that best represents load cell behaviour.



**Figure 4.7 Load cells readings during known weight application**

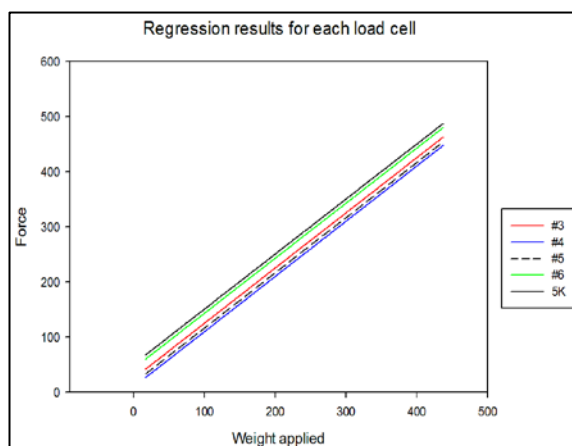


**Figure 4.8 Regression results for all load cells**

The results from the linear regression analysis are shown in Table 4.14. The  $Y_0$  value of each equation tells the initial deviation value of each load cell. Also the  $mx$  slope of the function has small deviations very close to the optimal value of 1 intended by the manufacturer's calibration. The regression graphs for each individual load cell are shown in the appendices.

Load Cell	Y	$R^2$
#3	$1,0015x+25,4690$	0,9978
#4	$1,0011x+10,4374$	0,9981
#5	$1,0016x+16,6947$	0,998
#6	$0,9987x+43,8583$	0,9973
5K	$0,9980x+51,5394$	0,9979

**Table 4.14 Regression equation for each load cell**

Linear regression is a method used to calculate an equation that minimizes the distance between the fitted line and the data points [27]. The R-squared is a statistical measure showing how closely the data fit the regression line. The closer the value is to 100%, the better the data fits the model. For example, a value of 0% shows it does not fit the model, and therefore explains none of the variability of the response data around its mean. On the other hand and a value of 100% indicates that the model explains all of the variability of the response data around its mean. In this case it can



be observed that the linear models obtained from the different regression analysis are suitable for determining the real force applied by the actuator.

Nevertheless, a shift offset was observed during the following tests. The “zero value” of the load cell without any load (only with its mounting flange attached), changed constantly by a few newtons. Important variations in temperature and other factors were not observed to contribute to this variation.

Considering that the load cells are calibrated by the manufacturer and that an offset was introduced by mounting the flanges; the regression analysis was made to ensure that the linearity behaviour of the sensor remained. Because the regression results were satisfactory, for future calculations the user can use the model to assess the initial deviations in the load cell readings.

- Shock effect on load cells readings

Considering that this is a novel method for testing load cells in a mechanical setup, an important point to consider is if the force readings might be affected greatly by the mechanics of force applications e.g. vibration or shocks that might generate high amplitude spikes that obstruct the accuracy of force readings and the performance of the control system.

A small series of tests were made in order to observe if this effect is present. To do this on each actuator a fixed force was set to be achieved by the ON/OFF system. To observe the possible shock/vibration effect in different cases the prefilling percentage was defined in order to see either an overshoot or a spike when the system switches from the prefilling phase to the control phase.

The readings were captured with a 0.004 second time step, while recording a set of 250 values. The results below are for one actuator paired with its own specific load cell. The force was applied on each actuator by connecting it to a beam mounted on the rack. The test on each actuator setting was performed three times.

- Actuator B, load cell #6, target force 1400N, prefilling phase overshoot, then control phase enters, higher prefilling percentage

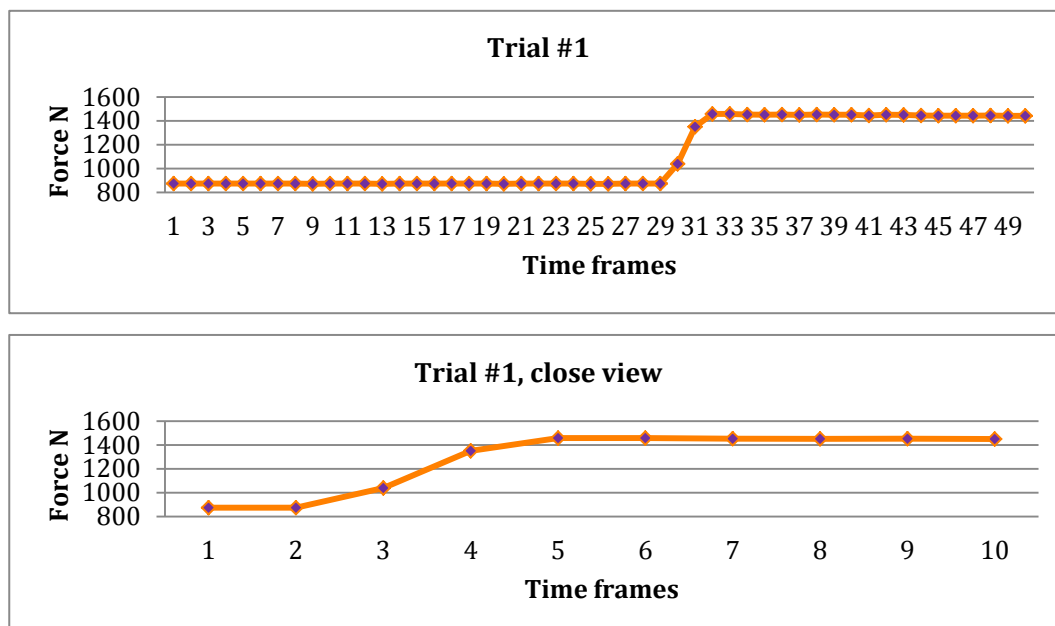


**Figure 4.9 Trial on actuator B. A) Full graph on Trial #1, B) Closer view of the force overshoot**

It is evident that the small changes seen on the graph are the result of the mechanical effect of the physical elements of the rack in the control systems, like the actuators



themselves, as well as rope and beam deformation. As no remarkable high amplitude oscillation that hindered force readings was seen, there was no need for further testing to be performed. The conclusion reached is that the user can rely on the fact that sensor readings will not be affected by the actuator activation mechanical effect. The rest of the vibration test graphs can be found in the appendices.

## 4.5. Redirection effect

Considering the high forces applied a special redirection system was designed and built, as explained in the previous chapter. To design the proper redirection mechanisms different elements were tested, for instance metal hooks, pulley wheels, etc. The test was done by mounting the redirection element on a beam of the metal frame. A load cell (#4), was left hanging at an approximate height of 30cm and pulled by a rope connected to the sensor end of an actuator. The difference in readings between the load cells show force loss due to redirection. Preliminary tests showed that metal hooks had an average force loss of 356N while applying 1000N by an actuator. This amount of force loss is extremely high, so the redirection mechanism was composed at the end of fixed pulley wheels and especially high-load sailing pulleys.

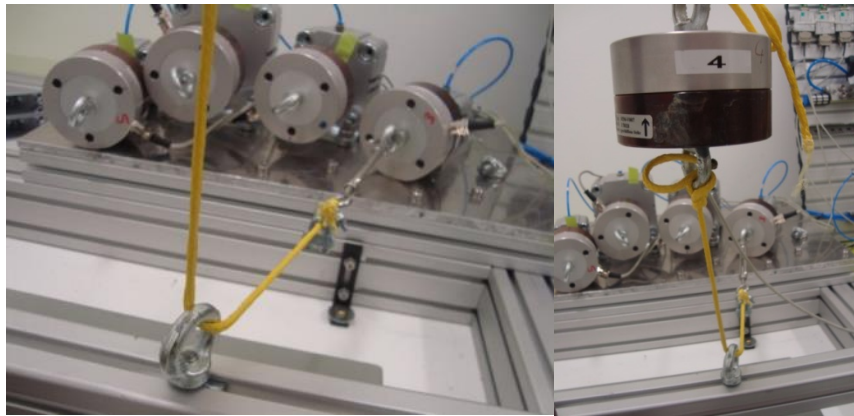


**Figure 4.10 Preliminary redirection test**

As avoiding losses during force application is not possible, a similar test was performed, but now using the final redirection configuration for each actuator, so the “error” on the force applied to the specimen can be assessed. For example, by increasing the control force level in order to obtain the desired force on the specimen after redirection.

The test was performed by activating each actuator and generating force levels in 10% increments of the maximum force magnitude desired for testing. For the small actuators the maximum target force was the maximum achievable force. For actuators A and B the top force was 2000N. The forces were recorded at a frequency of 250Hz. The number of data frames analysed was 125.

The results of the output forces from the sensors were analysed through regression, and a function of the real force vs control force was obtained.

The average forces for each trial were fed to the statistical software and analysed through linear regression. A set of equations was obtained; those show the function of the force applied by the actuators vs the real force (load cell #4 readings) after redirection losses.

Actuator	Y	R <sup>2</sup>
A	0,9162x+2,9932	0,9996
B	0,8523x+16,3080	0,9998
C	0,8676x+17,6156	0,9996
D	0,8146x+19,5471	0,9965

**Table 4.15 Regression analysis results for each actuator**

The regression functions show a clear linear behaviour of the force losses during force application for each actuator with a R-square value of >0.99. For future test adaptations and calculations the force loss function should be considered in order to obtain the force applied to the specimen and correlate the deformation results to the computer model.

## 4.6. Final setup test

In order to prove the capacity of the AMBR of performing biomechanical tests and to verify its suitability to apply the forces generated by the computer model developed at the DLR, a functionality test on the system's performance while running a routine biomechanical test was conducted.

The initial setup of the systems was performed according to the ones shown in the previous chapter.

The force plate captured reaction forces and moments during 20 seconds at a rate of 250 datasets per second. The hardware zero was made after positioning the specimen (establish a zero in all reaction forces and moments readings to avoid introducing initial errors).

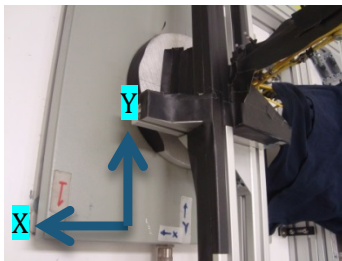


**Figure 4.11 Specimen position and orientation on the force plate coordinate system. The Z axis is pointing upwards from the top of the force plate**

The MoCap system was calibrated using 2000 wand counts until the error was lower than 0.5. As many phantom markers appeared, those were masked by a non-reflecting black tape. Many elements like metal beams, ropes, binders, and marker cluster frames were covered; also it was necessary to mask bone due to its polished surface. The actuator platform was producing phantom markers as well. For that a dark cotton fabric covered the actuators and eliminated these disturbances. In the end the result was a clear view of the markers without any disturbing signals, therefore increasing the precision of the data captured. The strobe and intensity of the cameras was optimized as well.

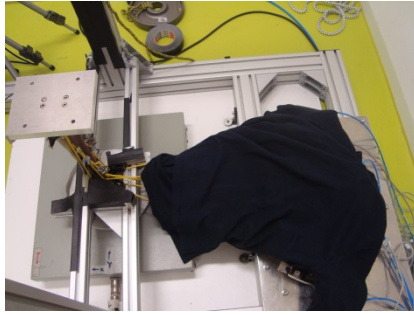


**Figure 4.12 Actuators covered for phantom markers elimination**

The coordinate system origin for the MoCap system was set positioning the calibration wand next to the specimen facing the cameras. The orientation of the coordinate axes used in the 3-D virtual space is shown in figure 4.13.

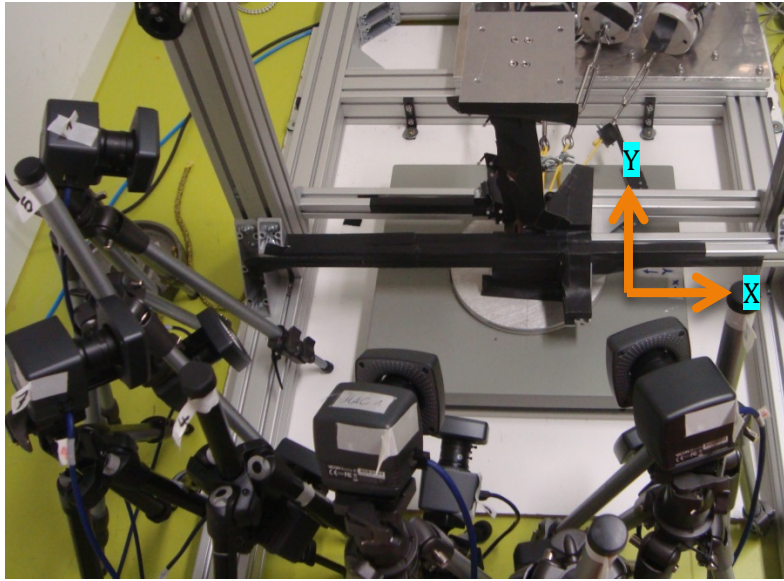


**Figure 4.13 Coordinate system origin and orientation for the MoCap system. The Z axis is pointing upwards from the specimen base**

The control system was set to only apply forces at a 25% of the maximum physiologically feasible capacity. For actuator A: 750N with an 8N window; actuator B: 600N with a 6N window; actuator C: 220N with 5N window and actuator D: 120N with a 5N window. The force windows were established in order to maintain a smooth control action and avoid high oscillations. The window and flow level were regulated manually until a desired behaviour was achieved.

The testing procedure was focused on applying the forces by activating the actuators simultaneously while recording ground reactions and bending data. Three trials were conducted by keeping the control system regulation for a few seconds (Continuous setup) and three more trials by stopping the ON/OFF control and closing the valves maintaining pressure in the actuators once a desired level of force was reached (Stop setup). By implementing the prefilling phase the rig started to vibrate due to the application of fast forces. Therefore only the ON/OFF control phase was used to regulate muscle forces.

- Control system

Choosing a 125 frames interval of the control force readings, the average force and standard deviation was calculated for each trial with the data collected on those frames. The results are shown in Table 4.16.

	Continuous					
Reference force	Trial 1 Measured	Trial 1 SD	Trial 2 Measured	Trial 2 SD	Trial 3 Measured	Trial 3 SD
120	124,8	3,299	124,15	4,638	124,33	3,8
220	230,95	10,901	226,02	2,632	225,72	19,917
600	606,11	14,823	609,55	3,923	613,18	6,974
750	749,82	5,666	757,14	3,006	754,62	6,737
	Stop					
Reference force	Trial 1 Measured	Trial 1 SD	Trial 2 Measured	Trial 2 SD	Trial 3 Measured	Trial 3 SD
120	119,07	2,655	122,67	0,819	123,84	1,288
220	249,1	1,049	229,21	2,581	233,27	0,641
600	608,43	2,811	600,81	3,007	618,98	3,905
750	721,04	5,614	743,35	7,94	748,64	8,01

**Table 4.16 Results of the control system. Average results and standard deviation**

A statistical analysis was made using Statgraphics Centurion XV, the accuracy for each trial is shown in table 4.17. The test was performed by comparing the average results of each trial individually and then the combined result used from all trials within a control setup (Continuous/Stop).

	Continuous			
	Trial 1	Trial 2	Trial 3	Combined
Bias	0,86%	1,07%	1,11%	1,01%
	Stop			
	Trial 1	Trial 2	Trial 3	Combined
Bias	0,30%	0,24%	1,38%	0,64%

**Table 4.17 Statistical analysis results for the control system performance. Bias percentage**

Both control actions show advantages and disadvantages. Both have an acceptable accuracy, being in the Stop setup (pressure maintained) better than the Continuous setup. The Stop setup might lead to problems due to the gradual relaxation effect that generates force losses over time. In order to keep a suitable level of force it might be advisable to set the force to a higher level to compensate for the loss over time. The variation in the data was considerable in the Continuous control setup due to the control window of operation for each actuator. As both schemes show a good accuracy, the decision on which one to use during future tests will be made by the operator regarding the kind of results expected from the test.

- Ground reaction forces and moments

The force plate recorded the reaction forces and moments at the specimen base during testing, the main objective is to verify if the sensing operation runs normally and captures the data without problems.

In Figures 14.14 and 14.15, the reactions recorded during one trial are shown.

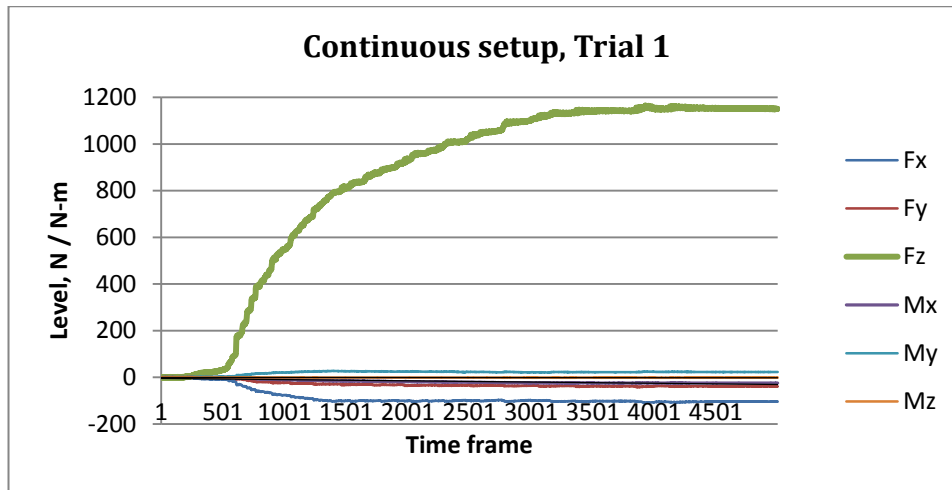


Figure 4.14 Reactions recorded during Continuous control

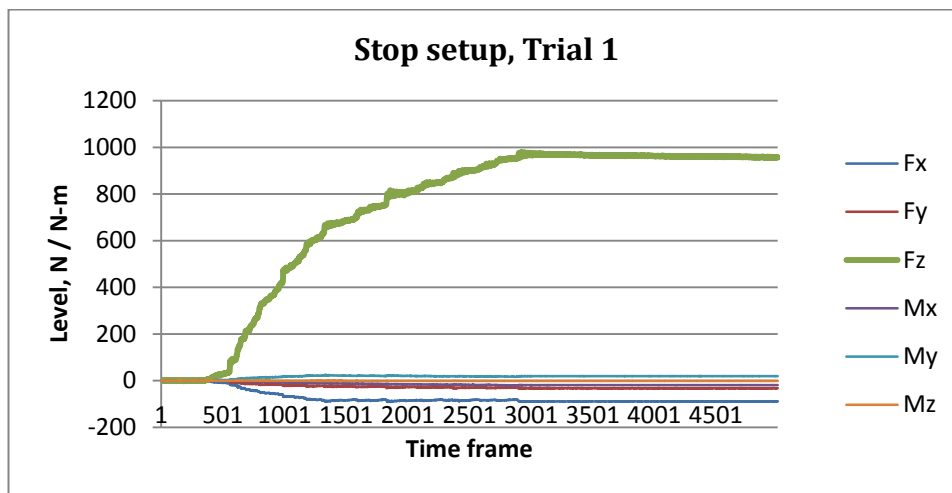


Figure 4.15 Reactions recorded during Stop control

The last 125 frames captured were averaged so the level of forces and moments reached on the test can be shown.

	Continuous		
	Trial 1	Trial 2	Trial 3
Fx	-103,77	-103,2	-103,76
Fy	-38,37	-38,02	-37,4
Fz	1150,92	1150,66	1155,23
Mx	-24,28	-24,26	-24,24
My	22,75	22,5	22,683
Mz	-1,38	-1,34	-1,35
	Stop		
	Trial 1	Trial 2	Trial 3
Fx	-88,56	-87,16	-90,08
Fy	-32,44	-31,65	-31,86
Fz	958,21	981,14	1004,63
Mx	-19	-19,71	-20,17
My	19,62	18,5	19,42
Mz	-1,01	-1,11	-1,18

Table 4.18 Average reaction forces and moments. Recorded during the last 125 frames of the tests

The magnitude of the forces and moments captured in these tests are shown, and the proper function of the force plate can be seen. During tests no source of mechanical disturbances was present, proving the adequacy of this system for the AMBR.

A statistical analysis was made to discover if significant differences between the reaction forces and moments within the two different setups are present. The repeatability percentage of the trials within the two schemes was of 0.6587%, proving that the high repeatability of the ground reactions recorded during biomechanical tests. The reproducibility percentage between the two different schemes was 4.012%. Although this percentage is not significantly high, it shows that the ground reactions generated when applying the continuous setup can differ from the ones obtained with the stop scheme. The user should decide which scheme retrieves more accurate and significant reaction data.

- Motion capturing system

The main output data for the validation of the computer model is the deformation magnitude present in the specimen during force application. For the purposes of this thesis the verification of the MoCap system during biomechanical tests is done by checking its ability to record specimen deformations. A deep analysis of the results obtained from the test is not within the scope of this thesis, nevertheless general conclusions from the bending information behaviour will be provided.

It will be shown an example of data captured during the first trial of the continuous control scheme. First for each marker clusters the center coordinate was calculated for each of the captured frames.

$$\text{Center coordinates} = \frac{x1+x2+x3}{3}, \frac{y1+y2+y3}{3}, \frac{z1+z2+z3}{3} \quad (\text{Eq. 7})$$

The following figure shows how the marker clusters are seen on the 3D space on the Vicon monitor during testing, the bending is small but perceptible when muscle-like forces are applied. The red lines help to visualize the change in position of the markers

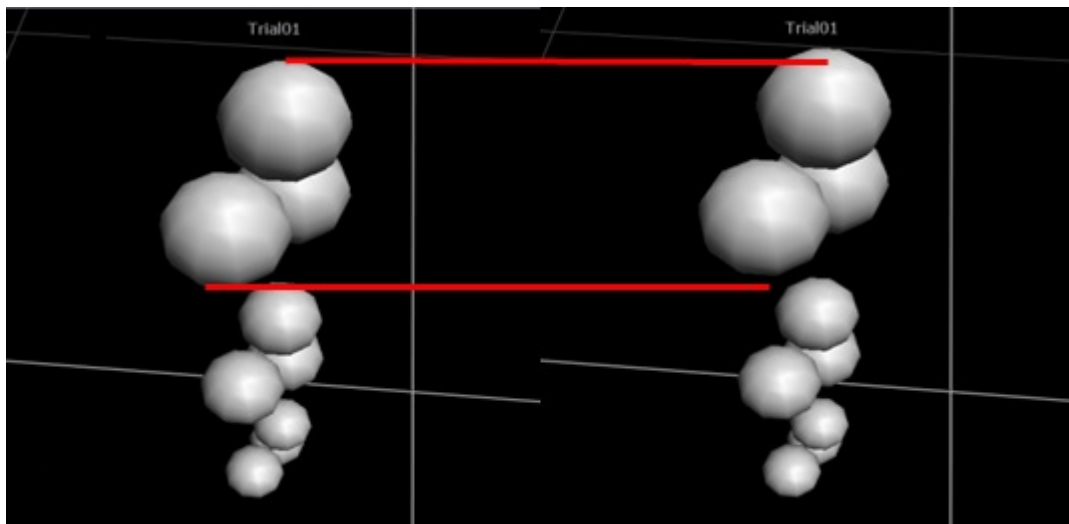


**Figure 4.16 Before/after picture showing marker's displacement on the 3D space while performing biomechanical tests**

To have an idea of the markers trajectory, the displacement on each coordinate axis for the center of one the three marker clusters can be seen in figure 4.17. The displacement of the medium marker cluster' center in the three coordinate axes is shown during the first trial of the Continuous setup.



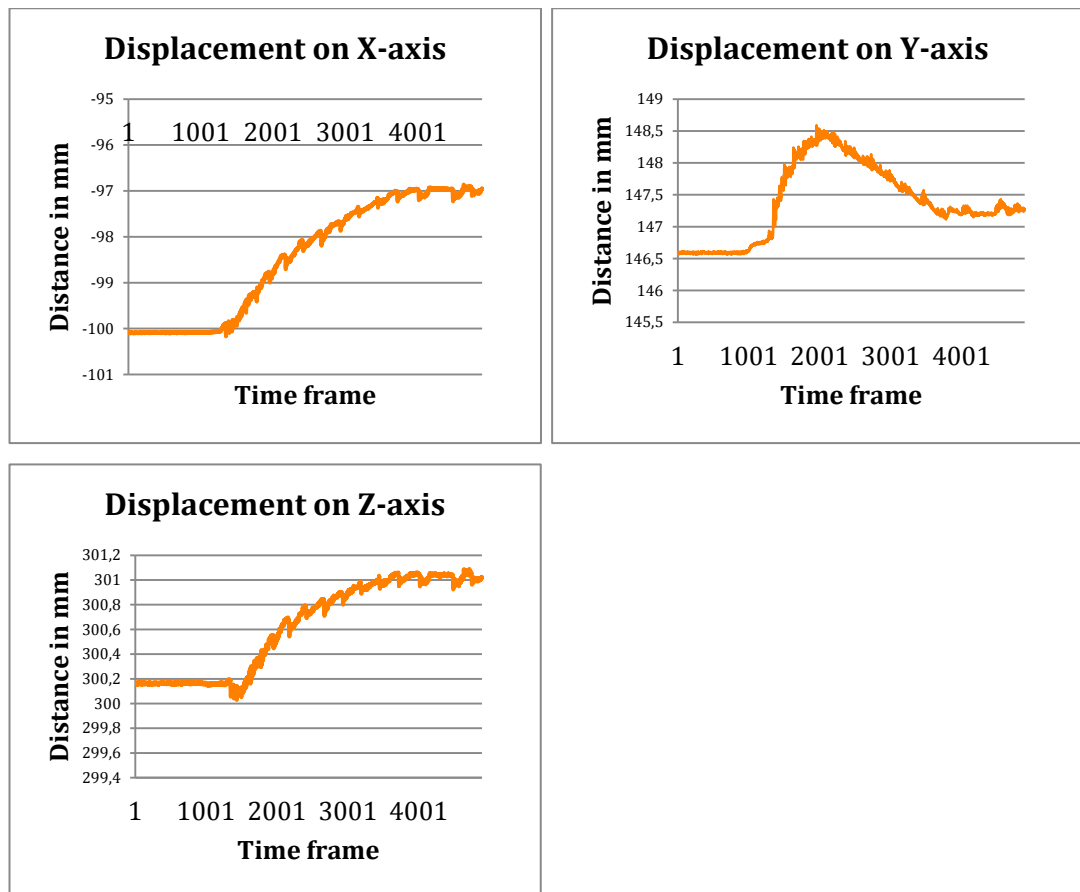


**Figure 4.17 Marker cluster center displacement on each axis. Medium cluster**

As it can be depicted from Figure 4.17, the displacement of the center of the medium marker cluster shows an interesting behaviour. In the X and Z axes it can be seen an increase of the distance that converged after a certain time while the system regulated the force applied by the actuators. The displacement curve in the Y axis show an increase of the distance followed by a decrease that almost returns to the initial position. Possible causes of this behaviour might be the mechanical behaviour proper of the material of the specimen, a relaxation due to the change in length of the ropes during force application or an offset in the deformation that is eliminated once the actuators achieved the desired force.

Displacement graphs for the top and bottom marker clusters are included in the appendices.

Another option to visualize bone deformation is to obtain the distance of the marker cluster center from the origin of the coordinate system. This will show the total displacement and bring the real biomechanical behaviour is intended to be recorded during biomechanical testing.

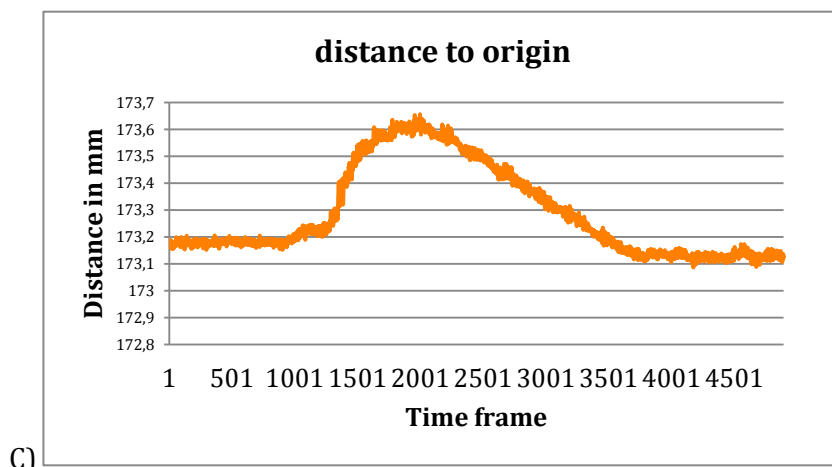
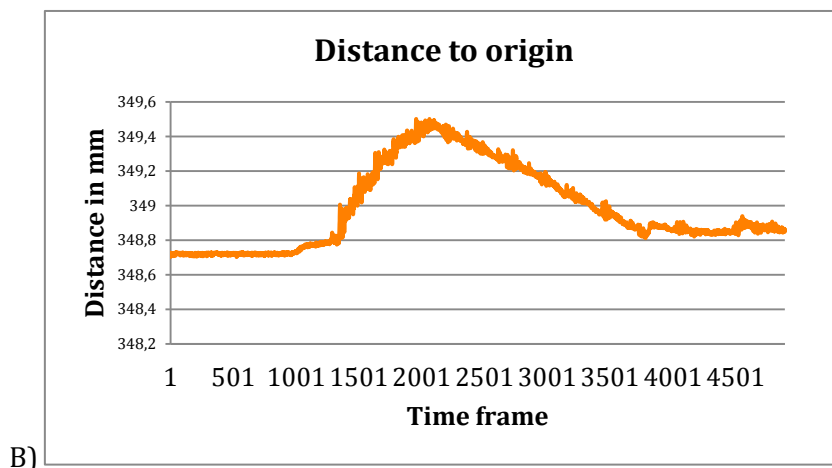


**Figure 4.18 Distance to origin of the 3 marker cluster centers. A) Top, B) Medium, C) Bottom**

It can be observed in Figure 4.18 an interesting behaviour of the distance to origin curves. The curves show an increase in the distance between the different marker cluster centers and after time a decrease in the distance, reaching the initial starting point or as it can be seen for the bottom cluster, the distance decreased. A possible reason for this might be that the movement pattern experienced by the marker clusters is a consequence of the bending and change in geometry of the bone during force application.



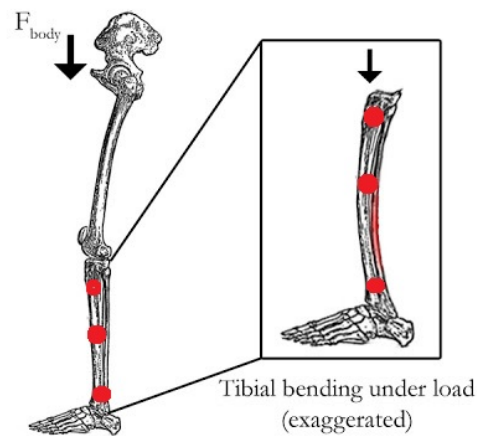


**Figure 4.19 Bone bending during load application. A possible explanation of the behaviour of the marker clusters changes in the coordinate system might be the special change in geometry that bone experiences under force loading [28]**

Considering that this data shows only the magnitude of the distance of the center of the marker clusters to the origin, it is important to verify other parameters in order to understand the detailed behaviour of the bone under muscle loading. The bending of the bone due to torsion might be seen by analysing the distance between one marker of the bottom cluster and one from the top. The relative changes between markers might show more conclusive and clear information about the specimen behaviour during these biomechanical tests.

As the numerical result is not a focus of this work, by observing the magnitude of the system outputs the conclusion is that the MoCap system works without any constraints, being able to capture bone deformation data in similar magnitude to the obtained during the MUST study.



## 5. CONCLUSIONS

Performing biomechanical tests that closely resemble real models is not an easy task. During several studies different human locomotion aspects were isolated and reproduced using different methods; from physical to computer models. Trying to represent a model that is as close to reality as possible entails several challenges. The AMBR is proposed as a tool for the realization of biomechanical tests. It will help to understand the influence of muscle forces in tibial loading by implementing different systems to generate and transmit muscle forces and record output data from the specimen.

The implemented artificial muscle system was composed by a pneumatic setup that offered the advantages of simple control and design. The control of the artificial muscles was proven suitable for the application but improvements can be made regarding force accuracy during testing procedures. The hardware can be customized in order to allow faster control and therefore a more accurate force regulation.

The designed computer interface was suitable for user operation during regular biomechanical tests. It allowed the operator to define the desired force and to manipulate control parameters that resulted in an expected behaviour of the actuators during force application. It is suggested to find a screen able to display completely the control panel for the user to be able to observe all details of the controls and information displays. The pneumatic hardware necessary to control the process was collocated next to the rig and close to the user there were only the main regulation hardware that poses no risk, like the EasyPort and the emergency stop.

The mechanical frame and redirection system were strong enough to avoid any mechanical disturbances during verification tests. Special attention should be paid to the behaviour of the whole setup while performing biomechanical tests that require the activation of all actuators with high forces at the same time. Control refinement as well as a more robust setup might strengthen the structure and ensure the longevity of its different components. Vibrations were present when actuators were activated too fast. This particular point should be addressed for future redesigns where dynamic tests will be performed.

The resulting data of bone deformation was captured and proven adequate for comparison to previous study results like the MUST study. The MoCap system was capable of recording small specimen deformations and the force plate captured ground reaction data without problems. Specimen handling must be improved in order to represent more accurately the real mounting and loading of a human tibia.

This is a big challenge considering the irregular geometry of the specimen and the difficulty of attaching muscles directly to the bone surface.

Finally, a full rig composed of different technologies was built and tested. Recalling the computer model developed at the Space physiology Department, the rig was proven able to reproduce muscular forces and generate bone specimen deformations in order to validate the model.

Future redesign and reconstruction will enable the AMBR to perform accurately with the human lower leg model. Other biomechanical test rigs have required between 2 and 3 years from design to construction and testing, and each has undergone different phases to generate improved versions from things that were learned from the past. The AMBR has currently one year of work on design, construction, testing and improvement, and is now capable of performing static positions of tibial loading. Improvements to this rig may one day make it a top biomechanical testing machine helping researchers model and prove special loading conditions on the human tibia, understanding on a deeper level the behaviour of bone tissues and develop rehabilitation therapies for astronauts and contributing to the treatment of bone diseases on earth.

## 6. REFERENCES

- [1] P. Yang, M. Sanno, G.-P. Brüggemann and J. Rittweger, "Evaluation of the performance of a motion capture system for small displacement recording and a discussion for its application potential in bone deformation in vivo measurements," in *Journal of engineering in medicine*, 2012.
- [2] H. Frost, *The Utah paradigm of skeletal physiology: an overview of its insights for bone, cartilage and collagenous tissue organs*, 2000.
- [3] L. Lanyonw, G. Hampsona , E. Goodship and J. Shah, *Bone deformation recorded in vivo from strain gauges attached to the human tibial shaft*, 1975.
- [4] Vicon Motion Systems Ltd., "Bonita, Affordable motion capture for any application," [Online]. Available: <http://www.vicon.com/System/Bonita>.
- [5] N. Bennell, *Characterisation of Bone Deformation Elicited by Artificial Muscles*, Sydney: The University of Sydney, 2014.
- [6] A. Zavatsky , "A kinematic-freedom analysis of a flexe-knee-stance testing rig," in *Biomechanics*, 1997.
- [7] O. Müller , J. Lo and M. Wünschel, "Simulation of force loaded knee movement in a newly developed in vitro knee simulator," in *Biomed Tech*, 2009.
- [8] P. Yang, *Relation of muscular contractions to mechanical deformation in the human tibia during different locomotive activities*, German Sports University Cologne, 2013.
- [9] HWFL, "Specialised knee and hip arthritis disease management program," [Online]. Available: <http://oa.hwfl.com.au/static.php?item=overview>.
- [10] E. P. Widmaier, *Human physiology: The mechanisms of body function*, McGraw-Hill Higher Education, 2004.
- [11] F. C. Anderson and M. G. Pandy, "A dynamic optimization solution for vertical jumping in three dimensions," in *Computer methods in biomechanics and biomedical engineering*, 2007.

- [12] DYNALLOY, Inc., "FLEXINOL, Actuator ribbon technical and design data," 2014. [Online]. Available: <http://www.dynalloy.com/TechDataRibbon.php>.
- [13] maxon motor ag, "maxon X drives," 2014. [Online]. Available: <http://www.maxonmotor.de/maxon/view/content/DCX-Detailsite>.
- [14] Exlar, "Tritex II DC Linear Actuator," 2014. [Online]. Available: [http://www.exlar.com/product\\_lines/38-Tritex-II-DC-Linear-Actuator](http://www.exlar.com/product_lines/38-Tritex-II-DC-Linear-Actuator).
- [15] Festo AG & Co.KG, "Compact cylinders ADVU, AEVU, metric," 2014. [Online]. Available: [http://www.festo.com/cat/en-us\\_us/products\\_ADVU\\_AEVU](http://www.festo.com/cat/en-us_us/products_ADVU_AEVU).
- [16] Festo AG & Co.KG, "Compact cylinders ADVU, AEVU, metric. 157295. AEUZ-100-15-A-P-A," 2014. [Online]. Available: [http://www.festo.com/cat/en-us\\_us/search?query=AEVUZ-100-15-A-P-A](http://www.festo.com/cat/en-us_us/search?query=AEVUZ-100-15-A-P-A).
- [17] R. Hernández Gaviño, *Introducción a los sistemas de control: Conceptos, aplicaciones y simulación con MATLAB*, Prentice Hall, 2010.
- [18] M. P. Trejo Ramírez, Writer, *Internship report*. [Performance]. Fachhochschule Lübeck, 2014.
- [19] M. More, "Comparison of different methods for pneumatic artificial muscle control," in *IEEE 11th International symposium on applied machine intelligence and informatics*, 2013.
- [20] Festo AG & Co.KG, "Proportional.pressure regulator VPPM," 2014. [Online]. Available: [http://www.festo.com/cat/en-us\\_us/products\\_VPPM](http://www.festo.com/cat/en-us_us/products_VPPM).
- [21] Advanced Mechanical Technology, Inc., "OR6-6-2000 specifications," [Online]. Available: [http://www.amti.biz/AMTIpibrowser.aspx?\\_\\_VIEWSTATE=%2FwEPDwULLTE0NzQ1NDQ3OTNkZA%3D%3D&iListbox1=350&iListbox2=397&iListbox3=OR6-6&iUnits=&iNewpageURL=&iScrollTop=0&iScrollTop2=0&iScrollTop3=533&iArrImage\\_URL=.%2FImage%2520file%2Fprogress\\_1.gif%2C.%2FImage](http://www.amti.biz/AMTIpibrowser.aspx?__VIEWSTATE=%2FwEPDwULLTE0NzQ1NDQ3OTNkZA%3D%3D&iListbox1=350&iListbox2=397&iListbox3=OR6-6&iUnits=&iNewpageURL=&iScrollTop=0&iScrollTop2=0&iScrollTop3=533&iArrImage_URL=.%2FImage%2520file%2Fprogress_1.gif%2C.%2FImage).
- [22] SAWBONES, P.R.L., "Fourth generation tibia," 2013. [Online]. Available: <http://www.sawbones.com/Catalog/Biomechanical/Composite%20Bones/3402>.
- [23] HowToMedia, Inc., "Muscles of the leg and foot," InnerBody, [Online]. Available: <http://www.innerbody.com/anatomy/muscular/leg-foot>.
- [24] Festo AG & Co.KG, "EasyPort USB – An interface for measuring, open-loop control, closed-loop control. Connects the simulation to the real world," [Online]. Available: <http://www.festo-didactic.com/int-en/learning-systems/software-e-learning/easyveep/easyport-usb-an-interface-for-measuring,open-loop-control,closed-loop-control.-connects-the-simulation-to-the-real-world.htm>.
- [25] ABB, "PID control. Application guide," [Online]. Available: [http://www05.abb.com/global/scot/scot267.nsf/veritydisplay/cdbe4d3a1be553ee852578e80071e77c/\\$file/2104301aiab.pdf](http://www05.abb.com/global/scot/scot267.nsf/veritydisplay/cdbe4d3a1be553ee852578e80071e77c/$file/2104301aiab.pdf).
- [26] GraphPad Software, Inc., "Detecting outliers with Grubbs' test," 2014. [Online]. Available: <http://www.graphpad.com/support/faqid/1598/>.
- [27] Minitab, "Regression analysis: How do i interpret R-squared and assess the

- goodness-of-fit?," 2014. [Online]. Available: <http://blog.minitab.com/blog/adventures-in-statistics/regression-analysis-how-do-i-interpret-r-squared-and-assess-the-goodness-of-fit>.
- [28] J. Davis, "Injury Series: Tibial stress fractures and stress reactions: The role of bone structure, impact, and calf strength," 2012. [Online]. Available: <http://www.runningwritings.com/2012/05/injury-series-tibial-stress-fractures.html>.
- [29] C.-L. Chen, "Tunning PID controllers," [Online]. Available: [http://pse.che.ntu.edu.tw/chenc1/Process\\_Control/2006/12%20Tuning%20PID%20Controllers.pdf](http://pse.che.ntu.edu.tw/chenc1/Process_Control/2006/12%20Tuning%20PID%20Controllers.pdf).
- [30] Advanced Mechanical Technology, Inc., *NetForce User manual*.
- [31] C. Oatis, Kinesiology, the mechanics and pathomechanics of human movement, Lippincott Williams & Wilkins, 2008.
- [32] G. K. Klute, J. M. Czerniecki and B. Hannaford, "Mckibben artificial muscles: pneumatic actuators with bioechnical intelligence," in *International conerence on Advanced intelligen mechatronics*, 1999.
- [33] J. M. Winters, "Hill-based muscle models: a systems engineering perspective," in *Multiple muscle systems*, Springer, 1990, pp. 69-93.





## 7. ACKNOWLEDGEMENTS

Studying in Germany has been a fascinating journey in my life. It was my first time living alone in a foreign country; it was not easy but along the way I was surrounded by people that helped me and guided my steps in this land.

I would like to thank Prof. Stephan Klein, Silke Venker and Gesche Lindemann-Heins for their guidance and support to all students from the master's program, especially to those of us coming from other countries. Without their help it will have been impossible to start a living in Lübeck and adapt to the learning system in Germany.

I am very grateful to the whole Space Physiology Department at the German Aerospace Center in Köln. Since I started my internship my colleagues have welcomed me and made me feel part of the team. Special thanks to Prof. Jörn Rittweger for his trust and support that allowed me to continue in the department and work on my master thesis there. Thanks to Dr. Uwe Mittag for his support and finally my deepest appreciation to my supervisor Andreas Kriechbaumer for his advice.

Special thanks to the CONACYT and DAAD for the scholarship that made this possible. Also I would like to thank all my friends and colleagues to whom I shared life-changing experiences with throughout the way.

I would like to express my deepest appreciation to my professors in México that motivated me to study biomedical engineering. Thanks to Dr. Juan Manuel López Ramírez and Dr. Enoch Gutiérrez Herrera for always being on my side willing to help and provide me with words of encouragement during all these years. Special thanks to Dr. Mario Adrián Flores Castro for his trust and continuing support.

Last but not least I would like to thank my parents Bertha and Manuel for their patience, unconditional support and love through these two long years we've been living so far from each other, but has somehow brought us closer. Also thanks to all my family for their encouragement.



# LIST OF TABLES

TABLE 2.1 AMTI FORCE PLATE OR6-6-2000.....	18
TABLE 2.2 VICON BONITA B3 SPECIFICATIONS [4].....	19
TABLE 3.1 ACTUATORS EMPLOYED TO SIMULATE LOWER LEG MUSCLES.....	28
TABLE 3.2 EASYPORT CHARACTERISTICS [24].....	31
TABLE 4.1 FORCES APPLIED AND RESULTS ON ACTUATOR D. CYLINDER OF 32MM DIAMETER. MAXIMUM FORCE OF 382N AT 6 BAR. MOUNTED TO LOAD CELL #3.....	42
TABLE 4.2 REPEATABILITY AND REPRODUCIBILITY RESULTS FOR EACH ACTUATOR.....	43
TABLE 4.3 ACCURACY OF THE CONTROL SYSTEM FOR EACH ACTUATOR. THE ANALYSIS WAS DONE WITH A 95% CONFIDENCE INTERVAL.....	44
TABLE 4.4 VARIATIONS MADE APPROXIMATELY ALONG X-AXIS IN MM .....	46
TABLE 4.5 VARIATIONS MADE APPROXIMATELY ALONG Y-AXIS IN MM .....	46
TABLE 4.6 VARIATIONS MADE APPROXIMATELY ALONG Z-AXIS IN MM .....	46
TABLE 4.7 COMPARISON OF VARIATIONS MADE APPROXIMATELY ALONG X-AXIS. ERROR DIFFERENCE IN MM OBTAINED BY COMPARING BOTH RESULTS.....	46
TABLE 4.8 COMPARISON OF VARIATIONS MADE APPROXIMATELY ALONG Y-AXIS. ERROR DIFFERENCE OBTAINED BY COMPARING BOTH RESULTS.....	46
TABLE 4.9 COMPARISON OF VARIATIONS MADE APPROXIMATELY ALONG Z-AXIS. ERROR DIFFERENCE OBTAINED BY COMPARING BOTH RESULTS .....	47
TABLE 4.10 SPECIMEN REACTION FORCES AND MOMENTS.....	48
TABLE 4.11 SPECIMEN REACTION FORCES AND MOMENTS DUE TO TOP PLATE MOUNTING.....	48
TABLE 4.12 AVERAGE READINGS OF REACTION FORCES AND MOMENTS DUE TO WEIGHT STACKING. ALSO THE STANDARD DEVIATION OF THE MEASUREMENTS IS SHOWN.....	49
TABLE 4.13 AVERAGE FORCE READINGS ON LOAD CELLS DUE TO THE APPLICATION OF A KNOWN WEIGHT .....	50
TABLE 4.14 REGRESSION EQUATION FOR EACH LOAD CELL.....	51
TABLE 4.15 REGRESSION ANALYSIS RESULTS FOR EACH ACTUATOR.....	54
TABLE 4.16 RESULTS OF THE CONTROL SYSTEM. AVERAGE RESULTS AND STANDARD DEVIATION.....	56
TABLE 4.17 STATISTICAL ANALYSIS RESULTS FOR THE CONTROL SYSTEM PERFORMANCE. BIAS PERCENTAGE.....	56
TABLE 4.18 AVERAGE REACTION FORCES AND MOMENTS. RECORDED DURING THE LAST 125 FRAMES OF THE TESTS .....	57



# LIST OF FIGURES

FIGURE 2.1: MECHANOSTAT MODEL [2] .....	4
FIGURE 2.2 MUST STUDY. A MoCAP SYSTEM RECORDED TIBIAL DEFORMATION DURING HUMAN LOCOMOTION [1] .....	4
FIGURE 2.3 BASIC PRINCIPLE OF THE COMPUTER MODEL .....	5
FIGURE 2.4 FIRST MECHANICAL FRAME FOR AMBR RACK. A) COMPUTER DESIGN, B) PHYSICAL CONFIGURATION [5].....	6
FIGURE 2.5 THE OXFORD KNEE-TESTING RIG [6] .....	8
FIGURE 2.6 TOTAL FORCES IN THREE SIMULATED QUADRICEPS MUSCLES. FORCES APPLIED DURING VARIOUS KNEE LOADING CONDITIONS FOR ONE SPECIMEN [7] .....	8
FIGURE 2.7 THE TÜBINGEN KNEE SIMULATOR [7] .....	9
FIGURE 2.8 THE LELD RIG .....	10
FIGURE 2.9 THE MUSCLES RESPONSIBLE FOR HUMAN LOCOMOTION HAVE A DIRECT IMPACT ON BONE REMODELLING DURING SPECIFIC ACTIVATION PATTERNS [9] .....	10
FIGURE 2.10 TIME RELATIONS BETWEEN A SKELETAL MUSCLE FIBER ACTION POTENTIAL. RESULTING CONTRACTION AND RELAXATION OF THE MUSCLE FIBER [10].....	11
FIGURE 2.11 MEASUREMENT OF TENSION DURING A SINGLE ISOMETRIC TWITCH OF A SKELETAL MUSCLE FIBER [10] .....	11
FIGURE 2.12 SAMPLE OF VALUES OF THE MAXIMUM ISOMETRIC STRENGTH OF EACH MUSCLE [11] .....	12
FIGURE 2.13 AEVUZ PNEUMATIC CYLINDER [16].....	13
FIGURE 2.14 POSITION/SPEED/TIME DIAGRAM. OBTAINED FROM FESTO ONLINE ENGINEERING TOOL [15] .....	14
FIGURE 2.15 OPEN-LOOP CONTROL SYSTEM .....	14
FIGURE 2.16 CLOSED-LOOP CONTROL SYSTEM .....	15
FIGURE 2.17 INNER CONNECTION OF PROPORTIONAL PRESSURE REGULATOR [19] .....	15
FIGURE 2.18 PROPORTIONAL PRESSURE REGULATOR FORM FESTO [20] .....	16
FIGURE 2.19 DIAGRAM OF CASCADE THROTTLE VALVES ASSEMBLY [19] .....	16
FIGURE 2.20 CIRCUIT OF A CONTROL SYSTEM USING A PROPORTIONAL VALVE [19] .....	17
FIGURE 2.21 A) AMTI FORCE PLATE B) DIMENSIONS AND ORIENTATION OF THE FORCE PLATE [21].	17
FIGURE 2.22 VICON BONITA B3 CAMERA [4] .....	19
FIGURE 3.1 FORCE PLATE. A) ALIGNMENT OF FORCE PLATE B) FIXATION OF THE PLATE TO THE WOODEN BASE USING SCREWS.....	22
FIGURE 3.2 ARTIFICIAL TIBIA MODEL. A) MATERIAL PROPERTIES, B) MODEL [22] .....	22
FIGURE 3.3 BOTTOM FIXATION. BOTTOM MOLD ATTACHMENT OF THE SPECIMEN .....	23
FIGURE 3.4 NEW SPECIMEN TOP ATTACHMENT. THE PLATE WAS DRILLED IN ORDER TO MATCH THE GEOMETRY OF THE TIBIA SPECIMEN .....	23
FIGURE 3.5 NEW REDIRECTION SYSTEM. PULLEY WHEELS AND SPECIAL HIGH-LOAD PULLEYS WERE EMPLOYED TO CONSTRUCT THE FORCE REDIRECTION MECHANISM.....	24
FIGURE 3.6 NEW LOAD CELL MOUNTINGS. METAL FLANGES MOUNTED ON THE FORCE SENSORS.....	24
FIGURE 3.7 PNEUMATIC CONFIGURATION. A) PREVIOUS ARRANGEMENT OF PNEUMATIC COMPONENTS. ALL THE CONTROL VALVES WERE NEXT TO THE USER CAUSING DISTURBANCES AND EXPOSURE TO	

POTENTIAL RISK. B) NEW ARRANGEMENT OF COMPONENTS. ONLY THE MAIN VALVE AND EMERGENCY STOP ARE NEXT TO THE USER .....	25
FIGURE 3.8 AMBR FINAL SETUP AFTER REDESIGN AND RECONSTRUCTION .....	25
FIGURE 3.9 FINAL AMBR CONFIGURATION OF MAIN ELEMENTS.....	26
FIGURE 3.10 ON/OFF CONTROL SYSTEM FOR MANAGING FORCE (PRESSURE) IN PNEUMATIC ACTUATORS.....	27
FIGURE 3.11 MUSCLES SIMULATED BY ACTUATORS. A) TIBIALIS ANTERIOR, B) SOLEUS, C) TIBIALIS POSTERIOR, D) FLEXOR DIGITORUM LONGUS [23].....	28
FIGURE 3.12 ACTUATORS MOUNTED ON THE METAL PLATE. THE ACTUATORS ARE ALREADY ALIGNED IN THE CORRECT ANGLES FOR FORCE APPLICATION .....	28
FIGURE 3.13 ACTUATOR CONTROL CONFIGURATION .....	28
FIGURE 3.14 GENERAL CIRCUIT FOR ACTUATION CONTROL .....	29
FIGURE 3.15 DETAILED CIRCUIT FOR INDIVIDUAL ACTUATOR ACTIVATION .....	29
FIGURE 3.16 SENSING ELEMENT. LOAD CELLS MODEL 8531 AND IN-LINE AMPLIFIER MODEL 9235 ...	30
FIGURE 3.17 PHYSICAL CONFIGURATION OF FESTO EASYPORT.....	31
FIGURE 3.18 FLOW CHART SHOWING THE MAIN LOGIC APPLIED IN THE CONTROL SOFTWARE .....	32
FIGURE 3.19 FRONT PANEL DISPLAYING GRAPHICALLY FORCE LEVEL AS WELL AS CURRENT VOLTAGE. ...	33
FIGURE 3.20 FRONT PANEL FOR SELECTING AND ACTIVATING ACTUATORS .....	33
FIGURE 3.21 FRONT PANEL FOR FORCE SETTINGS .....	34
FIGURE 3.22 STOP BUTTON ACTIVATED. WHEN THE BUTTON IS PUSHED IT REMAINS IN THAT STATE AND DEACTIVATES ALL OUTPUTS UNTIL USER PUSHES THE BUTTON AGAIN TO CONTINUE WITH TESTING .....	35
FIGURE 3.23 PID CONTROL DIAGRAM .....	36
FIGURE 3.24 TUNING OF INTEGRAL GAINS. CURVES WITH DIFFERENT INTEGRATIVE GAINS RECORDED. A) 2, B) 64, C) 128.....	36
FIGURE 3.25 TUNING OF DERIVATIVE GAINS. A) 2, B) 4, C) 16.....	36
FIGURE 3.26 PHYSICAL CONFIGURATION OF THE MoCAP SYSTEM.....	37
FIGURE 3.27 EXAMPLE OF OPTIMAL STROBE INTENSITY AND THRESHOLD VIEW ON THE MARKERS .....	38
FIGURE 3.28 POSITION OF THE CAMERAS IN THE VIRTUAL WORKSPACE.....	38
FIGURE 3.29 PHYSICAL CONFIGURATION FOR FORCE PLATE DATA CAPTURING USING THE GEN 5 AMPLIFIER [21] .....	39
FIGURE 3.30 FORCE PLATE COORDINATE SYSTEM.....	39
FIGURE 3.31 GRAPH CONFIGURATION. A) FORCE AND MOMENTS UNITS CONFIGURATION. B) GRAPH SHOWING THE VALUES OF THE THREE FORCES AND THREE MOMENTS .....	39
FIGURE 4.1 PHYSICAL CONFIGURATION FOR ACTUATOR CONTROL TESTING .....	41
FIGURE 4.2 FORCES READ ON EACH TRIAL FOR ACTUATOR D. A) ASCENDING ORDER B) RANDOM ORDER .....	43
FIGURE 4.3 CONFIGURATION OF MOTION CAPTURING SYSTEM TEST. A) MARKERS ATTACHED TO THE CALLIPER MEASURING TIPS OF THE FIXED JAW BLADES OF THE CALLIPER AT AN INITIAL SPANSE OF 20MM B) EXAMPLE SHOWING THE CALLIPER MOUNTED ON THE MECHANICAL VISE C) EXAMPLE OF COORDINATE SYSTEM SETUP OF THE VICON SYSTEM USING THE CALIBRATION WAND. THE WAND WAS POSITIONED ABOVE THE VISE .....	44

FIGURE 4.4 EXAMPLES OF THE DIFFERENT OFFSETS PRESENT ON MARKER'S MOUNTING AS WELL AS MARKER IMPERFECTIONS .....	45
FIGURE 4.5 FORCE PLATE LOADING WITH SPECIMEN. THE SPECIMEN HAS ATTACHED TOP AND BOTTOM FLANGES .....	48
FIGURE 4.6 VIBRATION ON Fx AND Fy DUE TO VIBRATIONS.....	49
FIGURE 4.7 LOAD CELLS READINGS DURING KNOWN WEIGHT APPLICATION .....	51
FIGURE 4.8 REGRESSION RESULTS FOR ALL LOAD CELLS .....	51
FIGURE 4.9 TRIAL ON ACTUATOR B. A) FULL GRAPH ON TRIAL #1, B) CLOSER VIEW OF THE FORCE OVERSHOOT .....	52
FIGURE 4.10 PRELIMINARY REDIRECTION TEST .....	53
FIGURE 4.11 SPECIMEN POSITION AND ORIENTATION ON THE FORCE PLATE COORDINATE SYSTEM. THE Z AXIS IS POINTING UPWARDS FROM THE TOP OF THE FORCE PLATE .....	54
FIGURE 4.12 ACTUATORS COVERED FOR PHANTOM MARKERS ELIMINATION.....	55
FIGURE 4.13 COORDINATE SYSTEM ORIGIN AND ORIENTATION FOR THE MoCAP SYSTEM. THE Z AXIS IS POINTING UPWARDS FROM THE SPECIMEN BASE .....	55
FIGURE 4.14 REACTIONS RECORDED DURING CONTINUOUS CONTROL.....	57
FIGURE 4.15 REACTIONS RECORDED DURING STOP CONTROL .....	57
FIGURE 4.16 BEFORE/AFTER PICTURE SHOWING MARKER'S DISPLACEMENT ON THE 3D SPACE WHILE PERFORMING BIOMECHANICAL TESTS.....	58
FIGURE 4.17 MARKER CLUSTER CENTER DISPLACEMENT ON EACH AXIS. MEDIUM CLUSTER.....	59
FIGURE 4.18 DISTANCE TO ORIGIN OF THE 3 MARKER CLUSTER CENTERS. A) TOP, B) MEDIUM, C) BOTTOM .....	60
FIGURE 4.19 BONE BENDING DURING LOAD APPLICATION. A POSSIBLE EXPLANATION OF THE BEHAVIOUR OF THE MARKER CLUSTERS CHANGES IN THE COORDINATE SYSTEM MIGHT BE THE SPECIAL CHANGE IN GEOMETRY THAT BONE EXPERIENCES UNDER FORCE LOADING [28] .....	61





# APPENDICES

APPENDIX 1: PNEUMATIC CYLINDERS SPECIFICATIONS

APPENDIX 2: FORCE PLATE SPECIFICATION SHEET

APPENDIX 3: VICON SYSTEMS TECHNICAL DATA

APPENDIX 4: LOAD CELLS FORCE SENSORS SPECIFICATION SHEET

APPENDIX 5: LOAD CELLS AMPLIFIER SPECIFICATION SHEET

APPENDIX 6: EASYPORT USB TECHNICAL DATA

APPENDIX 7: MAIN CONTROL PANEL IN LABVIEW

APPENDIX 8: CONTROL PROGRAM CIRCUIT IN LABVIEW

APPENDIX 9: ELECTRIC CIRCUITS OF THE CONTROL SYSTEM.

APPENDIX 10: PHASE CONTROL VALVES FOR PNEUMATIC ACTUATORS SPECIFICATION SHEETS

APPENDIX 11: VALVES FOR ON/OFF CONTROL SPECIFICATION SHEET

APPENDIX 12: PID CONTROL PANEL

APPENDIX 13: PID CONTROL CIRCUIT IN LABVIEW

APPENDIX 14: FORCE CONTROL TEST RESULTS FOR EACH ACTUATOR

APPENDIX 15: STATISTICAL RESULTS OF THE CONTROL SYSTEM FOR EACH ACTUATOR (SPANISH)

APPENDIX 16: LINEAR REGRESSION RESULT GRAPHS FOR EACH LOAD CELL. DATA FROM KNOWN WEIGHT APPLICATION.

APPENDIX 17: VIBRATION EFFECT ON LOAD CELL READINGS GRAPHS

APPENDIX 18: FORCE LOSS DUE TO REDIRECTION EFFECT. LINEAR REGRESSION RESULTS GRAPHS

APPENDIX 19: STATISTICAL RESULTS OF THE CONTROL SYSTEM DURING THE VERIFICATION TESTS (SPANISH)

APPENDIX 20: STATISTICAL RESULTS OF THE GROUND REACTION DATA DURING THE VERIFICATION TESTS (SPANISH)

APPENDIX 21: CENTER DISPLACEMENT GRAPHS OF THE CENTER OF THE THREE MARKER CLUSTERS DURING THE FIRST TRIAL OF THE CONTINUOUS SETUP



# APPENDIX 1

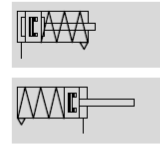
## Specification sheet for AEVUZ pneumatic cylinders from Festo

### Compact cylinders AEVU/AEVUZ

Technical data – Single-acting, basic version

**FESTO**

#### Function

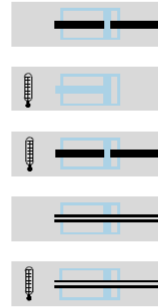


- Diameter  
12 ... 100
- Stroke length  
1 ... 25

• [www.festo.com](http://www.festo.com)

Wearing parts kits  
→ 45

#### Variants



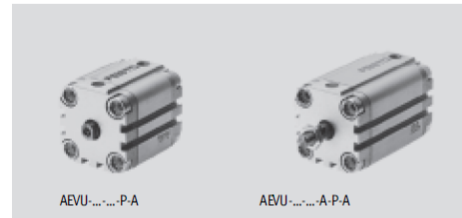
S2

S6

S26

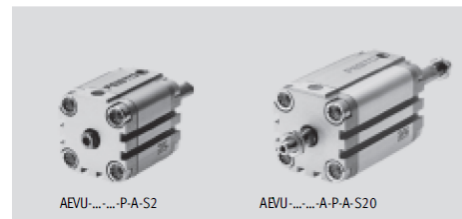
S20

S206



AEVU-...-P-A

AEVU-...-A-P-A



AEVU-...-P-A-S2

AEVU-...-A-P-A-S20

General technical data											
Piston $\varnothing$	12	16	20	25	32	40	50	63	80	100	
Pneumatic connection	M5	M5	M5	M5	G $\frac{1}{8}$	G $\frac{1}{8}$	G $\frac{1}{8}$	G $\frac{1}{8}$	G $\frac{1}{8}$	G $\frac{1}{4}$	
End of piston rod	Female thread	M3	M4	M5	M5	M6	M6	M8	M8	M10	M12
	Male thread	M6	M8	M10x1.25				M12x1.25		M16x1.5	M20x1.5
Operating medium	Compressed air in accordance with ISO 8573-1:2010 [7:4:4]										
Note on operating/pilot medium	Operation with lubricated medium possible (in which case lubricated operation will always be required)										
Constructional design	Piston										
	Piston rod										
Cushioning	Flexible cushioning rings/plates at both ends										
Position sensing	For proximity sensing										
Type of mounting	Via through-holes										
	Via female thread										
	Via accessories										
Mounting position	Any										

† Note: This product conforms to ISO 1179-1 and to ISO 228-1

Operating pressure [bar]											
Piston $\varnothing$	12	16	20	25	32	40	50	63	80	100	
Pushing variant AEVU											
Piston rod at one end	1.5 ... 10	1.3 ... 10	1.0 ... 10		0.8 ... 10			0.6 ... 10			
Through piston rod S2/S20	1.7 ... 10	1.5 ... 10	1.4 ... 10		1.2 ... 10			1.0 ... 10			
Pulling variant AEVUZ											
Piston rod at one end	1.5 ... 10	1.3 ... 10	1.0 ... 10		0.8 ... 10						

## Compact cylinders AEVU/AEVUZ

Technical data – Single-acting, basic version

FESTO

Ambient conditions		
Compact cylinder	Basic version	S6
Ambient temperature <sup>1)</sup> [°C]	–20 ... +80	0 ... +120
Corrosion resistance class CRC <sup>2)</sup>	2	2

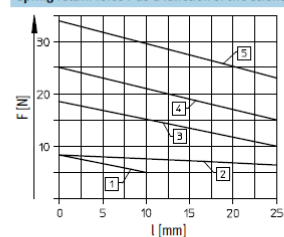
1) Note operating range of proximity sensors

2) Corrosion resistance class 2 according to Festo standard 940 070

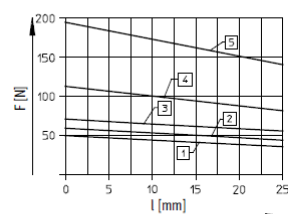
Components requiring moderate corrosion resistance. Externally visible parts with primarily decorative surface requirements which are in direct contact with a surrounding industrial atmosphere or media such as cooling or lubricating agents

Forces [N]										
Piston Ø	12	16	20	25	32	40	50	63	80	100
Pushing variant AEVU										
Theoretical force at 6 bar,	59	111	171	269	450	704	1121	1799	2902	4516
advancing	S2/S20	42	81	123	221	382	636	999	1679	2733
Pulling variant AEVUZ										
Theoretical force at 6 bar,	42	81	123	221	382	636	999	1679	2733	4222
advancing										

### Spring return force F as a function of the stroke l



- 1 AEVU/AEVUZ-12
- 2 AEVU/AEVUZ-16
- 3 AEVU/AEVUZ-20
- 4 AEVU/AEVUZ-25
- 5 AEVU/AEVUZ-32



- 1 AEVU/AEVUZ-40
- 2 AEVU/AEVUZ-50
- 3 AEVU/AEVUZ-63
- 4 AEVU/AEVUZ-80
- 5 AEVU/AEVUZ-100

Weights [g]										
Piston Ø	12	16	20	25	32	40	50	63	80	100
Product weight with 0 mm stroke	87	89	149	180	300	433	560	1059	1772	2797
Additional weight per 10 mm stroke	15	15	23	28	40	59	72	107	168	177
Moving load with 0 mm stroke	8	12	20	26	49	63	112	134	307	614
Additional load per 10 mm stroke	2	4	6	6	9	9	16	16	25	38

## APPENDIX 2

### Force plate specification sheet

Model: OR6-6-2000  
Serial Number: 7411M  
Number: 7411M-1-2  
Date: 08/30/11

ADVANCED MECHANICAL TECHNOLOGY INC.  
176 Waltham Street Watertown MA 02172-4800  
617-926-6700 [www.amti.biz](http://www.amti.biz)  
[support@amti.biz](mailto:support@amti.biz)

#### Environmental Information

Temperature: 24 degrees C  
Humidity: 46%

#### Multi-axis Force Transducer Calibration Data

##### Legend

N - Newtons (force)	N-m - Newton meters (moment)
lb - pounds (force)	in-lb - inch pounds (moment)
SI - System International (metric)	US - United States (English)
V - Volts	uV - micro Volts
Vex - excitation voltage	

#### Channel Sensitivities

The 'Sensitivities' (output/input) for each channel are:

	Forces			Moments	
	uV/V x N	uV/V x lb		uV/V x N-m	uV/V x in-lb
Fx	0.3481	1.5486	Mx	0.7906	0.0893
Fy	0.3472	1.5446	My	0.7833	0.0885
Fz	0.0882	0.3922	Mz	1.7413	0.1967

#### Electro-Mechanical Center

Location of the center of the top plate relative to the effective XYZ center of the transducer








	Xo	Yo	Zo
Millimeters	0.8	-1.0	-39.6
Inches	0.031	-0.040	-1.559

AMTI



# APPENDIX 3

## Vicon systems technical data

							
Resolution (Megapixels)	16.0	4.0	2.0	1.0	1.0	1.0	0.3
Maximum Frame rate at full frame resolution	120	515	690	1000	250	250	240
Sensor	Vicon Avalon-16	Vicon Vegas-S-4	Vicon Vegas-S-2	Vicon Vegas-S-1	Vicon Vegas-1	CMOSIS	CMOSIS
On-Board Marker Processing	Yes	Yes	Yes	Yes	Yes	Yes	Yes
On-Board Data Selection	Yes	Yes	Yes	Yes	Yes	No	No
Power	Giganet	Giganet	Giganet	Giganet	Giganet	POE/Giganet	POE/Giganet
Lens Options	12.5mm 18mm 35mm	12.5mm 18mm 35mm	8.5mm 12.5mm 18mm	6mm 8.5mm 12.5mm	6mm 8.5mm 12.5mm	4-12mm zoom	4-12mm zoom
Field of View (H° x V°)	73 x 57 54 x 41 29 x 22	67 x 52 49 x 37 26 x 20	67 x 56 48 x 39 35 x 28	66 x 55 50 x 41 35 x 28	66 x 55 50 x 41 35 x 28	70 x 70 - 26 x 26	82 x 66 - 32 x 24
Strobe Options	NIR VR	NIR VR	NIR VR	NIR VR	NIR VR	NIR	NIR
Shutter Type	Electronic Freeze Frame Shutter	Electronic Freeze Frame Shutter	Electronic Freeze Frame Shutter	Electronic Freeze Frame Shutter	Electronic Freeze Frame Shutter	Electronic Freeze Frame Shutter	Electronic Freeze Frame Shutter
Connection type	Lemo - Lemo	Lemo - Lemo	Lemo - Lemo	Lemo - Lemo	Lemo - Lemo	RJ45 - RJ45 RJ45 - Lemo	RJ45 - RJ45 RJ45 - Lemo
Updateable Firmware	Yes	Yes	Yes	Yes	Yes	Yes	Yes





# APPENDIX 4

## Load cells force sensors specification sheet



8523 EN - 2

### Technical Data

Dim. tolerances acc. ISO 2768-f

Order Code	Load Range	Accuracy <sup>1)</sup> [%v.E.]	Sensitivity [mV/V]	ø D [mm]	H [mm]	Natural Frequency [kHz]	Weight [kg]	Wrench Torque for Mounting Screw 12.9
8523-20	0 ... 20 N	≤ ± 0.5	nominal <sup>2)</sup> 1.0	54.5	16	0.5	0.15	3 Nm
8523-50	0 ... 50 N	≤ ± 0.5	nominal <sup>2)</sup> 1.0	54.5	16	0.75	0.15	3 Nm
8523-100	0 ... 100 N	≤ ± 0.5	standardized 1.5 ± 0.5 %	54.5	16	0.80	0.15	3 Nm
8523-200	0 ... 200 N	≤ ± 0.2	standardized 1.5 ± 0.2 %	54.5	16	1.1	0.15	3 Nm
8523-500	0 ... 500 N	≤ ± 0.2	standardized 1.5 ± 0.2 %	54.5	16	2.3	0.15	3 Nm
8531-1000	0 ... 1000 N	≤ ± 0.25	standardized 1.5 ± 0.2 %	89.5	22	1.0	0.35	6 Nm
8531-2000	0 ... 2000 N	≤ ± 0.15	standardized 1.5 ± 0.2 %	99.5	30	1.8	0.35	6 Nm
8531-5000	0 ... 5000 N	≤ ± 0.15	standardized 1.5 ± 0.2 %	99.5	30	3.0	0.35	6 Nm

<sup>1)</sup> Combined value consisting of non-linearity, hysteresis and non-repeatability in constant installation position.

<sup>2)</sup> More or less deviation from stated is possible.

### Electrical values

Bridge resistance (full bridges): foil strain gauges: 350 Ω, nominal<sup>2)</sup>

Calibration resistor: model 8523-20 150 kΩ ± 0.1 %  
model 8523-50 100 kΩ ± 0.1 %  
others 80 kΩ ± 0.1 %

The bridge output voltage resulting from a shunt resistor of these values is shown in the calibration certificate.

Excitation:

range 0 ... 20 N  
range ≥ 0 ... 50 N

max. 5 V DC or AC  
max. 10 V DC or AC

### Environmental condition

Temperature operating: - 30 °C ... + 80 °C

Temperature compensated: + 15 °C ... + 70 °C

Temperature effect:

model 8523 ≤ ± 0.01 % F.S./K  
model 8531 ≤ ± 0.02 % F.S./K

Temperature effect to span: ≤ ± 0.02 % Rdg./K

### Mechanical values

Kind of measurement: tension or compression direction  
(calibrated in compression direction)

Deflection full scale: approx. 80 µm

Overload safe: 130 % of capacity

Overload burst: approx. 300 % of capacity

Dynamic performance: recommended 50 % of capacity,  
not suitable for large number of load cycles in tension or compression direction.

Casing material: high-grade aluminium, anodized

Natural frequency: see table

Protection class: acc. EN 60529

model 8523 IP52  
model 8531 IP64

Electrical termination:

Screened, highly flexible cable with free soldered ends, length approx. 2 m, ø 4.5 mm, bending radius > 40 mm. For model 8523 range ≥ 0 ... 100 N the standardization is integrated in the sensor cable (length 7 cm, ø 8 mm, distance from cable end 30 cm).

Wiring code:

white	excitation	positive
brown	excitation	negative
yellow	signal output	positive
green	signal output	negative

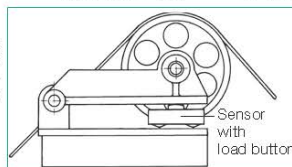
Dimension: see table and dimensions drawing

Weight: see table

Mounting: wrench torque for mounting screws, strength class 12.9 see table

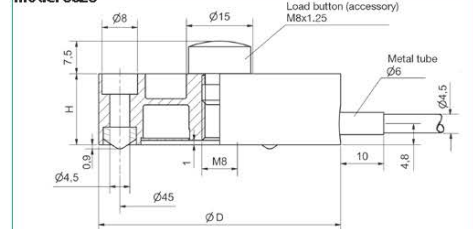
### Application example

A stable joint fastening of the arm protects the load cell against impermissible lateral and torsion forces.

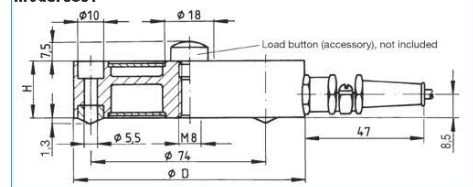


### Dimensional drawing

#### Model 8523



#### Model 8531



The CAD drawing (3D/2D) for this sensor can be imported online directly into your CAD system.

Download via [www.burster.com](http://www.burster.com) or directly at [www.traceparts.com](http://www.traceparts.com). For further information about the burster traceparts cooperation refer to data sheet 80-CAD-EN.

### Order Information

Compression and tension load cell, range 200 N **Model 8523-200**

### Accessories

**Mating connector**, 12 pin for burster desktop units except for 9163 **Model 9941**

**Mating connector**, 9 pins, for 9163-V3xxx, 9235 and 9310 **Model 9900-V209**

Mounting of mating connector to conductor cable for general use in preferential direction

in preferential direction (positive signal for compression)

**Order Code 99004**

Against preferential direction (positive signal for tension)

**Order Code 99007**

**Load button** for introduction of compressive forces polished and induction hardened (not included delivery) **Model 8580-V008**

**Pull plate** for measuring tension and compression forces (on both sides rings can be mounted)

for model 8523

**Model 8590-V002**

for model 8531 range 0...1 kN

**Model 8590-V006**

for model 8531 range 0...2 kN and 0...5 kN

**Model 8590-V007**

Amplifier, analysis and process control devices e.g. digital display 9180, in-line amplifier model 9235, modular amplifier model 9243, DIGIFORCE® 9307 **refer to section 9 of the catalog.**

### Factory Calibration Certificate (WKS)

Calibration of a load cell separately as well as connected to an indicator. Standard is a certificate with 11 points, starting at zero, running up and down in 20% increments covering the complete measuring range for preferential direction. Special calibrations on request. Calculation of costs by base price plus additional costs per point.

**Order Code 85WKS-85...**

Technical changes reserved -

Latest updates of data sheet always under [www.burster.com](http://www.burster.com)

burster praezisionsmesstechnik gmbh & co kg · Tel. +49-7224-6450 · Fax 64588  
Telstr. 1-5 · DE 76593 Gernsbach · [www.burster.com](http://www.burster.com) · [info@burster.com](mailto:info@burster.com)

1217-008523EN-5072-061519



# APPENDIX 5

## Load cells amplifier specification sheet



9235 EN - 2

### Technical Data

#### Connectable sensors

##### Strain gauges

Bridge resistance (full bridge):	350 Ω ... 5 kΩ
Connection technology:	4 wire
Sensor excitation voltage:	2.5 V
Excitation current:	10 mA max.
Power consumption:	approx 0.3 VA
Adjustable input:	0.8 mV/V ... 2.5 mV/V

#### Analog output

Voltage output:	0 ... ± 10 V
Output impedance:	470 Ω

#### General amplifier characteristics

Accuracy:	< 0,1 %
Temperature coefficient:	< 100 ppm/K
Power supply:	15 ... 30 V DC
Frequency response:	1 kHz
Operating temperature:	0 ... 60 °C

Plug connection model 9235

"Excitation and output" plug	pin 2 + excitation voltage
	pin 3 shield
	pin 5 - excitation voltage
	pin 7 ± output voltage
	pin 9 output ground

"Sensor" socket	pin 1 + sensor excitation
	pin 3 shield
	pin 5 - sensor excitation
	pin 6 + signal input
	pin 9 - signal input

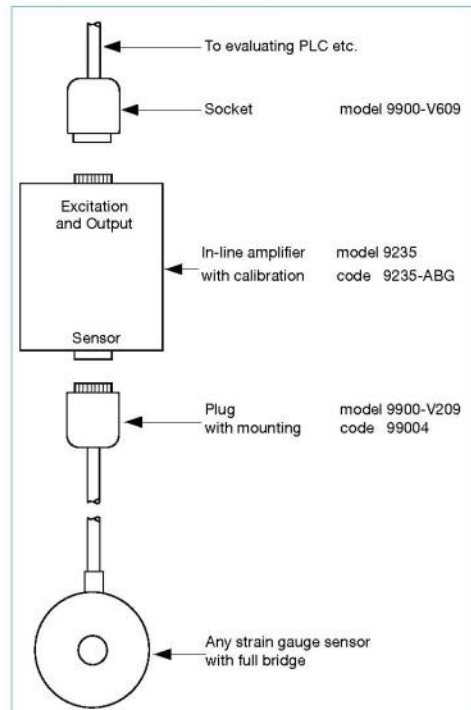
#### Housing

Connections:	Sub-D plug / mating connector
Dimensions (W x H x D):	62 x 55 x 16 [mm]
Material:	Aluminium
Mounting:	clamp or stick on
Protection class:	IP40
Weight:	< 65 g
Humidity:	10 ... 80 %, not dewing

#### Default setting

Sensor output:	1.5 mV/V
----------------	----------

### Example of a measuring chain



The CAD drawing (3D/2D) for this device can be imported online directly into your CAD system. Download via [www.burster.com](http://www.burster.com) or directly at [www.traceparts.com](http://www.traceparts.com). For further information about the burster traceparts cooperation refer to data sheet 80-CAD-EN.

### Order Information

In-line amplifier with housing including cable tie bracket **Model 9235**

Calibration of entire measuring chain Consisting of sensor and amplifier model 9235

Order Code **9235-ABG**

A sensor specific standard adjustment will be done, if no customer specific adjustment data are supplied.

### Accessories

Connectors	socket	<b>Model 9900-V609</b>
	plug	<b>Model 9900-V209</b>
not part of scope of delivery		



# APPENDIX 6

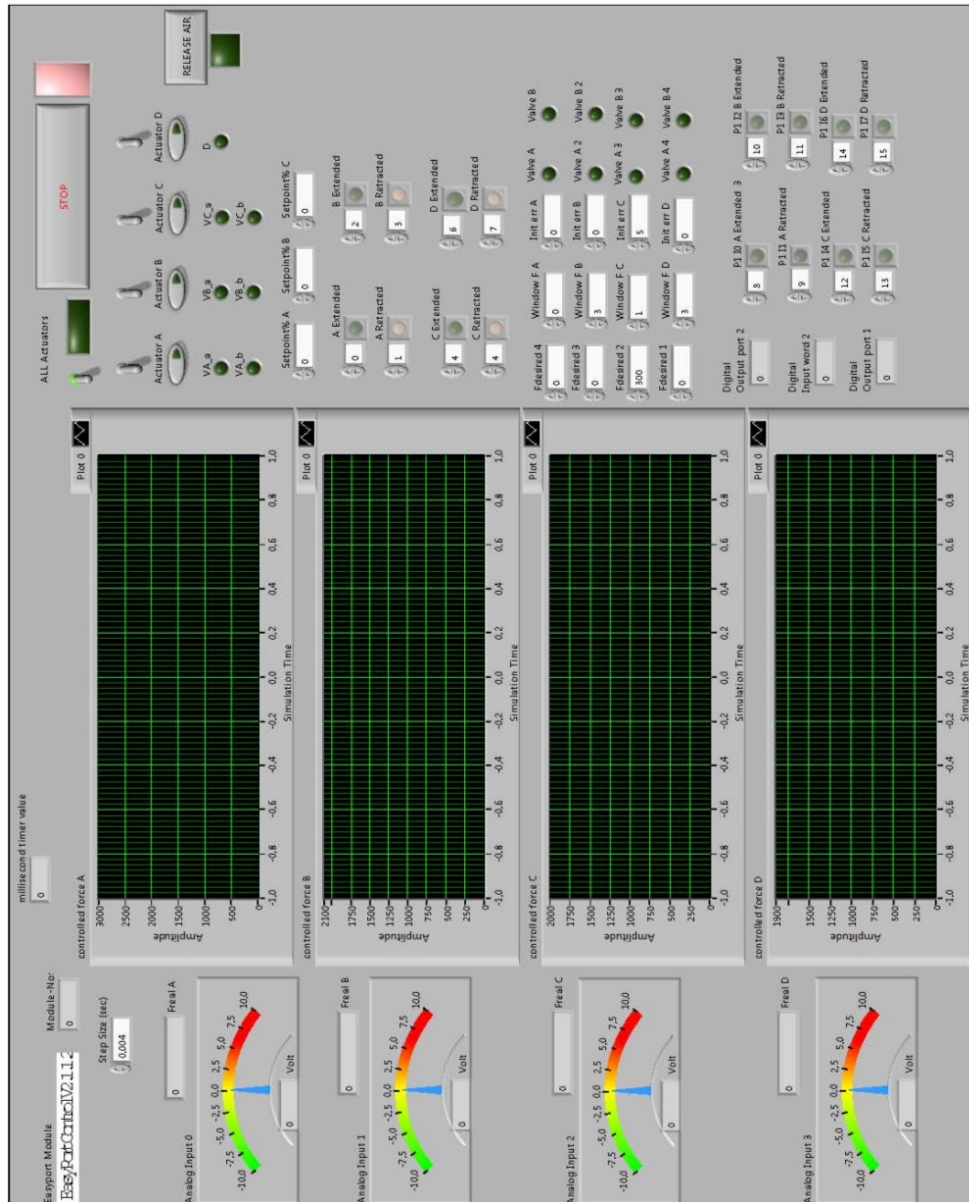
## EasyPort USB technical data

EasyPort USB D16A process interface	
Operating voltage	24 V DC $\pm 10\%$
Power consumption	3 VA
Number of outputs	16 digital: 24 V DC, 2 analogue: 0...10 V DC or -10...+10 V DC, 12 bit resolution
Output load capacity	0,7 A per digital output, 10 mA per analogue output
Short circuit protection	Yes
Number of inputs	16 digital: 24 V DC, 4 analogue: 0...10 V DC or -10...+10 V DC, 12 bit resolution
Digital input switching threshold	12 V DC
Digital input hysteresis	3 V
Filter	5 ms
Number of counters	2 inputs usable as high-speed counters, $f_{max} = 20 \text{ kHz}/U_{in} = 5 \text{ to } 24 \text{ V DC}$
Communication interfaces	RS 232, electrically isolated, USB 2.0, electrically isolated
Protocol	ASCII, 115.2 kBaud, 8, N, 1
Protection	IP 20
CE mark	Per EU/EMC directive
Permissible ambient temperature, operation/storage	0...55° C/0...70° C
Dimensions in mm (L x W x H)	135 x 167 x 37
Weight in kg	0,65



# APPENDIX 7

## Main control panel in LabVIEW

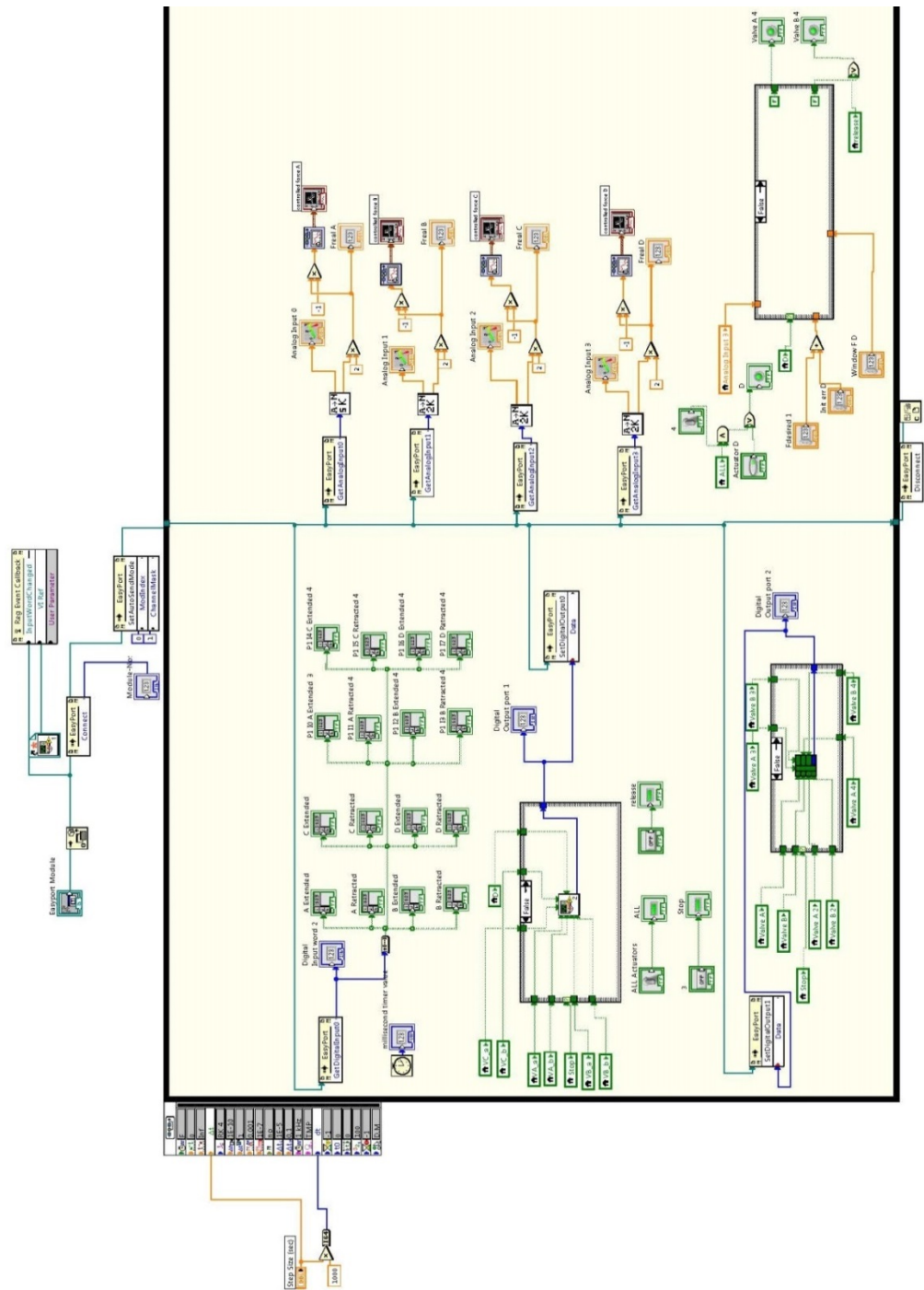


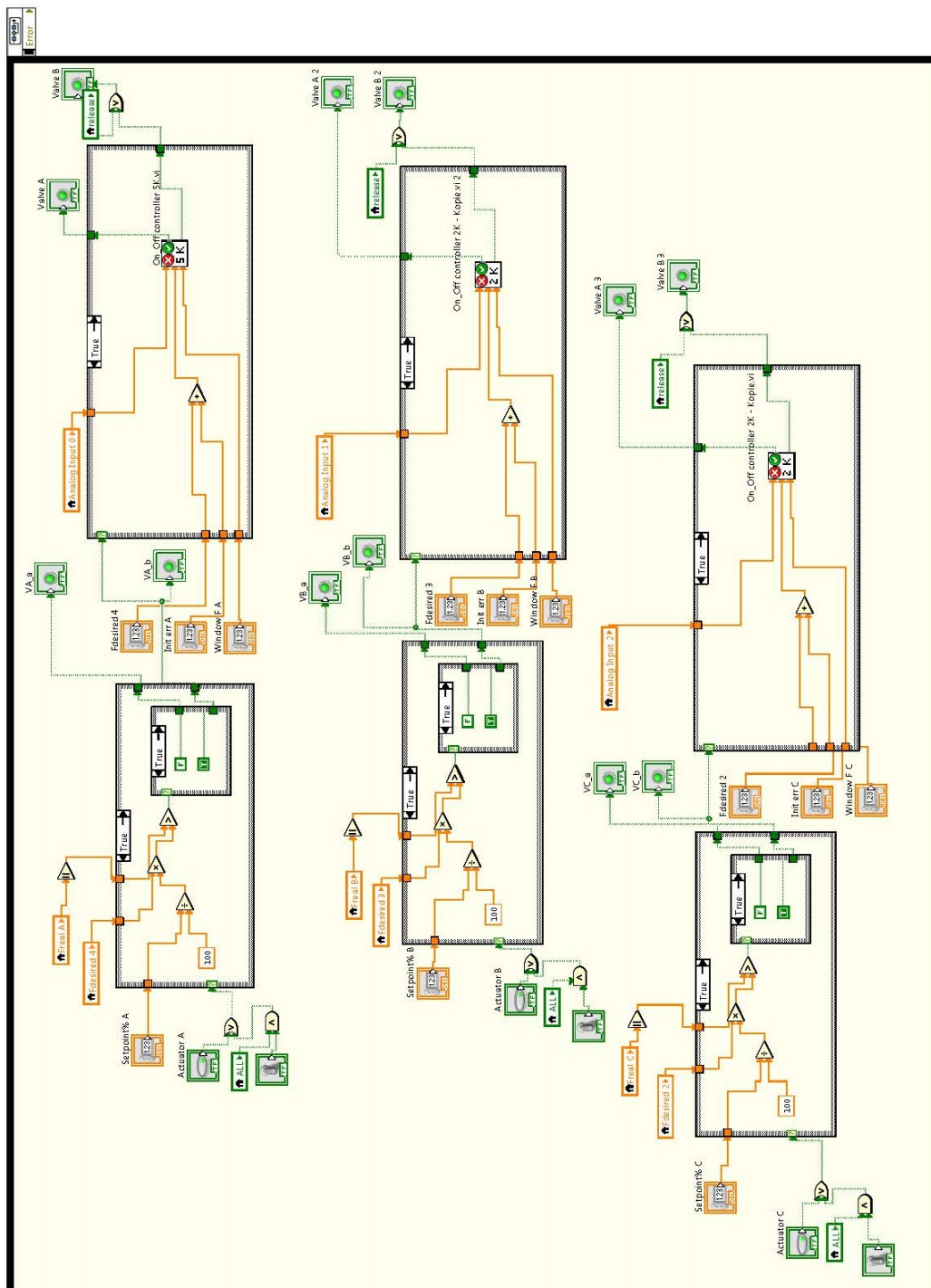




# APPENDIX 8

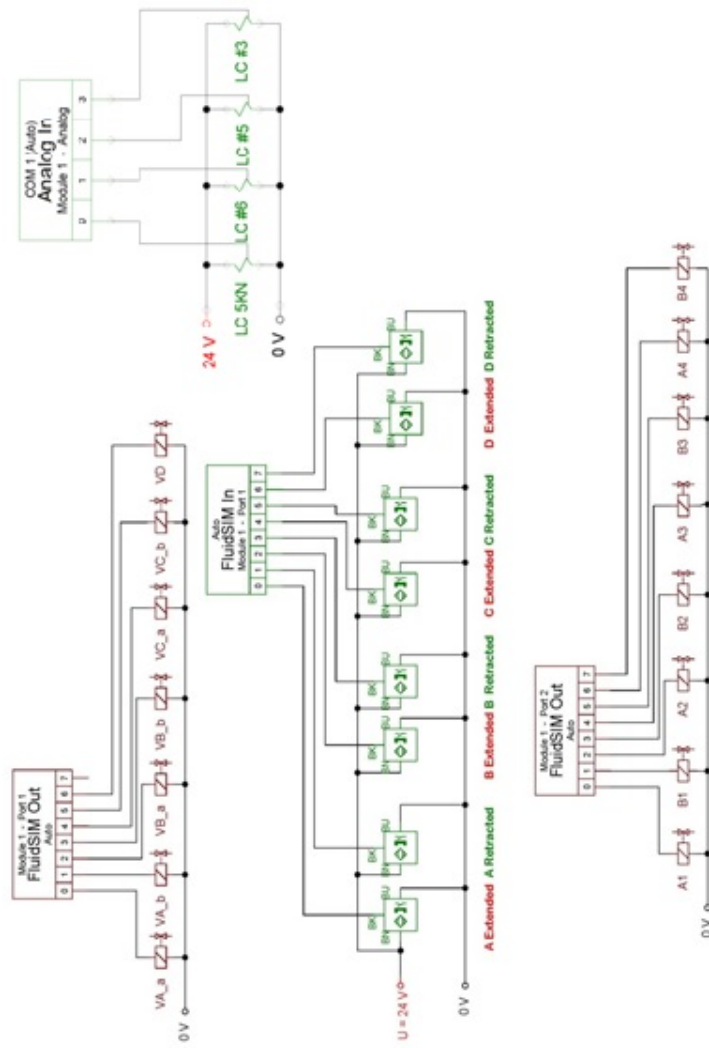
## Control program circuit in LabVIEW





# APPENDIX 9

## Electric circuits of the control system





# APPENDIX 10

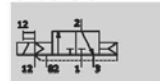
## Phase control valves for pneumatic actuators specification sheets

### Solenoid valves CPE14

Technical data

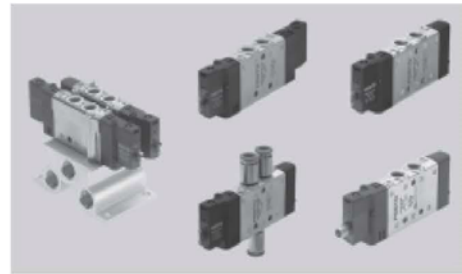
FESTO

Function  
3/2G, 3/2O  
5/2-way single solenoid  
5/2-way double solenoid  
5/3G, 5/3B, 5/3E



3/2-way valve with external pilot air supply,  
normally closed

- Width 14 mm
- Flow rate  
370 ... 900 l/min
- Voltage  
24 V DC



General technical data											
Valve function		3/2			5/2		5/3				
Normal position		G <sup>1)</sup>	O <sup>2)</sup>	–		–	G <sup>1)</sup>	B <sup>2)</sup>	E <sup>3)</sup>		
Memory stability		Single solenoid				Double solenoid	Single solenoid				
Pneumatic spring reset method		Yes				–	No				
Mechanical spring reset method		No				–	Yes				
Design		Piston spool									
Sealing principle		Soft									
Actuation type		Electric									
Control type		Piloted									
Pilot air supply		Internal or external									
Direction of flow		–			Reversible with external pilot air supply						
Exhaust function		–			Flow control						
Manual override		Non-detenting, detenting via accessory									
Type of mounting		Using through holes									
Mounting position		Any									
Pneumatic connection	1, 2, 4	Threaded connection: G $\frac{1}{8}$ ; QS connection: $\varnothing$ 6 or $\varnothing$ 8 mm									
	3, 5	Threaded connection: G $\frac{3}{8}$									
	12, 14	Threaded connection: M3; QS connection: $\varnothing$ 3									
	82, 84	Threaded connection: M3									
Nominal diameter		[mm]	6								
Standard nominal flow rate		G $\frac{1}{8}$	[l/min]	900		800		750		700	
Standard nominal flow rate		QS6	[l/min]	510		400		410		370	
Standard nominal flow rate		QS8	[l/min]	810		680		720		650	570
Switching time on/off		[ms]	16/27		24/32		–		20/42		
Changeover time		[ms]	–			12		–			
Duty cycle		[%]	100								
Width		[mm]	14								
Corrosion resistance class		CRC	2 <sup>4)</sup>								

1) G = Normally closed

2) O.B. = Normally open

3) E = Normally exhausted

4) Corrosion resistance class 2 as per Festo standard 940 070

Components subject to moderate corrosion stress. Externally visible parts with primarily decorative surface requirements which are in direct contact with a normal industrial environment or media such as coolants or lubricating agents.

## Solenoid valves CPE18

Technical data

FESTO

Functions:

3/2G, 3/2O

5/2-way single solenoid

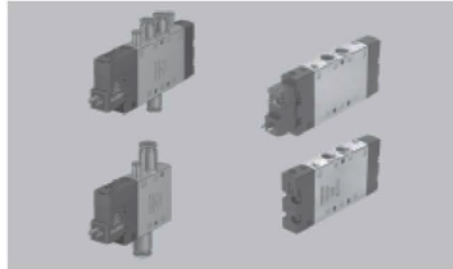
5/2-way double solenoid

5/3G, 5/3B, 5/3E



3/2G with external pilot air supply,  
normally closed

- Width 18 mm
- Flow rate  
850 ... 1,500 l/min
- Voltage for  
complete valves  
24 V DC, 110, 230 V AC  
basic valves  
12, 24 V DC, 24, 110,  
230 V AC



General technical data						
Valve function		3/2		5/2	5/3	
Normal position		G <sup>1)</sup>	O <sup>2)</sup>	–	G <sup>1)</sup>	B <sup>2)</sup> E <sup>3)</sup>
Memory stability		Single solenoid			Double solenoid	Single solenoid
Pneumatic spring reset method		Yes			–	No
Mechanical spring reset method		No			–	Yes
Design		Piston spool				
Sealing principle		Soft				
Actuation type		Electric				
Control type		Piloted				
Pilot interface		To ISO 15218 or none in the case of integrated pilot valve				
Pilot air supply		Internal or external				
Direction of flow		–		Reversible with external pilot air supply		
Exhaust function		–		Flow control		
Manual override		Non-detenting, detenting via accessory				
Type of mounting		Using through holes				
Mounting position		Any				
Pneumatic connection	1, 2, 4	Threaded connection: G¼; QS connection: Ø 8 or Ø 10 mm				
	3, 5	Threaded connection: G¼				
	12, 14	Threaded connection: M5; QS connection: Ø 4				
	82, 84	Threaded connection: M5				
Nominal diameter	[mm]	8				
Standard nominal flow rate	G¼	[l/min]	1,300	1,300	1,450	1,200 1,300
Standard nominal flow rate	QS8	[l/min]	850			780
Standard nominal flow rate	QS10	[l/min]	1,000		1,050	1,000
Switching time on/off	[ms]	28/18, 36/30 <sup>5)</sup>	26/20, 32/30 <sup>5)</sup>	–	20/38, 20/34 <sup>5)</sup>	
Changeover time	[ms]	–		13, 15 <sup>5)</sup>	–	
Duty cycle	[%]	100				
Width	[mm]	18				
Conforms to		ISO 15218 in the case of interface with pilot valve				
Corrosion resistance class	CRC	2 <sup>4)</sup>				

1) G = Normally closed

2) O, B = Normally open

3) E = Normally exhausted

4) Corrosion resistance class 2 as per Festo standard 940 070

Components subject to moderate corrosion stress. Externally visible parts with primarily decorative surface requirements which are in direct contact with a normal industrial environment or media such as coolants or lubricating agents.

5) Switching time for basic valve

# APPENDIX 11

## Valves for ON/OFF control specification sheet

### Isonic® V1000 Series (2 and 3-Way)

### Control Valves

Specifications	
Design :	Poppet
Media:	Air or Inert Gas
Lubrication:	None Required
Filtration:	40 micron
Cycle Life:	50,000,000 cycles
Orifice Size:	A: 0.025" / 0.65mm B: 0.035" / 0.90mm C: 0.055" / 1.4mm
Flow:	A: 0.01 C <sub>v</sub> B: 0.02 C <sub>v</sub> C: 0.05 C <sub>v</sub>
Maximum Pressure:	A: 120 PSI / 8.3 Bar B: 120 PSI / 8.3 Bar C: 30 PSI / 2.1 Bar
Vacuum:	to 28 in .Hg
Temperature Range:	0° - 120°F / 49°C
Tubing:	1/8" or 4mm
Mounting Holes:	0.156 diameter (1 hole, 1 slot)
Seals:	Viton® and Nitrile
Weight:	1.5 oz. (per valve)

#### Solenoid Data

Voltage	12DC	24DC	24AC	120 AC
Amps	0.133	0.058	0.058	0.014
Resistance	92Ω	406Ω	406Ω	8350Ω
Initial Power	1.6	1.4	1.4	1.7
Continuous On	1.3	1.2	1.2	1.5

Response Time: 10 milliseconds

Molex Connector: UL and CSA Listed

Din Connector: Protection Class- IP 65 according to DIN 40 050  
Insulation Class- Group C according to VDE 0110  
Conform to DIN 43650 Form C Specifications

#### Manifold

Common Air Inlet: Built-in, push-in fittings for 1/8" OD or 6mm tubing both ends

Foot Mounting: 4 slots, 11/16" diameter

DIN Rail Mounting: Attaches to 15mm DIN rail

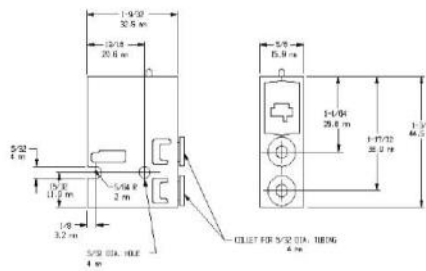
#### Valve Symbols:



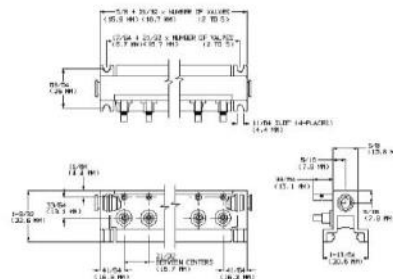
#### Dimensions



#### Valves:



#### Manifolds



#### Accessories



P1SA1



P1SA2



P1Q1

NOTE: (1) pc. is included with each "W" type valve. 24 AWG wire.



MM-019

Muffler shown here on V1 Valve with T1 option





## APPENDIX 12

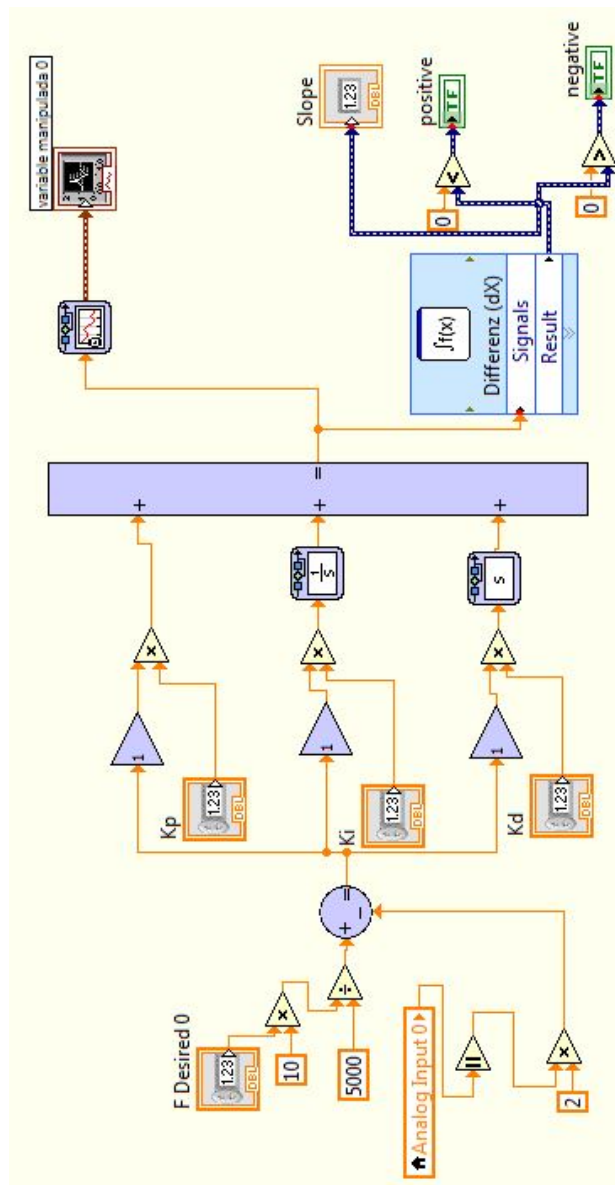
### PID control panel

F Desired A	F Desired B	F Desired C	F Desired D
<input type="text" value="1000"/>	<input type="text" value="0"/>	<input type="text" value="300"/>	<input type="text" value="0"/>
positive <input type="radio"/>	positive 2 <input type="radio"/>	positive 3 <input type="radio"/>	positive 4 <input type="radio"/>
negative <input checked="" type="radio"/>	negative 2 <input type="radio"/>	negative 3 <input type="radio"/>	negative 4 <input type="radio"/>
Slope <input type="text" value="-0,512"/>	Slope 2 <input type="text" value="-1,28"/>	Slope 3 <input type="text" value="-0,544"/>	Slope 4 <input type="text" value="0"/>
Kp <input type="text" value="0,1"/>	Kp 2 <input type="text" value="0,1"/>	Kp 3 <input type="text" value="0,1"/>	Kp 4 <input type="text" value="0"/>
Ki <input type="text" value="64"/>	Ki 2 <input type="text" value="128"/>	Ki 3 <input type="text" value="64"/>	Ki 4 <input type="text" value="0"/>
Kd <input type="text" value="4"/>	Kd 2 <input type="text" value="4"/>	Kd 3 <input type="text" value="4"/>	Kd 4 <input type="text" value="0"/>



# APPENDIX 13

## PID control circuit in LabVIEW





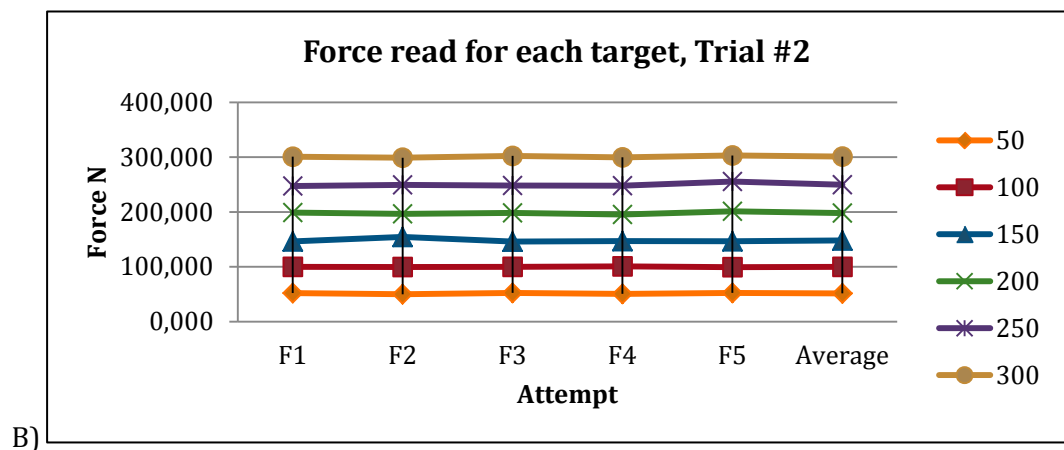
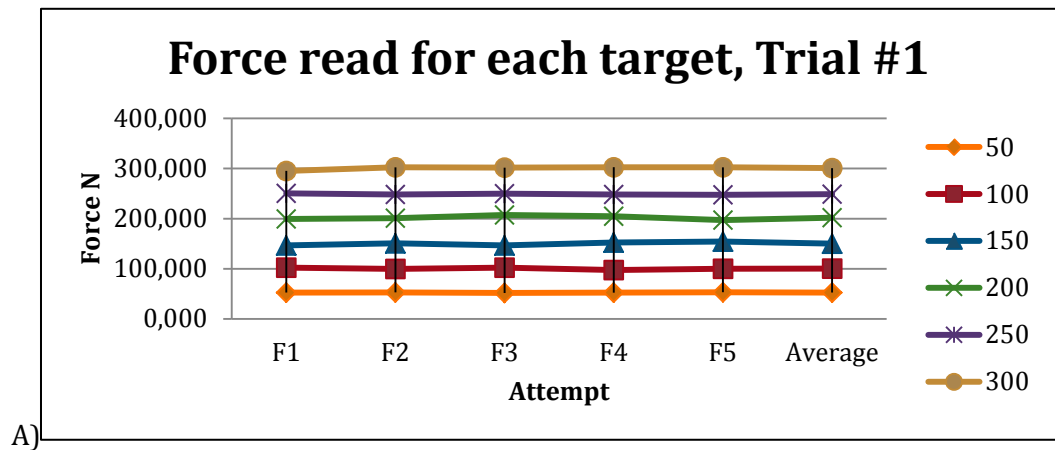
## APPENDIX 14

Force control test results for each actuator

Forces applied and results on Actuator D. Cylinder of 32mm diameter. Maximum force of 382N at 6 bar. Mounted to load cell #3.

TRIAL #1								
Force desired	F1	F2	F3	F4	F5	Average	Standard Dev	Order
50	52,599	52,895	51,848	52,451	53,284	52,615	0,534	1
100	102,249	99,810	102,257	97,647	100,230	100,439	1,925	2
150	146,788	150,823	146,764	152,402	154,211	150,198	3,346	3
200	199,485	201,092	207,329	204,905	197,185	201,999	4,098	4
250	250,419	248,104	249,956	248,291	247,715	248,897	1,207	5
300	295,292	302,373	301,696	302,556	302,342	300,852	3,125	6
TRIAL #2								
Force desired	F1	F2	F3	F4	F5	Average	Standard Dev	Order
50	52,206	49,965	52,401	50,770	52,397	51,548	1,117	3
100	99,892	99,588	99,966	100,837	99,394	99,935	0,555	2
150	146,399	154,600	146,185	146,858	146,780	148,164	3,608	1
200	198,827	196,703	198,469	195,427	201,278	198,141	2,228	4
250	247,509	249,299	248,299	247,925	255,617	249,730	3,357	6
300	300,895	298,953	302,338	299,658	303,093	300,987	1,744	5

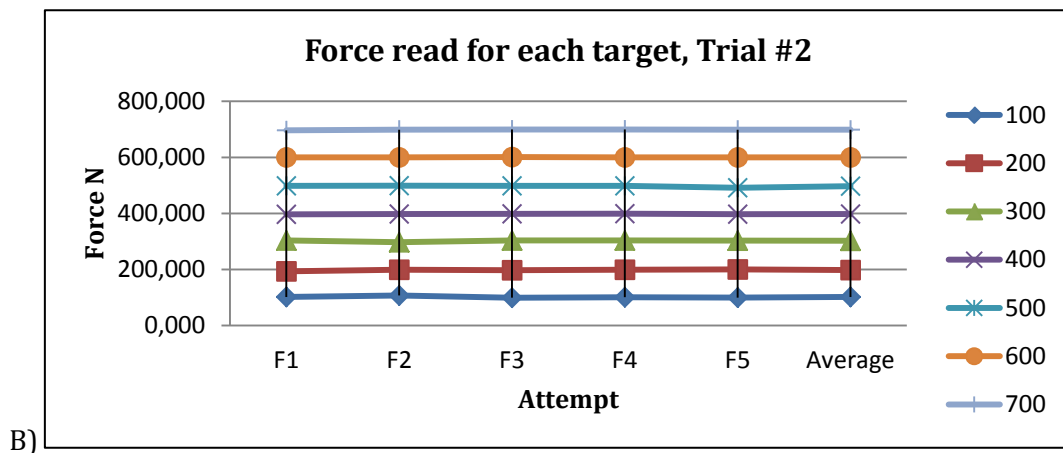
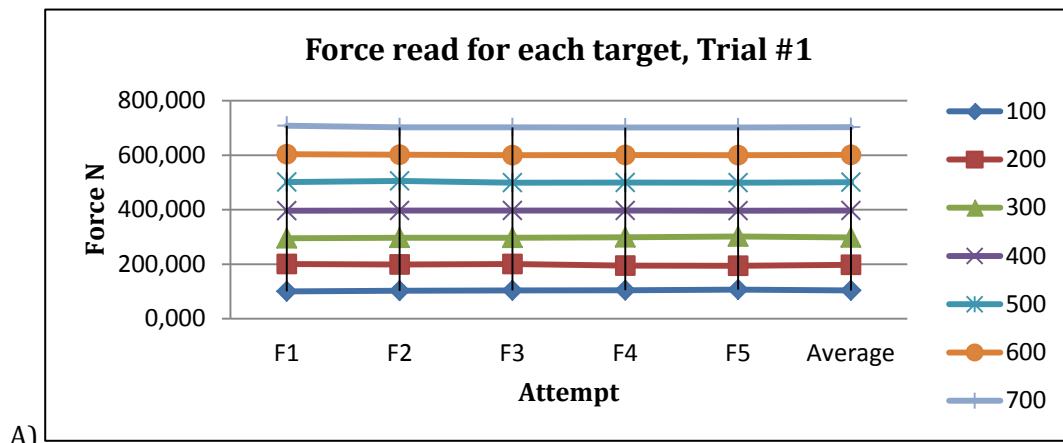
Forces read on each trial for actuator D. A) Ascending order, B) Random order.



Forces applied and results on Actuator C. Cylinder of 50mm diameter. Maximum force of 999N at 6 bar. Mounted to load cell #5.

<b>cylinder 50</b>	<b>999N</b>	<b>Load cell #5</b>						
	<b>at 6 bar</b>							
<b>TRIAL #1</b>								
<b>Force desired</b>	<b>F1</b>	<b>F2</b>	<b>F3</b>	<b>F4</b>	<b>F5</b>	<b>Average</b>	<b>Standard Dev</b>	<b>Order</b>
100	100,349	102,590	103,657	104,676	106,913	103,637	2,435	1
200	200,646	199,230	200,763	194,771	194,277	197,937	3,179	2
300	295,617	297,231	296,870	299,033	301,776	298,105	2,388	3
400	396,684	396,922	397,256	396,856	396,696	396,883	0,232	4
500	501,421	505,674	499,067	499,771	499,055	500,998	2,786	5
600	604,053	602,033	600,220	600,963	600,076	601,469	1,639	6
700	708,307	702,194	702,257	701,809	701,949	703,303	2,803	7
<b>TRIAL #2</b>								
<b>Force desired</b>	<b>F1</b>	<b>F2</b>	<b>F3</b>	<b>F4</b>	<b>F5</b>	<b>Average</b>	<b>Standard Dev</b>	<b>Order</b>
100	101,980	107,372	99,551	101,170	99,894	101,993	3,161	2
200	193,705	199,230	197,627	199,502	200,475	198,108	2,666	1
300	303,601	297,609	303,690	303,648	303,173	302,344	2,655	3
400	396,852	398,027	398,665	399,081	397,163	397,958	0,952	4
500	498,507	498,958	498,355	498,663	491,686	497,234	3,109	7
600	600,022	599,983	601,092	600,154	600,057	600,262	0,468	6
700	696,568	698,884	699,498	699,623	698,818	698,678	1,233	5

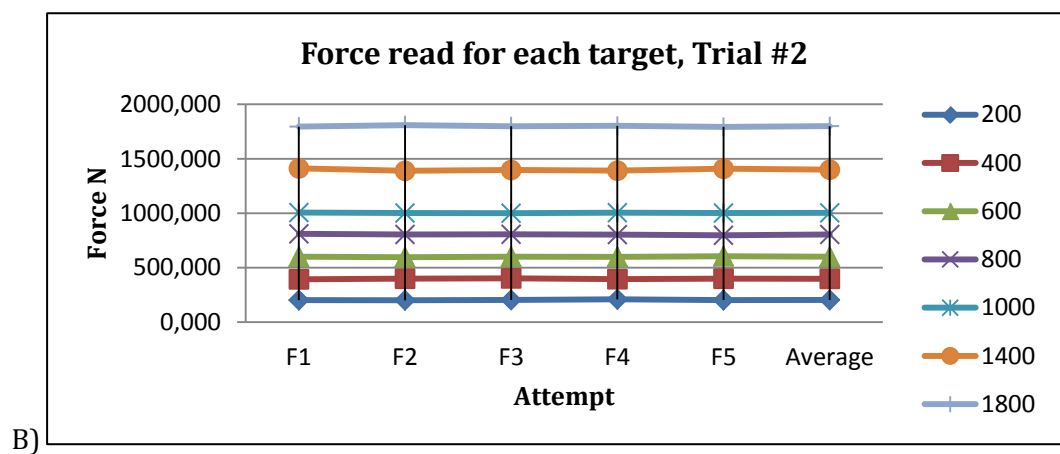
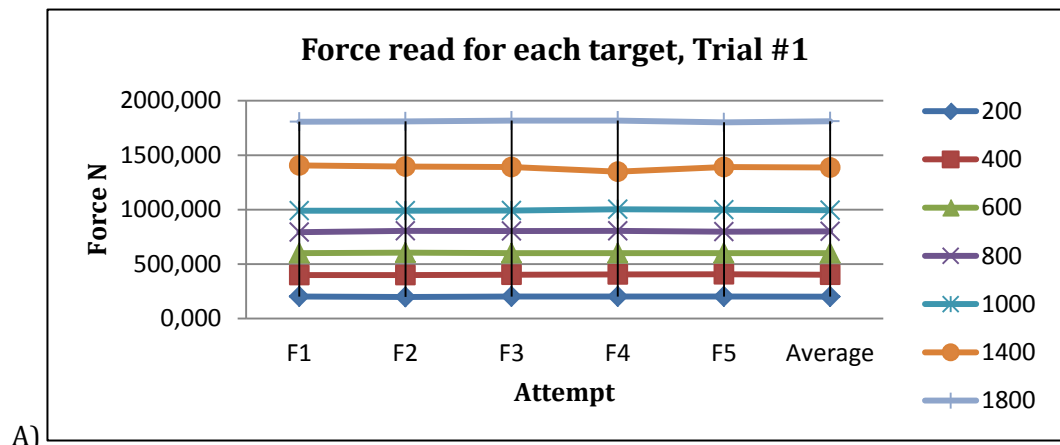
Forces read on each trial for actuator C. A) Ascending order, B) Random order.



Forces applied and results on Actuator B. Cylinder of 80mm diameter. Maximum force of 2733N at 6 bar. Mounted to load cell #6.

<i>cylinder 80</i>	<b>2733N</b>	<b>Load cell #6</b>						
	<b>at 6 bar</b>							
TRIAL #1								
Force desired	F1	F2	F3	F4	F5	Average	Standard Dev	Order
200	201,495	197,390	201,277	201,094	201,079	200,467	1,728	1
400	398,121	398,078	401,669	404,206	405,782	401,571	3,492	2
600	599,863	604,162	600,228	600,026	599,505	600,757	1,922	3
800	792,788	805,099	803,776	804,593	796,940	800,639	5,493	4
1000	990,041	989,535	990,675	1002,818	998,748	994,363	6,048	5
1400	1406,145	1395,312	1390,954	1348,369	1390,592	1386,275	22,101	6
1800	1807,653	1810,824	1818,013	1818,258	1801,709	1811,291	7,053	7
TRIAL #2								
Force desired	F1	F2	F3	F4	F5	Average	Standard Dev	Order
200	201,522	199,530	203,063	208,833	202,176	203,025	3,498	2
400	393,284	399,113	401,529	394,000	399,109	397,407	3,585	1
600	599,396	595,575	600,244	598,847	605,197	599,852	3,472	3
800	810,733	805,224	806,383	803,776	797,819	804,787	4,681	4
1000	1005,920	1001,355	1000,713	1005,122	1001,550	1002,932	2,400	7
1400	1411,242	1390,160	1397,288	1391,451	1408,261	1399,680	9,635	6
1800	1795,454	1808,715	1798,788	1802,701	1792,766	1799,685	6,269	5

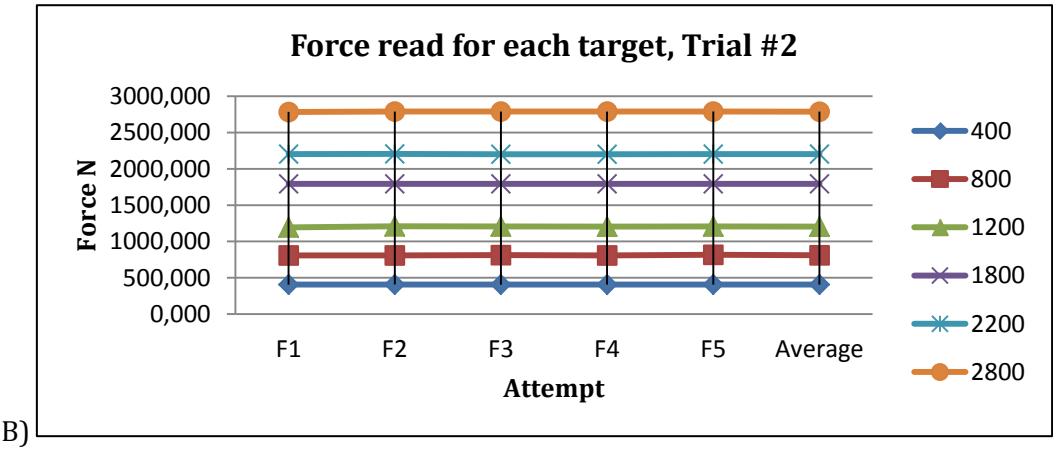
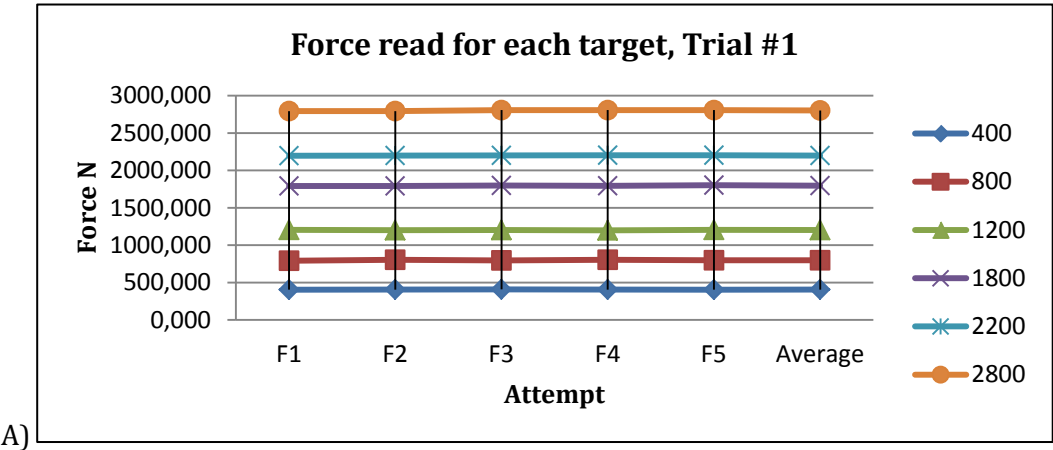
Forces read on each trial for actuator B. A) Ascending order, B) Random order.



Forces applied and results on Actuator A. Cylinder of 100mm diameter. Maximum force of 4222N at 6 bar. Mounted to load cell #7 (5K).

cylinder 100	4222N	Load cell 5K						
	at 6 bar							
TRIAL #1								
Force desired	F1	F2	F3	F4	F5	Average	Standard Dev	Order
400	404,879	406,747	408,965	406,124	404,976	406,338	1,665	1
800	792,880	805,691	796,051	805,117	797,822	799,512	5,666	2
1200	1206,062	1201,713	1203,921	1198,308	1205,866	1203,174	3,239	3
1800	1792,040	1792,749	1799,645	1793,518	1803,186	1796,228	4,926	4
2200	2196,140	2198,416	2201,091	2202,453	2202,326	2200,085	2,738	5
2800	2793,395	2793,832	2807,218	2807,393	2807,889	2801,945	7,611	6
TRIAL #2								
Force desired	F1	F2	F3	F4	F5	Average	Standard Dev	Order
400	406,105	406,465	405,667	405,667	405,074	405,796	0,524	3
800	806,994	807,325	811,410	807,062	815,855	809,729	3,896	1
1200	1193,066	1208,000	1207,706	1205,606	1206,190	1204,114	6,257	2
1800	1793,138	1792,672	1792,944	1793,547	1793,955	1793,251	0,506	5
2200	2202,696	2204,934	2201,053	2202,453	2202,900	2202,807	1,392	6
2800	2784,816	2789,777	2789,540	2790,030	2790,458	2788,924	2,322	4

Forces read on each trial for actuator A. A) Ascending order, B) Random order.



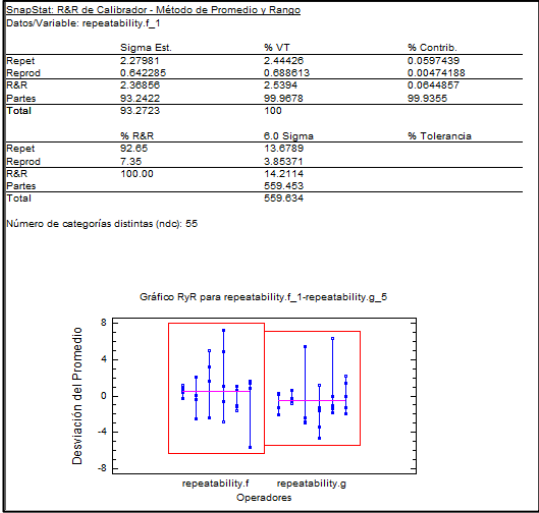


# APPENDIX 15

## Statistical results of the control system for each actuator (Spanish)

### Actuator D

#### Repeatability and Reproducibility. Percentages chart and results graph.



Con base en un estudio involucrando 2 operadores, cada uno midiendo 6 partes 5 veces, la desviación estándar estimada del proceso de medición es igual a 2.36856. De la varianza total, 7.35% es debida a diferencias entre operadores (Reproducibilidad) en tanto que 92.65% es debida al instrumento (Repetibilidad).

Comparando la variabilidad del proceso de medición con la variabilidad total en repeatability.f\_1, el proceso de medición contribuye 0.06%, con el resto 99.94%, atribuible a las diferencias entre partes.

También se muestra una gráfico de rangos. Esta gráfico muestra el rango de cada grupo de 5 mediciones hechas por 2 operadores en 6 partes. El límite superior se coloca a la distancia usual de 3 sigmas para la gráfico de rangos. En este caso, no hay grupos fuera del límite de control, lo que implica un nivel consistente de variabilidad entre los grupos.

#### Accuracy. Percentages chart.

Partes: accuracy.Part  
Mediciones: accuracy.f\_1  
Valores de referencia: accuracy.reference  
Variación de proceso:

Número de Partes: 60  
Número total de mediciones: 60  
Número de mediciones excluidas: 0  
Rango de valores de referencia: 50 - 300

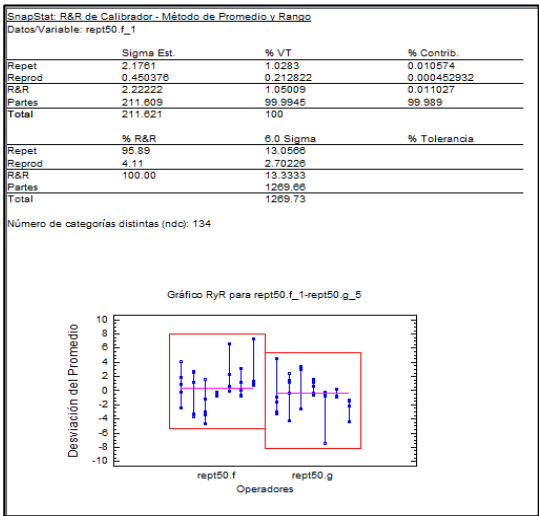
Estimados	Estimado	Porcentaje
Bias	0.292185	0.117
Linealidad	1.07731	0.431

Modelo de bias: 1.0463 - 0.00430925x

Parámetro	Estimado	Error Estnd.	Estadístico t	Valor_P
Intercepto	1.0463	0.784027	1.33453	0.1872
Pendiente	-0.00430925	0.00402639	-1.07025	0.2889

Actuator C

Repeatability and Reproducibility. Percentages chart and results graph.

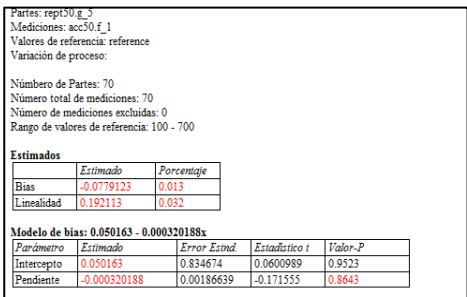


Con base en un estudio involucrando 2 operadores, cada uno midiendo 7 partes 5 veces, la desviación estándar estimada del proceso de medición es igual a 2.22222. De la varianza total, 4.11% es debida a diferencias entre operadores (Reproducibilidad) en tanto que 95.89% es debida al instrumento (Repetibilidad).

Comparando la variabilidad del proceso de medición con la variabilidad total en rept50\_f\_1, el proceso de medición contribuye 0.01%, con el resto 99.99%, atribuible a las diferencias entre partes.

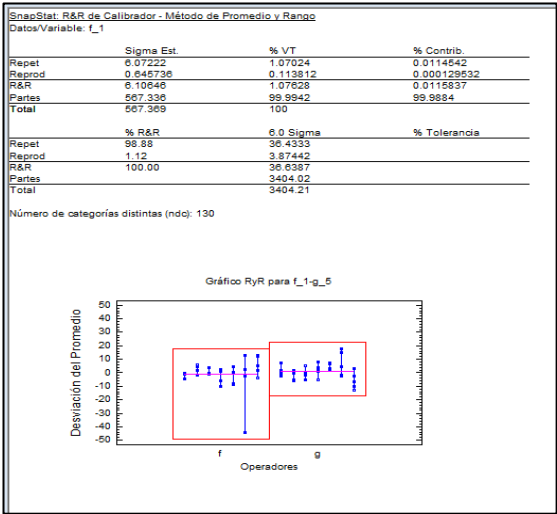
También se muestra una gráfico de rangos. Esta gráfico muestra el rango de cada grupo de 5 mediciones hechas por 2 operadores en 7 partes. El límite superior se coloca a la distancia usual de 3 sigmas para la gráfico de rangos. En este caso, no hay grupos fuera del límite de control, lo que implica un nivel consistente de variabilidad entre los grupos.

Accuracy. Percentages chart.



Actuator B

Repeatability and Reproducibility. Percentages chart and results graph.

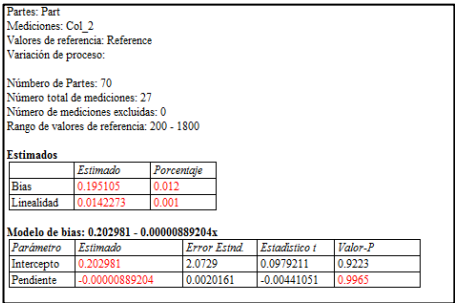


Con base en un estudio involucrando 2 operadores, cada uno midiendo 7 partes 5 veces, la desviación estándar estimada del proceso de medición es igual a 6.10646. De la varianza total, 1.12% es debida a diferencias entre operadores (Reproducibilidad) en tanto que 98.88% es debida al instrumento (Repetibilidad).

Comparando la variabilidad del proceso de medición con la variabilidad total en f\_1, el proceso de medición contribuye 0.01%, con el resto 99.99%, atribuible a las diferencias entre partes.

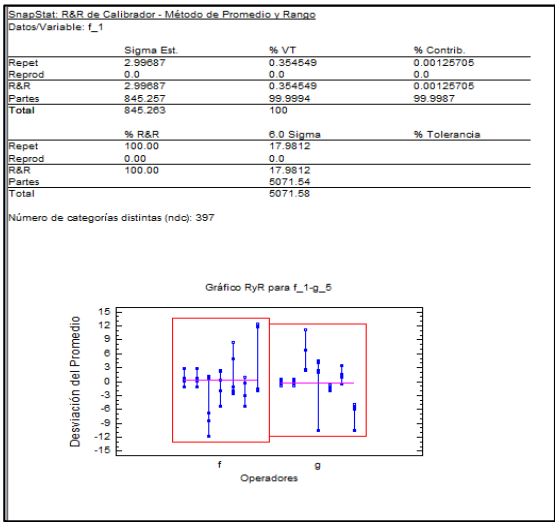
También se muestra una gráfico de rangos. Esta gráfico muestra el rango de cada grupo de 5 mediciones hechas por 2 operadores en 7 partes. El límite superior se coloca a la distancia usual de 3 sigmas para la gráfico de rangos. En este caso, no hay grupos fuera del límite de control, lo que implica un nivel consistente de variabilidad entre los grupos.

Accuracy. Percentages chart.



Actuator A

Repeatability and Reproducibility. Percentages chart and results graph.

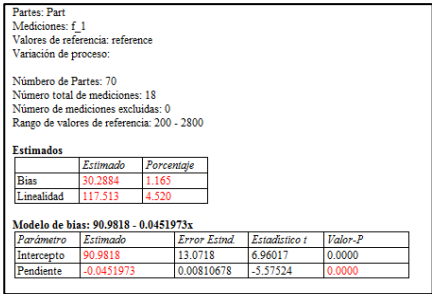


Con base en un estudio involucrando 2 operadores, cada uno midiendo 7 partes 5 veces, la desviación estándar estimada del proceso de medición es igual a 2.99687. De la varianza total, 0.00% es debida a diferencias entre operadores (Reproducibilidad) en tanto que 100.00% es debida al instrumento (Repetibilidad).

Comparando la variabilidad del proceso de medición con la variabilidad total en f\_1, el proceso de medición contribuye 0.00%, con el resto 100.00%, atribuible a las diferencias entre partes.

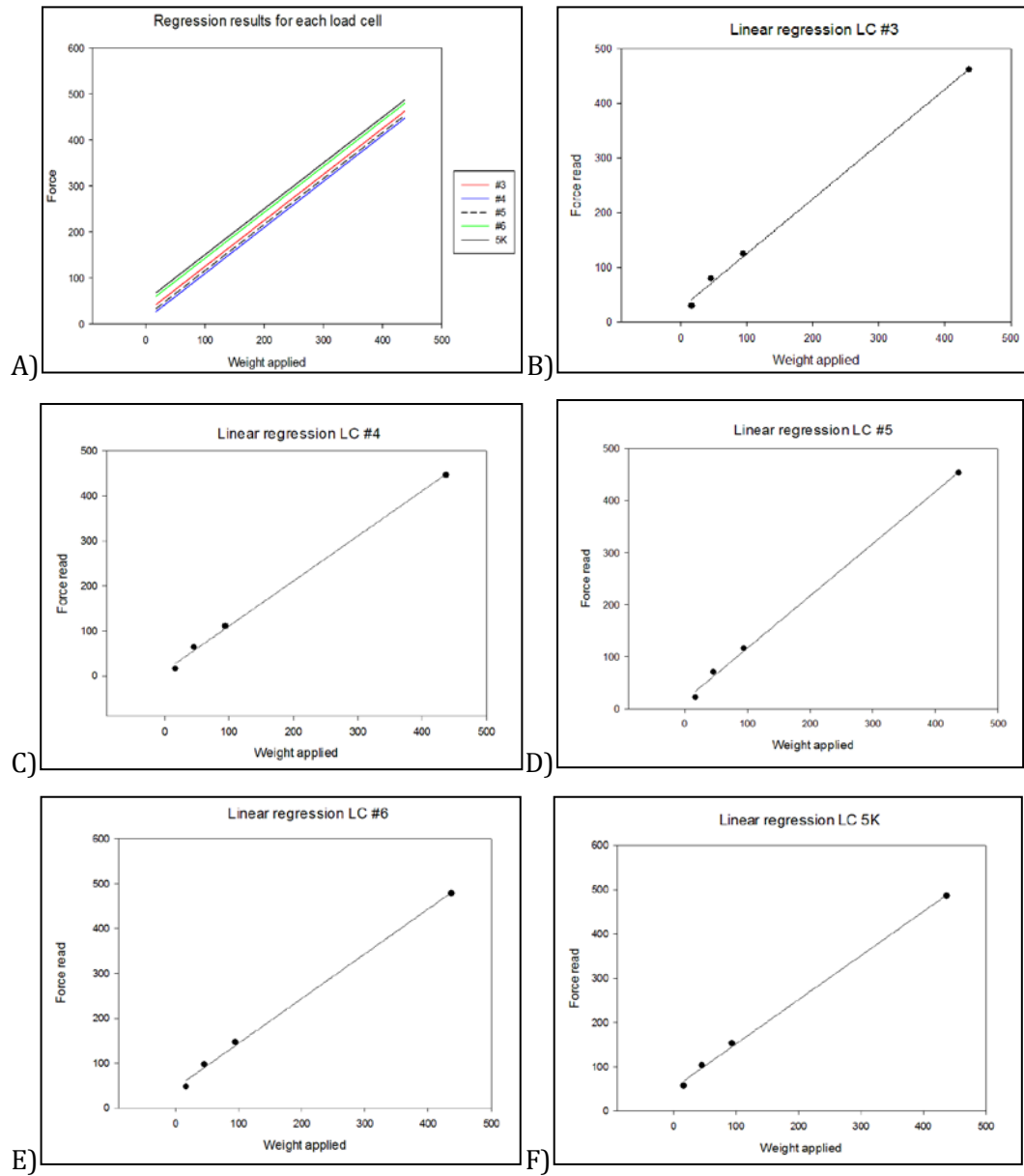
También se muestra una gráfico de rangos. Esta gráfico muestra el rango de cada grupo de 5 mediciones hechas por 2 operadores en 7 partes. El límite superior se coloca a la distancia usual de 3 sigmas para la gráfico de rangos. En este caso, no hay grupos fuera del límite de control, lo que implica un nivel consistente de variabilidad entre los grupos.

Accuracy. Percentages chart.



## APPENDIX 16

Linear regression result graphs for each load cell. Data from known weight application



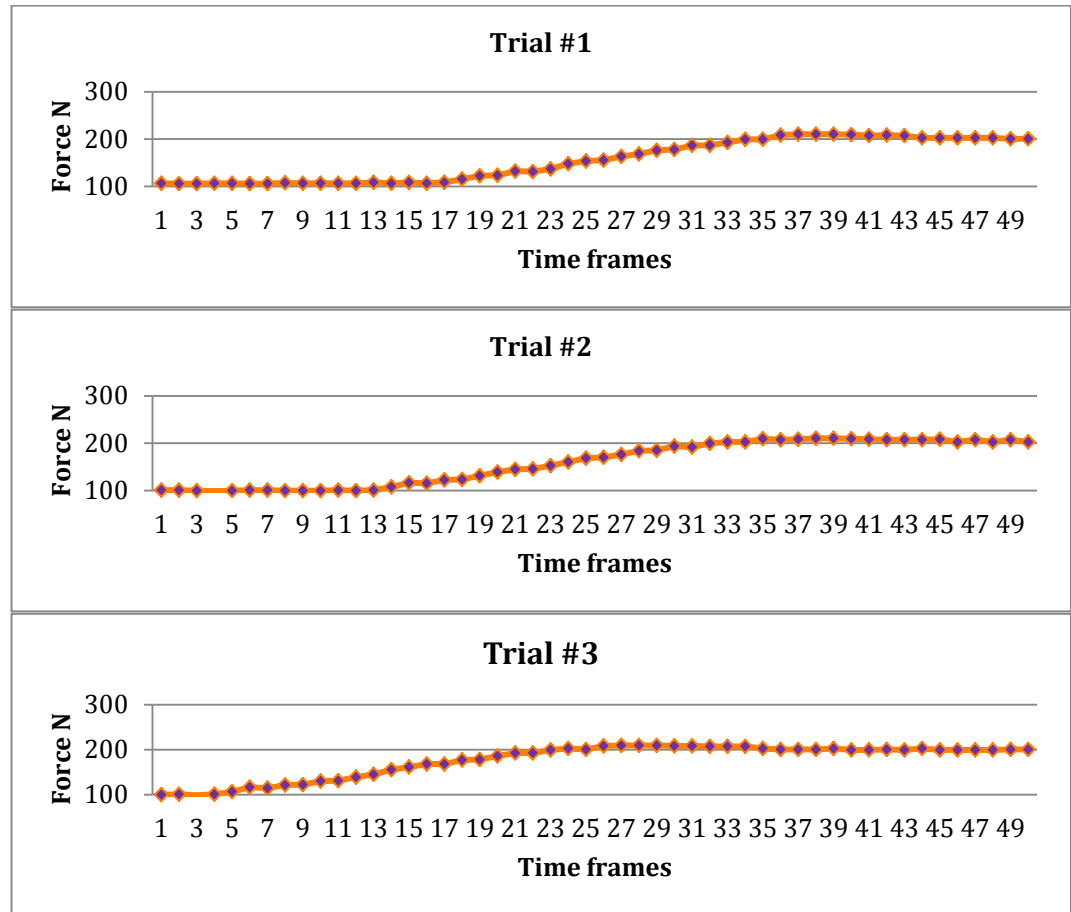
Regression results of the force sensors. A) All load cells B) Load cell #3 C) Load cell #4 D) Load cell #5 E) Load cell #6 F) Load cell #7 (5KN)



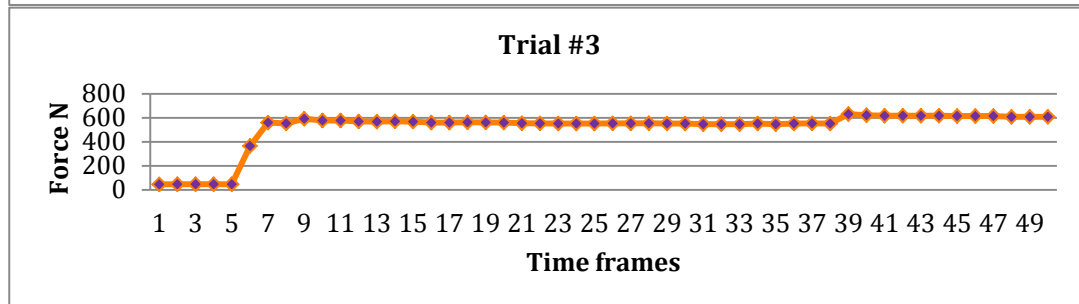
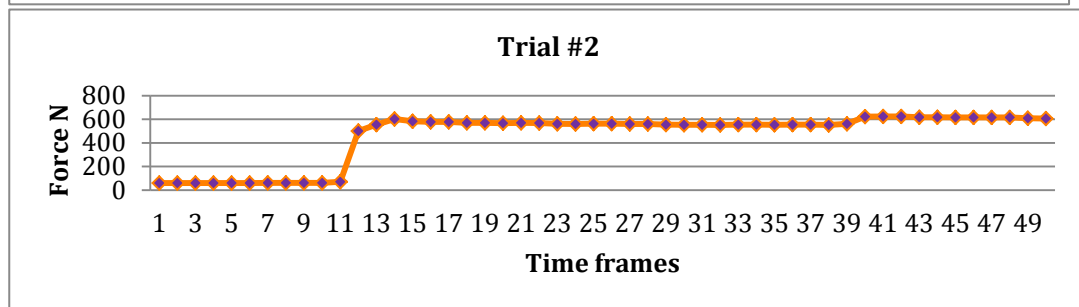
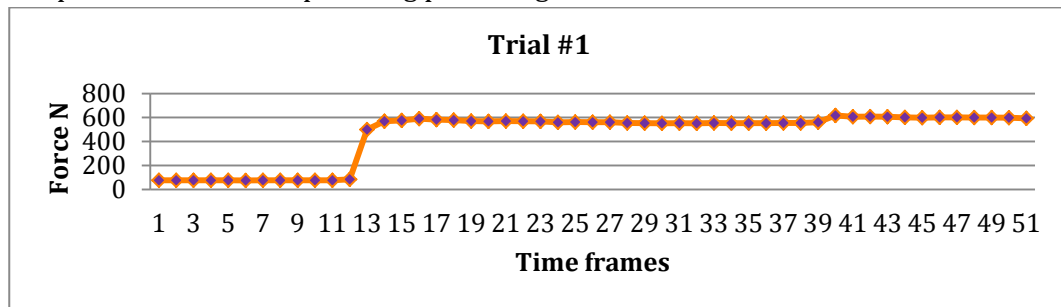
# APPENDIX 17

## Vibration effect on load cell readings graphs

- Actuator D, load cell #3, target force 200N, high force overshoot

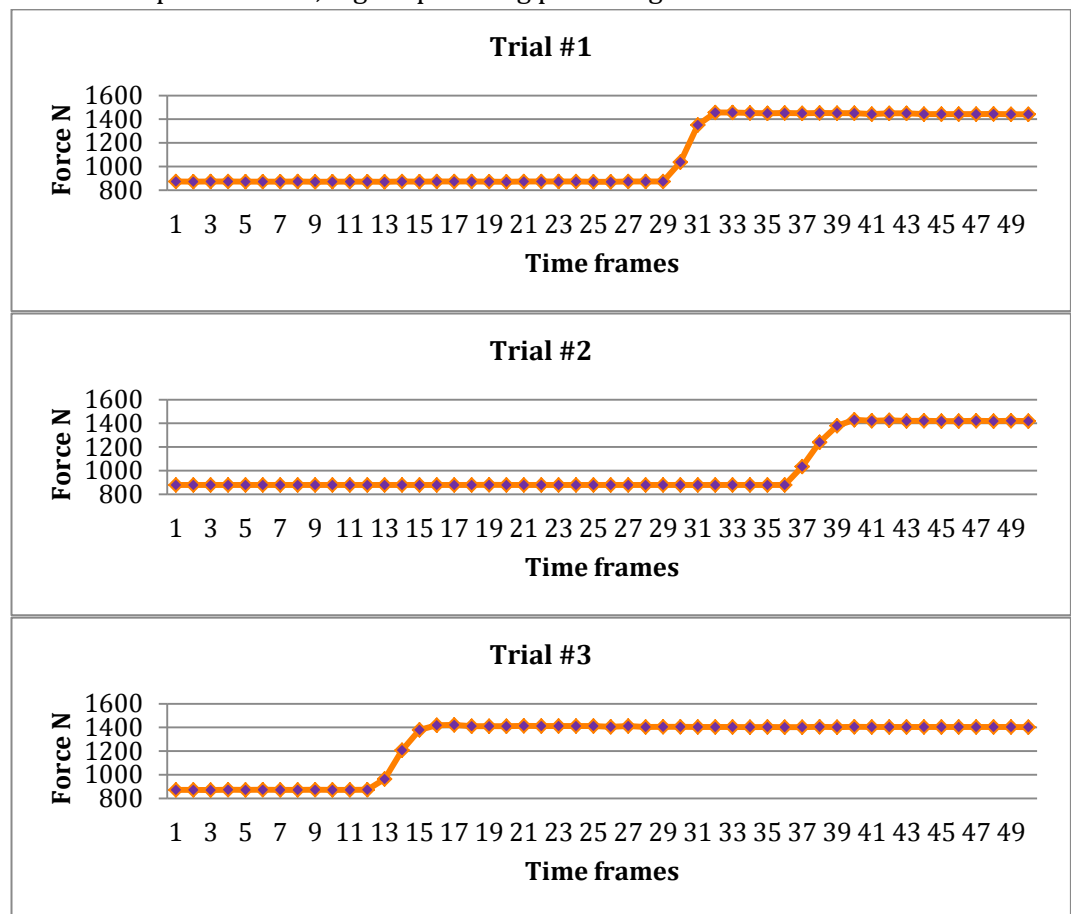


- Actuator C, load cell #5, target force 600N, prefilling phase overshoot, then control phase enters, small prefilling percentage

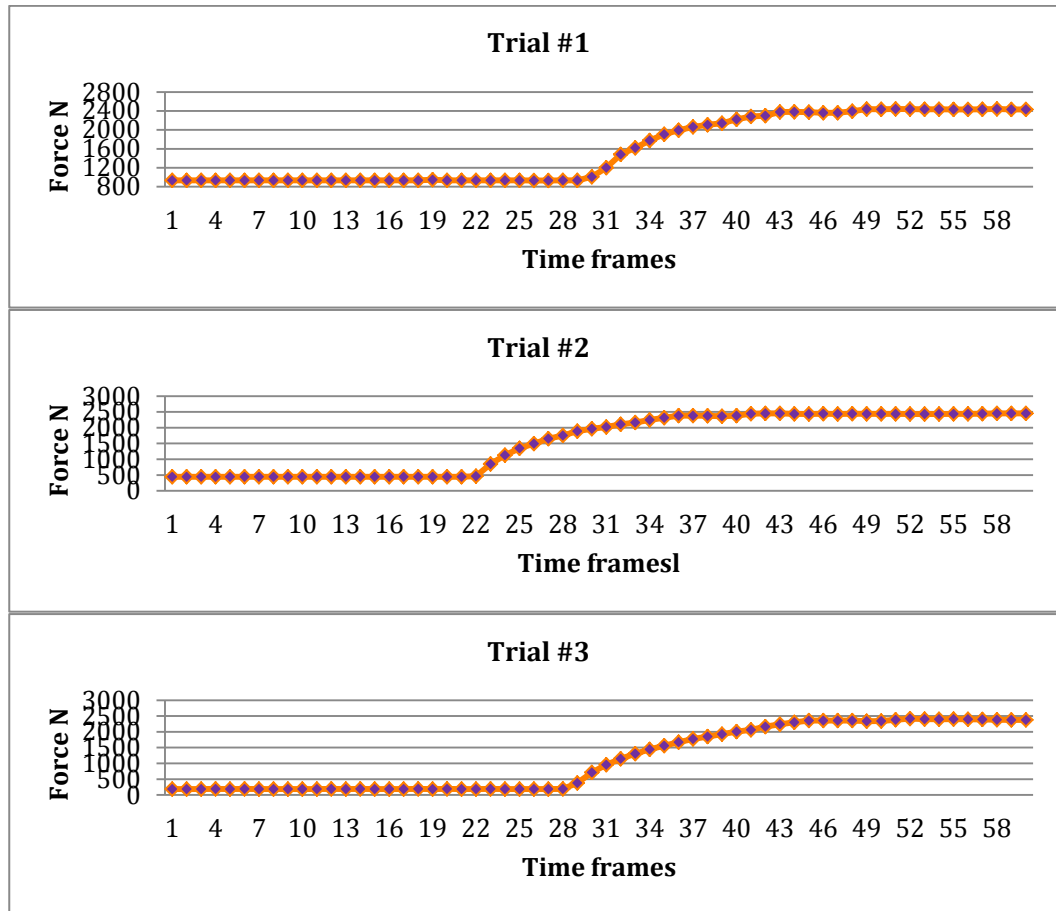




- Actuator B, load cell #6, target force 1400N, prefilling phase overshoot, then control phase enters, higher prefilling percentage

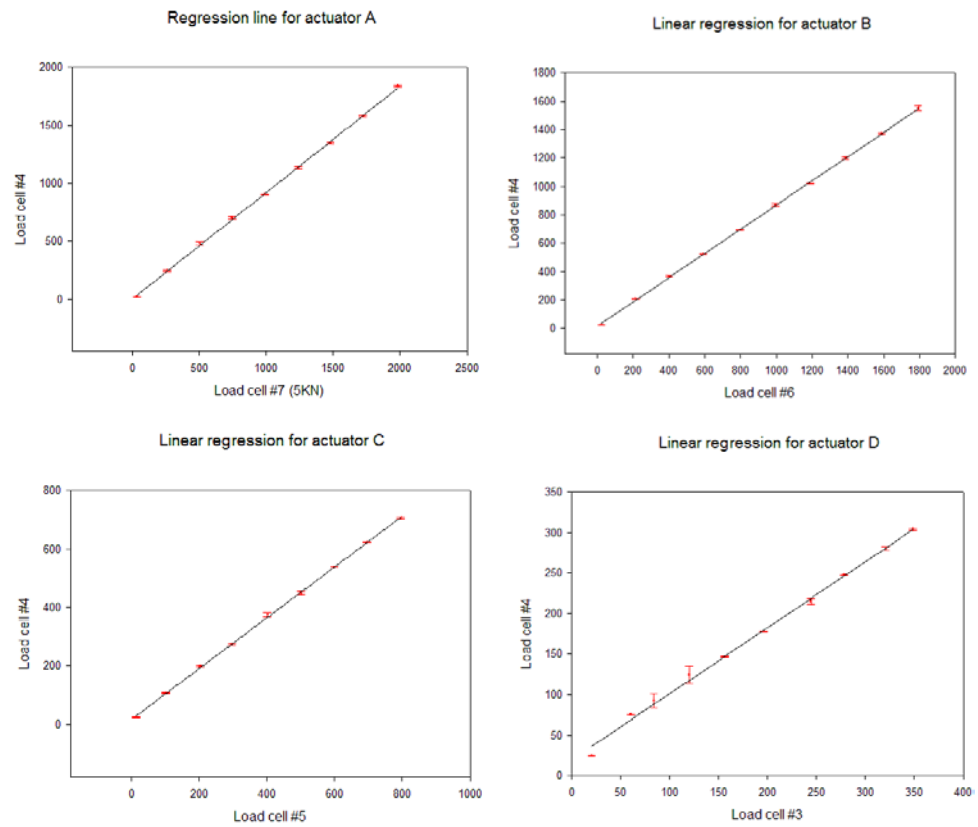


- Actuator A, load cell 5KN, target force 2500N, small prefilling overshoot



## APPENDIX 18

Force loss due to redirection effect. Linear regression results graphs



Regression lines for each artificial muscle redirection loss. The graphs also show the average forces obtained during testing as well as the standard deviation range



# APPENDIX 19

## Statistical results of the control system during the verification tests (Spanish)

- Accuracy results from Continuous setup

### Accuracy of the complete setup

Mediciones: ts1

Valores de referencia: ref

Variación de proceso:

Número de Partes: 12

Número total de mediciones: 12

Número de mediciones excluidas: 0

Rango de valores de referencia: 120 - 750

Estimados

	Estimado	Porcentaje
Bias	6.3705	1.011
Linealidad	0.234258	0.037

Modelo de bias:  $6.2134 + 0.000371837x$

Parámetro	Estimado	Error Estnd.	Estadístico t	Valor-P
Intercepto	6.2134	2.03051	3.06002	0.0120
Pendiente	0.000371837	0.00409119	0.0908872	0.9294

El StatAdvisor

Basado en un total de 12 mediciones en 4 partes, el bias medio estimado del dispositivo es 6.3705 unidades. Esto representa 1.011% de la variación de proceso, la cual se ha especificado como 630.0 unidades. La linealidad, o cambio de bias a lo largo del rango de variación de producto, representa 0.037% de ese rango.

También de interés es el valor-P de la pendiente. Puesto que el valor-P es mayor o igual que 0.05, no hay un cambio estadísticamente significativo en el bias a lo largo del rango de los valores de referencia a un nivel de significancia del 5.0%.

### Trial1

Partes: part  
Mediciones: tc1  
Valores de referencia: reference  
Variación de proceso:  
  
Número de Partes: 4  
Número total de mediciones: 4  
Número de mediciones excluidas: 0  
Rango de valores de referencia: 120 - 750

Estimados

	Estimado	Porcentaje
Bias	5.42417	0.861
Linealidad	6.14675	0.976

Modelo de bias: 9.54639 - 0.00975674x

Parámetro	Estimado	Error Estnd.	Estadístico t	Valor-P
Intercepto	9.54639	4.10054	2.32808	0.1453
Pendiente	-0.00975674	0.00826203	-1.18091	0.3590

El StatAdvisor

Basado en un total de 4 mediciones en 4 partes, el bias medio estimado del dispositivo es 5.42417 unidades. Esto representa 0.861% de la variación de proceso, la cual se ha especificado como 630.0 unidades. La linealidad, o cambio de bias a lo largo del rango de variación de producto, representa 0.976% de ese rango.

También de interés es el valor-P de la pendiente. Puesto que el valor-P es mayor o igual que 0.05, no hay un cambio estadísticamente significativo en el bias a lo largo del rango de los valores de referencia a un nivel de significancia del 5.0%.

## Trial 2

Partes: part

Mediciones: tc2

Valores de referencia: reference

Variación de proceso:

Número de Partes: 4

Número total de mediciones: 4

Número de mediciones excluidas: 0

Rango de valores de referencia: 120 - 750

Estimados

	<i>Estimado</i>	<i>Porcentaje</i>
Bias	6.71965	1.067
Linealidad	3.62839	0.576

Modelo de bias: 4.28633 + 0.00575935x

<i>Parámetro</i>	<i>Estimado</i>	<i>Error Estnd.</i>	<i>Estadístico t</i>	<i>Valor-P</i>
Intercepto	4.28633	1.69521	2.52848	0.1272
Pendiente	0.00575935	0.00341563	1.68618	0.2338

El StatAdvisor

Basado en un total de 4 mediciones en 4 partes, el bias medio estimado del dispositivo es 6.71965 unidades. Esto representa 1.067% de la variación de proceso, la cual se ha especificado como 630.0 unidades. La linealidad, o cambio de bias a lo largo del rango de variación de producto, representa 0.576% de ese rango.

También de interés es el valor-P de la pendiente. Puesto que el valor-P es mayor o igual que 0.05, no hay un cambio estadísticamente significativo en el bias a lo largo del rango de los valores de referencia a un nivel de significancia del 5.0%.

## Trial 3

Partes: part

Mediciones: tc3

Valores de referencia: reference

Variación de proceso:

Número de Partes: 4

Número total de mediciones: 4

Número de mediciones excluidas: 0

Rango de valores de referencia: 120 - 750

Estimados

	Estimado	Porcentaje
Bias	6.96767	1.106
Linealidad	3.22113	0.511

Modelo de bias:  $4.80747 + 0.0051129x$

Parámetro	Estimado	Error Estnd.	Estadístico t	Valor-P
Intercepto	4.80747	4.54781	1.0571	0.4013
Pendiente	0.0051129	0.00916321	0.557981	0.6330

El StatAdvisor

Basado en un total de 4 mediciones en 4 partes, el bias medio estimado del dispositivo es 6.96767 unidades. Esto representa 1.106% de la variación de proceso, la cual se ha especificado como 630.0 unidades. La linealidad, o cambio de bias a lo largo del rango de variación de producto, representa 0.511% de ese rango.

También de interés es el valor-P de la pendiente. Puesto que el valor-P es mayor o igual que 0.05, no hay un cambio estadísticamente significativo en el bias a lo largo del rango de los valores de referencia a un nivel de significancia del 5.0%.

- Accuracy results from Stop setup

## Accuracy of the complete setup

Partes: part  
Mediciones: ts1  
Valores de referencia: ref  
Variación de proceso:

Número de Partes: 12  
Número total de mediciones: 12  
Número de mediciones excluidas: 0  
Rango de valores de referencia: 120 - 750

Estimados

	Estimado	Porcentaje
Bias	4.03927	0.641
Linealidad	14.8896	2.363

Modelo de bias: 14.0248 - 0.0236343x

Parámetro	Estimado	Error Estnd.	Estadístico t	Valor-P
Intercepto	14.0248	7.37578	1.90146	0.0864
Pendiente	-0.0236343	0.0148612	-1.59034	0.1428

El StatAdvisor

Basado en un total de 12 mediciones en 4 partes, el bias medio estimado del dispositivo es 4.03927 unidades. Esto representa 0.641% de la variación de proceso, la cual se ha especificado como 630.0 unidades. La linealidad, o cambio de bias a lo largo del rango de variación de producto, representa 2.363% de ese rango.

También de interés es el valor-P de la pendiente. Puesto que el valor-P es mayor o igual que 0.05, no hay un cambio estadísticamente significativo en el bias a lo largo del rango de los valores de referencia a un nivel de significancia del 5.0%.

## Trial1

Mediciones: ts1

Valores de referencia: ref

Variación de proceso:

Número de Partes: 4

Número total de mediciones: 4

Número de mediciones excluidas: 0

Rango de valores de referencia: 120 - 750

Estimados

	Estimado	Porcentaje
Bias	1.91727	0.304
Linealidad	31.583	5.013

Modelo de bias: 23.0979 - 0.0501318x

Parámetro	Estimado	Error Estnd.	Estadístico t	Valor-P
Intercepto	23.0979	21.949	1.05234	0.4030
Pendiente	-0.0501318	0.0442243	-1.13358	0.3746

El StatAdvisor

Basado en un total de 4 mediciones en 4 partes, el bias medio estimado del dispositivo es 1.91727 unidades. Esto representa 0.304% de la variación de proceso, la cual se ha especificado como 630.0 unidades. La linealidad, o cambio de bias a lo largo del rango de variación de producto, representa 5.013% de ese rango.

También de interés es el valor-P de la pendiente. Puesto que el valor-P es mayor o igual que 0.05, no hay un cambio estadísticamente significativo en el bias a lo largo del rango de los valores de referencia a un nivel de significancia del 5.0%.

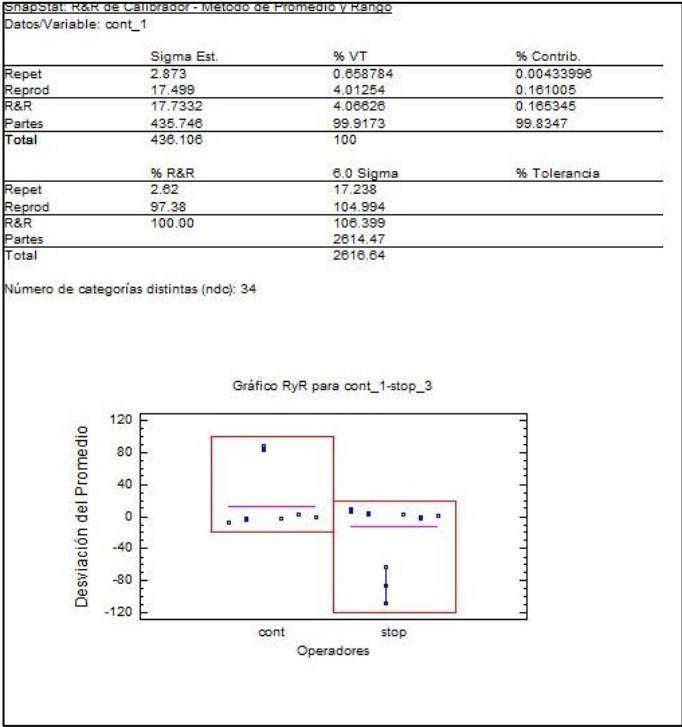
También de interés es el valor-P de la pendiente. Puesto que el valor-P es mayor o igual que 0.05, no hay un cambio estadísticamente significativo en el bias a lo largo del rango de los valores de referencia a un nivel de significancia del 5.0%.



# APPENDIX 20

Statistical results of the ground reaction data during the verification tests (Spanish)

Repeatability and reproducibility percentage chart and graph.



Con base en un estudio involucrando 2 operadores, cada uno midiendo 6 partes 3 veces, la desviación estándar estimada del proceso de medición es igual a 17.7332. De la varianza total, 97.38% es debida a diferencias entre operadores (Reproducibilidad) en tanto que 2.62% es debida al instrumento (Repetibilidad).

Comparando la variabilidad del proceso de medición con la variabilidad total en cont\_1, el proceso de medición contribuye 0.17%, con el resto 99.83%, atribuible a las diferencias entre partes.

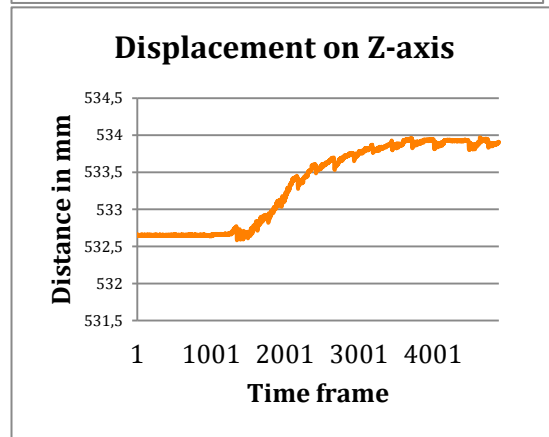
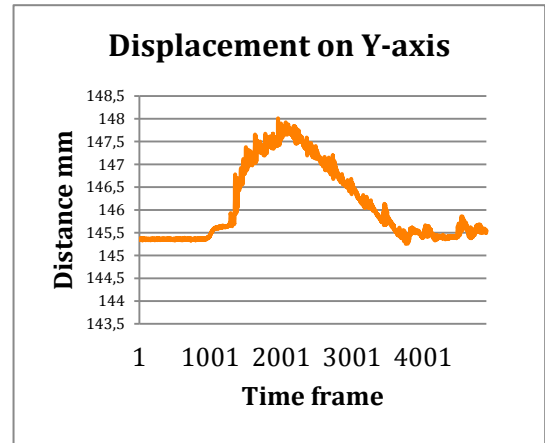
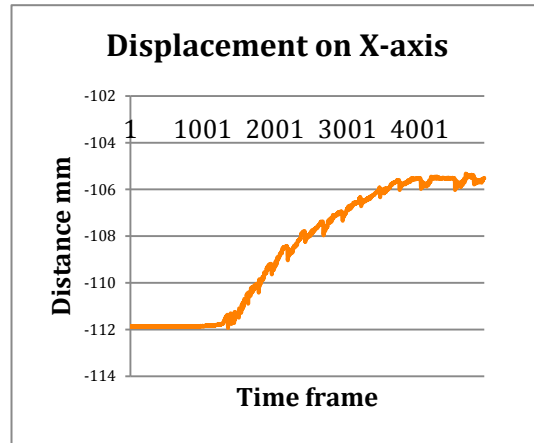
También se muestra una gráfica de rangos. Esta gráfica muestra el rango de cada grupo de 3 mediciones hechas por 2 operadores en 6 partes. El límite superior se coloca a la distancia usual de 3 sigmas para la gráfica de rangos. En este caso, no hay grupos fuera del límite de control, lo que implica un nivel consistente de variabilidad entre los grupos.



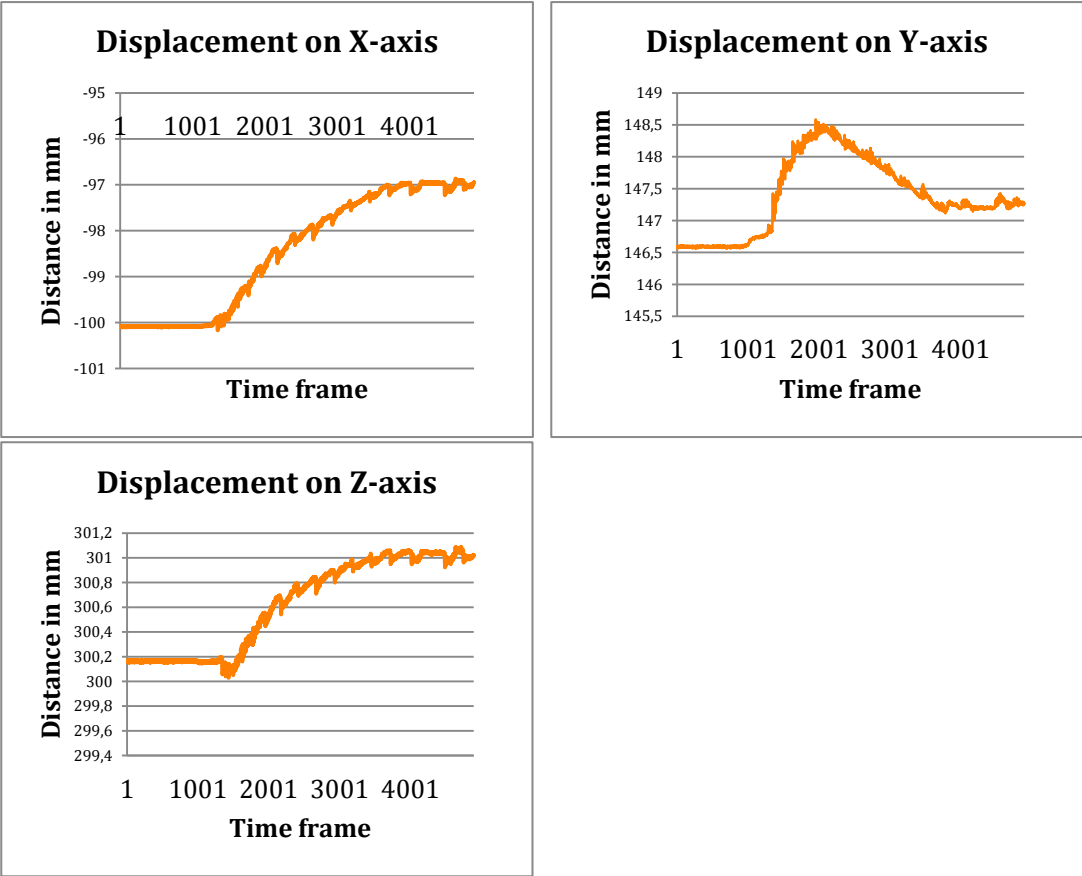
## APPENDIX 21

Center displacement graphs of the center of the three marker clusters during the first trial of the Continuous setup

Marker cluster center displacement on each axis. Top cluster



Marker cluster center displacement on each axis. Medium cluster



Marker cluster center displacement on each axis. Bottom cluster

